Active Independent Front Steering for Yaw-Rate Control and Tire Work-Load Equalization in Road Vehicles

Vaibhav Rawat

A Thesis

in

The Department

of

Mechanical and Industrial Engineering

Presented in Partial Fulfillment of the Requirements
for the Degree of Master of Applied Science (Mechanical Engineering) at
Concordia University
Montreal, Quebec, Canada

February, 2007

Your file Votre référence
ISBN: 978-0-494-52316-2
Our file Notre référence
ISBN: 978-0-494-52316-2

Abstract

Active Independent Front Steering for Yaw-Rate Control and Tire Work-Load Equalization in Road Vehicles

Vaibhav Rawat

Several control strategies can be implemented in road vehicles to avoid roll over, improve ride quality or customize handling performance. Handling performance is one of the crucial areas of research from the safety point of view. Most of the control strategies depend on manipulating the motion of the tires, which are the prime source of the forces acting on the vehicle. Some of the common control strategies for handling explored in recent years include: active control of tractive and/or braking torque; and a wide variations in active steering control. For vehicle stability and handling improvement, Active Front and Rear Steering (AFS, ARS) prove to be excellent control techniques, as active torque control fails to generate required forces and moments in certain situations. In recent years, major research effort has been directed towards active steering control, where the steer angle of the wheels is actively controlled to improve handling performance at high speeds. Such controls, however, have limitations as they do not attempt to utilize tires' force generating potential. The present study proposes a new Active Independent Front Steering (AIFS) technique with independent control for each front wheel. A non-linear 4-wheel vehicle model incorporating tire 'Magic formula' and load shifts in longitudinal and lateral direction is studied. This model agrees well with a simpler bicycle model and CarSim simulation. The 4-wheel vehicle model with proposed AIFS is simulated for step and sinusoidal lane-change inputs. A simple PI control

algorithm that differentiates between under and oversteer handling characteristics is developed and utilized for the simulations. The results show that by controlling one wheel only, AIFS can provide the ideal yaw-rate and trajectory responses at any speed, and the performances are as good as those obtained by AFS and significantly better than conventional uncontrolled system. Furthermore, AIFS is shown to equalize the tire work-load at the left and right front tires improving the vehicle's ability to generate maximum possible lateral force. Only exception to this is when the vehicle is strongly oversteer. It is also shown that this limitation can be overcome by introducing an AIFS where both wheels are actively controlled. A physical design using tandem planetary gear trains is proposed for the AIFS that can provide the required control and is fail safe. The present is a first investigation of AIFS control that has significant potential for the integrated control of road vehicles and is identified in proposed future studies.

Acknowledgments

Writing this thesis has certainly been a long journey and a great learning experience. I would like to take this opportunity to thank all those who made it easier with their support and intellectually satisfying with their critique.

I would like to express sincere gratitude to my supervisors, Dr. Waizuddin Ahmed and Dr. Rama Bhat, for their intellectual and financial support which made this research possible. Dr. Ahmed's belief in my potential to carry out this research, and his continuous encouragement, certainly are the key factors in this success.

I would also like to thank the members of the examination committee, Dr. Subhash Rakheja and Dr. Michelle Nokken, for their constructive comments. I wish to express my special thanks to Akanksh Vashisth, research assistant in the Dept. of Computer Science, Concordia University, whose excellence in Computer Graphics made it possible to transform my ideas into 3D design.

Finally, I would like to thank: my family for being supportive in my quest; my friends for the great times thus making my stay in Montreal extremely pleasant.

Dedicated to Dishita, Ruchi, late Mrs. and Mr. Ravindra Shrivastava

Contents

List of Figures and Tables

List of Symbols

Symbol	Description	Unit
a_x	Longitudinal acceleration of the vehicle CG	m/s^2
a_y	Lateral acceleration of the vehicle CG	m/s^2
b, c	Distance of CG from the front and rear axles	m
C_{ff}	Linear cornering force stiffness for each front tire (Bicycle model)	N/rad
$C_{f.r}$	Linear cornering force stiffness for each rear tire (Bicycle model)	N/rad
$C_{m.f}$	Linear aligning moment stiffness for each front tire (Bicycle model)	N.m/rad
$C_{m.r}$	Linear aligning moment stiffness for each rear tire (Bicycle model)	N.m/rad
$F_{i.j.k}$	$i=y, z; j=f, r; k=R, L;$ Lateral/Normal force on front/rear – Right/Left tire (4-wheel model)	N
F_{max}	Maximum allowable lateral force	N
$F_{y.f}, F_{y.r}$	Lateral force on front and rear tires (Bicycle model)	N
G_{acc}	Lateral acceleration gain	1/rad
G_{yaw}	Yaw-rate gain	1/s
h_{cg}	Height of CG above the ground	m
I_{zz}	Mass moment of inertia of the vehicle about vertical (z) axis	$kg.m^2$
K	Ratio of track width and wheel base	_
K_{st}	Steering gain	s
K_{us}	Understeer coefficient	_

L	Wheel base	m
m	Mass of the vehicle	kg
M_f	Aligning moment on front tire (Bicycle model)	N.m
M_r	Aligning moment on rear tire (Bicycle model)	N.m
$M_{i,j}$	$i=f, r; j=R, L;$ aligning moment on front/rear – Right/Left tire (4-wheel model)	N.m
R	Radius of the curved path	m
R_{ref}	Reference radius of the curved path	m
T_f, T_r	Half front and rear track widths	m
V	Forward velocity of the vehicle	m/s
V_{max}	Maximum allowable forward velocity of the vehicle	m/s
V_o	Initial velocity of the vehicle	m/s
V_f, V_r	Front and rear tire velocity (Bicycle model)	m/s
V_x	Longitudinal velocity of the vehicle	m/s
V_y	Lateral velocity of the vehicle	m/s
W	Weight of the vehicle	N
W_d	Work done by cornering forces and aligning moments	N.m
W_f, W_r	Weight on the front and rear axles	N
x, y, z	Vehicle co-ordinate system	_
X, Y, Z	Global co-ordinate system	_
α	Side slip-angle	rad

α_f, α_r	Front and rear side slip-angles (Bicycle model)	rad
$\alpha_{i,j}$	$i=f, r; j=R, L$; Tire side slip-angle, front/rear-Right/Left (4-wheel model)	rad
δ_i, δ_o	Steering angle at inner and outer wheels	rad
δ_L, δ_R	Steering angle at left and right wheels	rad
δ_{st}	Driver steering command	rad
δ_c	Controller steering command	rad
$\Delta\delta_{st}$	Differential steering command	rad
ΔE	Change in energy	N.m
$\Delta\Omega$	Yaw-rate error	rad/s
θ	Yaw angle	rad
μ	Coefficient of friction between tire and road surface	_
Ω	Yaw-rate	rad/s
Ω_{act}	Actual yaw-rate	rad/s
Ω_{ref}	Reference yaw-rate	rad/s

List of Abbreviations

4WS	Four Wheel Steering
ABS	Anti-lock Braking System
AFS	Active Front Steering
AGV	Autonomous Ground Vehicles
AIFS	Active Independent Front Steering
ARS	Active Rear Steering
CG	Centre of Gravity
DOF	Degree-of-Freedom
DYC	Direct Yaw-moment Control
TCS	Traction Control System
UAV	Unmanned Aerial Vehicles

1 Introduction & Literature Review

"The shortest distance between two points is under construction."

~Noelie Altito

1.1 Introduction

"Drive-by-wire" [1, 2], a concept derived from "fly-by-wire" [3], is a new step in automation. The ongoing research in the areas of vehicle handling and control all around the world promises that automated vehicles will be soon on the roads. National Advanced Driving Simulator (NADS) setup by National Highway Traffic Safety Administration (NHTSA) at Iowa State University, Partners for Automated Transit and Highways (PATH) at University of California at Berkeley and Transportation Data Center (TDC) at the University of Michigan Transportation Research Institute (UMTRI) are a few of the major attempts towards this goal [4, 5, 6]. Stanton and Marsden [7] presented a detailed summary of trends in drive-by-wire systems. Their arguments are based on three main assumptions: increased driver well-being as drivers will be relieved of several monotonous tasks, increased safety by avoiding possible driver errors as most of the road accidents are caused by driver's lack of attention or inability to control the vehicle in emergency maneuvers and finally, cost optimization as automation will enhance the desirability of the product and thus lead to substantial increase in unit sales, hence lower production cost. With the cutting edge technology already available, such as fly-by-wire

and glass-cockpit [8], Unmanned Aerial Vehicles (UAV's) [9] used as spy planes and Autonomous Ground Vehicles (AGV's) [10] used for space exploration, the concept of drive-by-wire appears to be easily achievable. But an important concern in vehicle automation is cost effectiveness. The maintenance cost and the simplicity of the operation are other major concerns as the road vehicles are maneuvered by a wide variety of people of all ages and not by a group of experts as in UAV's or AGV's. These challenges make it difficult to implement full automation in the road vehicles. In addition, vehicle system crucial components and sub-systems must be designed with fail-safe features such that lack of maintenance or partial failure does not jeopardize the safety.

In any development of a vehicle system it is essential to acquire a thorough understanding of tire mechanics and tire-road interaction, since the major forces and moments are developed at the tire-road interface. An understanding of resulting vehicle dynamics is also essential to carry out further development work in improving the performance, may it be in ride or handling. Vehicle models have been developed to understand the dynamic behavior for over six decades by engineers and researchers. Very simple 2-degrees of freedom (DOF) [11] to complex full vehicle 94-DOF models [12] were used to simulate the vehicle motion. Industries are working on developing tire models and new tire material to improve traction and control on dry asphalt and icy conditions. Control algorithms for Anti-lock-Braking System (ABS), Traction Control System (TCS) and Direct Yaw-moment Control (DYC) [13] have been developed to assist driver in extreme maneuvers. Active suspensions are designed to prevent roll over and improve the ride comfort [14, 15]. In recent years increasing attention has been directed towards control algorithm to improve vehicle handling performance under all

maneuvers and road conditions. The present study is focused on improving handling performance using simple control algorithm for steering system.

1.2 Motivation and Objective of this Research

The conventional road vehicle steering mechanism is designed to closely follow the Ackerman steering ratio which is based on different steer angle required at the inner and outer wheels at low speeds. The dynamics of a vehicle and its influence on the ability of inner and outer tires to generate forces are, however, significantly different at higher speeds than those at low speeds. Hence a fixed ratio at all speeds will fail to generate the forces each tire is capable of generating.

In attempts to overcome this limitation an actively controlled steering input is proposed to improve the stability [17]. This input is applied on both the front tires following the Ackerman geometry. Various sensors measure the vehicle state parameters, such as, longitudinal and lateral velocity, yaw-rate and steering command from the driver. Using a control algorithm the additional steering command is calculated. The only control variable in this case is the additional controlled steering input (δ_c). The next step to improve handling characteristics of vehicles is 4-Wheel Steering (4WS), where the rear wheels are also steered actively with respect to the front wheels. 4WS has shown an improvement in handling over Active Front steering (AFS) [18-20], but has not made a great impact on the marketplace due to its added complexity and cost [21]. The AFS control system can be presented in form of a block diagram as shown in Figure 1.1 [22], where, the front steering angle δ_f is composed of the driver commanded steering wheel angle, δ_{st} and an additional controller steering command, δ_c:

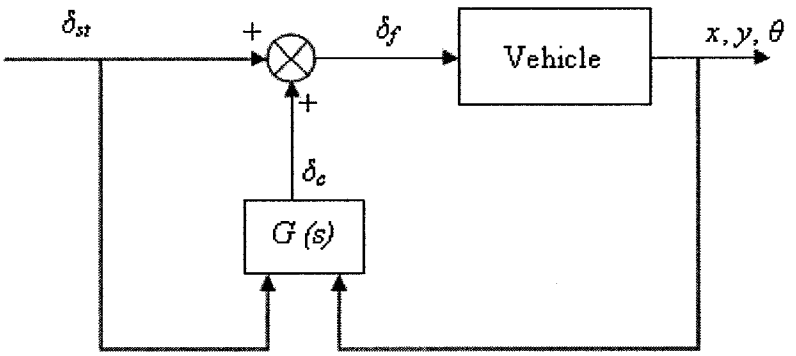

Figure 1.1: Block diagram of a vehicle with AFS [22]

$$\delta_f = \delta_{st} + \delta_c \tag{1.1}$$

The control law *G(s)* generally requires input of the driver commanded steering wheel angle as reference and measurement of dynamical variables, such as yaw-rate and lateral acceleration. The parameters to be matched to reference or set point values are yaw-rate and vehicle side-slip. Since there is only one control variable, front steering angle, only one of the two parameters can be controlled, yaw-rate in this case, and thus other techniques, such as Active Rear Steering (ARS) and Direct Yaw-moment Control (DYC) are incorporated to achieve a full control [18, 19, 23].

Most of the studies related to AFS employ a bicycle model and assume that both front tires can generate equal lateral forces. At high speeds, vehicle roll plays an important role in normal load transfer from inner to outer wheels. Since, the lateral force generated by tire depends on normal weight, the ability to generate lateral forces during cornering is different for inner and outer tires [24]. The inner tire with less normal load can generate less lateral force in cornering when compared to the outer tire and hence, becomes the limiting factor for the actively commanded steering angle. The outer tire, though can generate higher lateral force, can not be exploited to its capability so as to

prevent the skidding of the inner tire, which is a major concern in vehicle handling safety [15].

In the current study, it is proposed that if both front wheels are steered independently this limitation can be overcome. The independent steering will increase the number of control variables to 2 and an optimized ratio of the front wheels steering can lead to a better control when compared with the conventional AFS. Such a system proposed in this investigation is referred to as Active Independent Front Steering (AIFS). The AIFS can be designed to apply Ackerman steering ratio at low speeds and modify the steering angle at one or both front wheels to achieve improved vehicle control and tire work-load [19, 23]. Tire work-load is measure of utilization of frictional forces developed by each tire under a given normal load. Such control strategy would also be useful to enhance the performance of split-μ driving when the coefficient of friction at one side of the tire-road interface is not same as that at the other side [17, 23, 25, 26].

To examine the proposed AIFS it is essential to develop a 4-wheel vehicle handling model that includes tire non-linearity and vehicle roll dynamics. It further requires identification of response variables to be controlled. A thorough literature review is carried out on various aspects of the proposed investigation as presented in the following subsection.

1.3 Literature Review

Literature survey in various fields, such as, tire modeling and scrub, vehicle modeling, active steering control and parameter estimation is carried out to establish the state of the art.

1.3.1 Tire Modeling

Tires play the most important role in dictating vehicle handling performance. Tires transmit most of the external forces to the vehicle; other forces being air drag and gravity. Nonlinear characteristics of tire, wear with time and dependency on other factors such as temperature, normal load etc. make it difficult to model force-slip characteristics of the tire. Different researchers have developed mathematical and analytical models based on physical principles and empirical models derived from field test data. Chang *et al.* have done a thorough survey on the development of tire models [27]. It includes the comparison between different approaches such as lumped-parameter, semi-analytical and FEM models. The survey concentrates mainly on vertical and longitudinal motions of the tire.

Three different approaches are used for tire modeling. The first approach is to use a physical model of the tire where the tire is made up of discrete deformable radial spokes [28]. Other workers use a series of springs which produce forces in the contact patch [29]. A good review of this type of approach has been given in [30]. The parameters in these models must be set to create a match with measured tire data. A second approach entails the storage of a large amount of experimental data and use of interpolation to describe arbitrary conditions [31]. The final approach, which appears to be most popular, is to determine a function which relates tire forces and moments to physical parameters such as slip-angle and camber [24, 32-34].

In 1987 Pacejka, Bakker and Nyborg presented a semi-empirical approach for tire longitudinal and lateral force calculation [24]. Well known as "Magic formula", it utilizes the data from field tests to calculate the coefficients of stiffness, shape factor, etc. The

model also gives lateral and longitudinal forces in combined cornering and braking, along with self aligning moments. The work is limited to steady state conditions and has been used by several researchers for vehicle handling studies [12, 35-41] and for real-time tire-road friction estimation [42, 43]. It is also used extensively in the vehicle simulation software such as CarSim to predict vehicle behaviour [44]. Later, many researchers improved the model for transient analysis, yet using the simple bicycle model and neglecting the effects of self aligning moment [45, 46]. Liu and Peng improved the 'brush model' matched to the Magic formula curve for vehicle path prediction and to calculate 'time to lane crossing' (TLC) by road friction coefficient estimation [47]. A brush model is a physical tire model based on the tire-road contact patch properties of adhesion and sliding. The brush tire model was a popular method in the 1960's and 1970's before the empirical approaches became dominating, and is still used by researchers for various vehicle dynamics studies [42, 47-53]. A detailed description of brush model can be found in [54].

In 1988, just after the development of the Magic formula, Szostak *et al.* proposed another semi-empirical tire model [55]. Based on a physical tire model they used the Calspan tire test data to include effects of normal load and camber [56, 57]. The simulation results were compared to other test results and matched very well. The formulation had the ability to differentiate between radial and bias-ply tire. Being extensively computational, the model could not become as popular as Magic formula and is rarely used by the researchers. Ray has used Szostak's tire model to develop tire forces in a 9-DOF vehicle model and then estimated these forces from a 5-DOF and 8-DOF vehicle models [58, 59], respectively, using an Extended Kalman Filter [60, 61].

DiMaggio and Bieniek presented a new method of dealing with the force-producing mechanism at the tire-road interface [62]. The model consists of a representation of the tire elasticity and the relations between the interface forces and the contact patch displacement. The model appears to be capable of reproducing the tire behavior under both free-rolling and fully locked wheel conditions. Maurice developed a pragmatic tire model based on the analytical frequency response functions of the pneumatic trail of the brush type model [63]. The model consists of a phase leading system in series with the first-order model for the lateral force. The self aligning moment is calculated by multiplying the force with the pneumatic trail.

Beato *et al.* [41] obtained the relation between tire force and slip-angle as a function of normal load using a Milliken test [64] on a flat track roadway simulator (FTRS). This test has advantage over field tests as it has better repeatability and each tire/axle can be tested at a time, thus all tires are not damaged each time the test is run unlike other 'constrained tests' [64]. The results matched well with the Magic formula. Qu and Liu developed an empirical formula for qualitative analysis of nonlinear characteristics of the tire applying the approximate analytical methods of nonlinear vibration [65]. The coefficients in the formula are found by least mean square regression and it seems to give precise results when compared with experimental data. In another attempt, Lacombe developed an analytical model for lateral tire deflection using elastic beam theory [66]. Unlike the empirical formulae, the model requires limited set of easily obtained input parameters. Also it can be used in nonlinear range of operation unlike most of the analytical models available.

Although, the Magic formula predicts the tire forces under steady state conditions, many researchers have used it in transient vehicle handling analysis due to its ability to predict tire forces and moments under varying load and combined braking and cornering [12, 38, 67, 68]. In the current study same tire model based on Magic formula is used as presented in [24].

1.3.2 Vehicle Modeling

Several simple and complicated vehicle models have been formulated after Segel first developed a theoretical vehicle model for vehicle response prediction [69]. The less complex single track model, commonly known as bicycle model, was first developed by Marquard [11] in 1966 and was followed by McHenry [70] in 1968. This model takes advantage of the fact that the steering angle difference between inner and outer wheels is small and hence, both tires on each axle can be combined together to form a single track model and uses average steering angle for the front wheel. This model is explained in detail in texts such as [13, 16]. Shladover [71] has substantiated the use of such model for the vehicle performance analysis when effect of roll steering is not a concern and hence, the model has been extensively used by researchers even today, when high computing facilities are available. Bicycle model has proved to be an excellent choice for vehicle handling performance tests including vehicle state prediction [65, 72-74] and active steering [22, 26, 75]. Bicycle model also helps in understanding the vehicle handling characteristics such as understeer nature [16].

Though the bicycle model has its own advantages, it has limited application when the track width of the vehicle plays an important role, for example in vehicle roll-over [17, 20, 67, 76-78] and DYC [17, 23, 79-82] studies. Since most of the vehicle handling

studies consider only yaw, lateral and longitudinal motion, a yaw-plane [83] model is commonly used. This model considers the vehicle as a rigid body, neglecting the effect of the suspension, and hence can be defined by 3-DOF: longitudinal, lateral and yaw. Such a model is most commonly used in various vehicle dynamic studies [21, 25, 36-38, 42, 48, 83-85]. In other studies more complex vehicle models, such as 94-DOF model [12] developed by Hegazy *et al.* considers suspension stiffness, steering compliances and tire inertia. Takezono *et al.* [86] have taken the asymmetry of the vehicle into account to develop a vehicle model with off centered centre of gravity of the vehicle.

From the above studies it is clear that a bicycle model is sufficient for understanding the vehicle behavior and for active steering control, but a more complex 4-wheel model is necessary to take vehicle roll and lateral load shift into account. Also, for active traction control as in DYC, a 4-wheel model has to be employed. Although the current study deals only with active front steering and does not include any traction control, the importance of lateral load shift and the independent active steering command for both front wheels make it necessary to use a 4-wheel model. Both a bicycle and 4-wheel models are developed in this investigation, assuming rigid suspension and neglecting tire inertia. Although the effect of dynamic load shift due to roll is included, the vehicle in each case is only assigned lateral, longitudinal and yaw degrees-of-freedom.

1.3.3 Active Control

Vehicle control can be divided into two main categories: control algorithm and control technique. The control algorithm is the mathematical formulation which operates on the input variable to give the output. By improving a control algorithm, stability of the given

control system can be improved and the factors such as response time delay and overshoot can be reduced. A control technique is based on a physical phenomenon which defines the state variables to be matched to reference values (set points) by changing other parameters. The current study focuses on developing a new control technique by independently controlling the steering angles of the front wheels.

Various control techniques used for vehicle handling improvement and reported in literature, include Active Front Steering (AFS), Active Rear Steering (ARS), 4-Wheel Steering (4WS) and Direct Yaw-moment Control (DYC). While AFS, ARS and 4WS control the lateral forces acting on the tires, DYC controls the longitudinal forces. The state variables to be controlled are side-slip angle of the vehicle's CG and vehicle yaw-rate. AFS and ARS actively control the steering angle of the front and rear wheels, respectively, and hence control the lateral forces acting on the vehicle. These lateral forces can be used to generate yaw moment about the vehicle's CG and hence control the yaw-rate. By using a combination of AFS and ARS (4WS) one can control the side-slip of the vehicle by steering the rear wheels in proportion to the front steering angle. As early as 1969, Kasselmann and Keranen [87] developed an active steering system based on feedback from a yaw-rate sensor.

DYC uses the commonly used hardware of Antilock Braking System (ABS) and Traction Control System (TCS). DYC controls the longitudinal force of each tire in relationship with the vehicle motion which in turn controls the lateral motion of the vehicle to stabilize its behavior. The differential longitudinal forces generated at different tires result in a yaw-moment about the CG. A proper combination of this yaw-moment

along with the braking forces can be used to control either yaw-rate or vehicle side-slip. A detailed explanation about these control techniques can be found in [13] and [81].

Many researchers have shown the advantages of DYC over AFS and ARS [19, 81, 88]. The limitation of AFS and ARS lies in tire's inability to generate enough lateral forces in near saturation state [81], and hence such techniques fail to control the vehicle in combined braking and cornering. Furthermore, the longitudinal load shift from the rear axle to the front axle in braking decreases the ability of the rear tires to generate lateral forces, and hence deteriorates the ability of ARS [19]. A comparison of side-slip type DYC, yaw-rate type DYC and side-slip control by 4WS is presented in [88]. The results show that side-slip type DYC is better than yaw-rate type DYC. Similar results are shown in [18] and [81]. Also 4WS control seems to be as good as side-slip type DYC for certain situations. Hence, DYC alone has been used for vehicle control in various studies, [79, 82, 88]. However DYC is still not a popular practical choice due to its added complexity [81].

Even with its limitations, AFS has maintained its importance in research as well as in industry. AFS as an integral part of vehicle has been shown to control the yaw-rate in split-μ tracks [17] and side-force disturbance [80]. In other studies [65, 76] AFS has shown significant improvement in roll-over prevention. Similarly [21, 75, 77, 89] have shown the importance of 4WS control technique and its advantage over AFS [18-20]. A comparison of fixed-ratio, in-phase and out-of-phase response using 4WS system is presented in [89]. 'Quadrasteer system', currently used in General Motors' pick-up trucks, is one such active 4WS strategy implemented with electronic rear-wheel steering system. Control strategies and algorithm using 4WS system are, however, complex,

expensive and not practical for most general vehicle applications. Since all of the above techniques control only one of the two state variables, yaw-rate or vehicle side-slip, an integrated control technique is adopted for a full vehicle control. A review on integrated control and its applications is given in [90]. Several studies [18, 19, 23, 76, 80] show the improvement in vehicle handling by integrated control over any of the control techniques used individually. The test conditions used in these studies are step steer input, single/double lane-change and split-μ maneuver. Studies [26, 36, 77, 91-94] have been conducted using different control algorithms to improve the performance of above control strategies.

1.3.4 Parameter Estimation

For any of the above controls to be implemented in vehicles, the first task is parameter measurement/estimation: various vehicle state variables such as vehicle velocity, yaw-rate, roll angle, tire stiffness, tire-road friction, vehicle side-slip, tire slip-angle, tire longitudinal slip etc. should be known in order to employ a control strategy. Some of these variables are easily measured, such as velocity, roll-angle/rate, yaw-rate and acceleration by velocity sensors, accelerometers and gyro sensors [79] already available in production vehicles these days. But other variables such as tire-slip and forces can not be measured directly and can only be estimated from other known variables.

A new dynamic tire/road friction model is presented in [95-100] to estimate the longitudinal and lateral tire forces. It uses LuGre tire friction model based on Coulomb friction, Stribeck effect and hysteresis [101]. Shang *et al* [102, 103] have used tire modal parameters from experiments to model unsteady cornering properties of the tire. Cadiou *et al.* [104, 105] have presented two methods to calculate tire lateral forces. The methods

proposed are estimation based on simulation (EBS) and estimation based on observer (EBO). Fukada [106] combined such two methods utilizing a vehicle model and direct integration, to estimate the tire slip-angle. This model has the advantage of being independent of the tire properties as well as does not accumulate integration error.

Yi and Jeoung [107] estimated the tire-road friction using wheel speed measurement, which can easily be realized with RPM sensors. In [108] Umeno presented a novel way to estimate the tire-road friction using the rotational vibration of the tire. The method is based on the power spectrum density of the wheel angular velocity, which is related to the tire-road friction. Ray [58, 59, 109] has used an extended Kalman filter to estimate the tire stiffness as well as friction coefficient between tire and road from measured motion of vehicles on smooth surfaces. The method neither requires a priori knowledge of μ nor a tire force model. Hahn *et al.* [110] presented a Global Positioning System (GPS) based tire/road friction coefficient measurement technique using the lateral dynamics of the vehicle. In other attempts Gerdes *et al.* [73, 74] used the GPS sensors to directly measure vehicle side-slip, tire slip-angle and roll parameters. Researchers have also developed driver models to be used in vehicle dynamics simulations [111, 112].

With all these estimation techniques along with the tire hardware-in-loop systems to measure experimental data [113, 114], online estimation/measurement of most of the vehicle parameters is possible. The most practical system should, however, be the most simplest that requires the readily available and easily measurable parameters to achieve the control.

1.4 Contribution of the Thesis

Even after the development of many control strategies discussed above and advanced computing facilities available, it was not possible to exploit the advantages of AFS to full extent as explained earlier. The conventional AFS techniques rely on adding a small additional controlled input to the steering using compliance in rotational motion of the steering column or lateral motion of the steering rack [17]. This can provide 2-3° of active steering command, which may not be sufficient in emergency situations. Only after BMW's approach towards active steering through the use of a planetary gear in steering column, active front steering seems to be a promising control strategy [115, 116]. This steering mechanism uses a planetary gear train between the driver steering command and the rack-pinion mechanism of the steering. A planetary gear train is a 2-DOF system, which means that the output steering to the rack can be controlled by 2 separate inputs: driver command and controller command. Although with this steering mechanism it is possible to fully implement the AFS control, still the front wheels in all cases maintain the Ackerman ratio. In the current study it is proposed that the planetary steering mechanism can be improved to control both front wheels independently in order to accomplish a active independent steering control. This can be achieved by using 2 planetary gear trains and 2 separate rack-pinion mechanisms connected to the same driver steering command. This proposed mechanism, as opposed to steer-by-wire approach, is a fail-safe design that can be attractive for vehicle systems.

Other shortcoming of the conventional active steering control lies in the fact that the lateral forces can not be utilized fully due to the saturation of the forces on the inner tire in cornering. As explained earlier, the inner tire has less normal load and hence is less

capable of generating longitudinal and lateral forces in cornering maneuver [117]. Despite its inability to generate lateral forces, a conventional steering system and active steering strategy requires inner tire to be steered more than the outer tire (Ackerman geometry). A performance parameter, tire work-load, defined as the ratio of the total forces generated by a tire and the maximum capability to generate forces, is never optimized between the inner and outer tire [19, 23]. This leaves the outer tire at a very low tire work-load while the inner tire reaches near saturation state. If the inner tire reaches the saturation state, i.e., tire work-load = 1, wheel lockup or skid can occur which leads to loss of control and instability of the vehicle.

The present thesis focuses on equalizing the tire work-load between inner and outer tires, and hence, utilizing the maximum friction force available to control the vehicle. For this purpose anti-Ackerman geometry is followed for high speed turning by feed-forward and feedback algorithms. The primary objective achieved in this study is the improvement in tire work-load by AIFS when compared with the conventional control strategies, while maintaining the similar yaw-rate response. The secondary objectives, also achieved in the present work, are:

- To design a control algorithm that differentiates between understeer and oversteer vehicle.
- To conceptualize a mechanical steering mechanism to implement the independent steering control.

1.5 Organization of the Thesis

The thesis is divided in five main parts:

- Vehicle Modeling (chapters 2 and 3)
- Design of Control Technique (chapter 4)
- Design of Control Algorithm (chapter 5)
- Design of Hardware (chapter 6)
- Conclusion and Recommendations (chapter 7)

Chapter 2 describes the formulation of a simple 2-wheel bicycle linear model. The tire forces are analyzed for linear and non-linear models. Steady state analysis is carried out to define the understeer nature of the vehicle. Equations of motion are formulated and transient analysis is carried out which agrees with the steady state analysis. Also, loss of energy in cornering is accounted for.

In chapter 3 conventional steering mechanism with Ackerman geometry is analyzed. A detailed 4-wheel non-linear vehicle handling model is developed. The model is based on Pacejka's Magic formula that also incorporates load shifts and other factors. The developed vehicle model response matches with the well established bicycle model as well as CarSim simulations.

In chapter 4, control strategies using longitudinal and lateral forces are discussed. Vehicle response for no-control and conventional active steering control is analyzed. Tire work-load is defined and limitations of conventional AFS are shown. An Active Independent Front Steering (AIFS) technique is proposed which can overcome the limitations of the conventional AFS.

In chapter 5 a control algorithm using a PI controller is applied to the 4-wheel model presented in chapter 3. This algorithm is modified to take care of understeer and oversteer vehicle. The same active independent control is applied to lane-change maneuver. Tire work-load in AIFS is studied and compared to the conventional control strategies and improvements are shown.

A steering mechanism using planetary gear trains is proposed in chapter 6. This practical design for road vehicles can be used to realize the AIFS system investigated in this research.

Finally, chapter 7 presents the highlights of the study, major conclusions, possible other applications of independent steering control and recommendations for future work.

2 Bicycle Model

The basic model to study the vehicle handling response is a 'Bicycle Model'. In this model, both wheels on each axle are combined together to have a 2-wheel model. Each tire bears the total load of each axle and the tire stiffness is doubled. Average steering angle is used for the front wheel. Such model neglects roll dynamics and the resulting load shift between the wheels. Bicycle models are commonly used for assessment of handling performance and comparative studies. Typically, these models assume constant forward velocity and thus, are represented by lateral and yaw degrees-of-freedom (DOF). For handling performance the tire lateral properties play the most important role. Most handling studies assume small motions and tire characteristics to be linear [22, 72, 77, 80, 83, 85, 86]. For large motions, however, the tire characteristics are very non-linear, and one must therefore adopt a non-linear model. A steady-state handling model can provide useful performance characteristics and response to given fixed steering angle. For transient response, however, it is necessary to develop a transient model represented by a set of differential equations. This chapter is devoted to developing a vehicle handling model with bicycle assumptions. The non-linear tire model is developed using Pacejka's Magic formula [24]. This is followed by the formulation for steady-state and transient response along lateral, yaw and longitudinal DOF. These models are essential part of handling study as they can be validated against each other as well as the 4-wheel model developed later in this investigation for application of AIFS control system.

2.1 Tire Model

As discussed in the literature review, tire plays the most important role in vehicle dynamics as most of the forces act at the tire-road interface. Tire models have been extensively studied over the years. Although linear tire model can represent the forces reasonably well for small motion, it is known to be very non-linear for large motions. The most common non-linear tire model is Pacejka's Magic formula [24]. For linearized analysis, the initial slope of the curve can be utilized if the motion is small.

The Pacejka's tire model calculates lateral force and aligning moment based on slip-angle, and longitudinal force based on percent longitudinal slip. The model parameters are dependent on the normal force, F_z on the tire, where the normal force is given in kN. The formula is expressed as [24]:

$$y(x) = D \sin\{C \tan^{-1}[Bx\text{-}E(Bx\text{-}\tan^{-1}Bx)]\} \tag{2.1}$$

where $y(x)$ denotes cornering force, aligning moment, or braking effort, and x represents slip-angle (α) or percent slip. Different coefficients in Equation (2.1) are:

B = stiffness factor; C = shape factor; D = peak factor; E = curvature factor

The characteristic curve is assumed to pass through origin when initial conditions such as camber and conicity are neglected. The Magic formula further provides the coefficient values or the procedure to establish them as a function of normal load (F_z) using the following:

C = 1.30 (for cornering force); 2.40 (for aligning moment)

$$D = a_1 F_z^2 + a_2 F_z \;;\; E = a_6 F_z^2 + a_7 F_z + a_8$$

$BCD = a_3 \sin\left(\tan^{-1}\left(a_5 F_z\right)\right)$ (for cornering force); $\dfrac{a_3 F_z^2 + a_4 F_z}{e^{a_5 F_z}}$ (for aligning moment)

The coefficient B can thus be calculated from:

$$B = \frac{BCD}{CD}$$

where a_1 to a_8 are the empirical coefficients, given in the Table 2.1 below [24].

Table 2.1: Pacejka's Magic formula coefficients for a medium car tire [24]

	a_1	a_2	a_3	a_4	a_5	a_6	a_7	a_8
F_y, N	-22.1	1011	1078	1.82	0.208	0.000	-0.354	0.707
M_z, N.m	-2.72	-2.28	-1.86	-2.73	0.110	-0.070	0.643	-4.04

If a side force F_s is applied to a tire, at the tire-road interface a lateral force will be developed at the contact patch, and the tire will move along a path at an angle α with the wheel plane, as OA shown in Figure 2.1 [16]. The angle between the tire heading and tire travel direction is the slip-angle, α. The phenomenon of side slip is mainly due to the lateral elasticity of the tire.

The tire lateral (cornering) force (F_y) and self aligning moment (M_z) as a function of slip-angle (α) can be established using Equation (2.1) and corresponding parameters from Table 2.1. Sample results for the front tire normal load of 4018 N and rear tire normal load of 3482 N are shown in Figure 2.2. As the results show, both characteristics are non-linear for slip-angle beyond 2°.

For steady-state bicycle model, linearized tire stiffness can be established from the initial slope in each case, and can be derived from the Equation (2.1) as:

$$C_{i,j} = \frac{dy}{dx} = \left.\frac{d\left[D\sin\left\{C\tan^{-1}\left[Bx - E\left(Bx - \tan^{-1}Bx\right)\right]\right\}\right]}{dx}\right|_{x=0} = BCD \qquad (2.2)$$

where subscript i refers to the force or moment and subscript j refers to front or rear tire.

The values of $C_{i,j}$'s for the candidate vehicle calculated from Equation (2.2) are:

$C_{f,f}$ = 1028.60 N/deg (Cornering force stiffness for each front tire)

$C_{f,r}$ = 979.90 N/deg (Cornering force stiffness for each rear tire)

$C_{m,f}$ = -26.35 N.m/deg (Aligning moment stiffness for each front tire)

$C_{m,r}$ = -21.86 N.m/deg (Aligning moment stiffness for each rear tire)

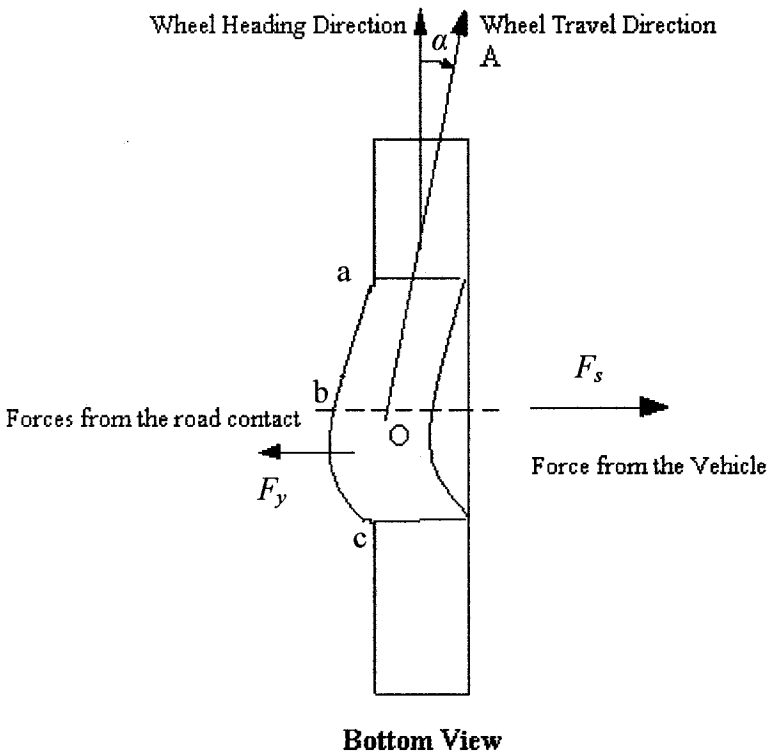

Figure 2.1: Bottom view of a tire showing deformation during cornering

For a bicycle model, as mentioned earlier, the influence of roll is neglected and the stiffness and normal load for both tires on each axle should be added consequently. Each axle's stiffness in this case becomes

$2*C_{f,f}$ = 2057.3 N/deg (Cornering force stiffness for front axle)

$2*C_{f,r}$ = 1959.8 N/deg (Cornering force stiffness for rear axle)

$2*C_{m,f}$ = -52.70 N.m/deg (Aligning moment stiffness for front axle)

$2*C_{m,r}$ = -43.72 N.m/deg (Aligning moment stiffness for rear axle)

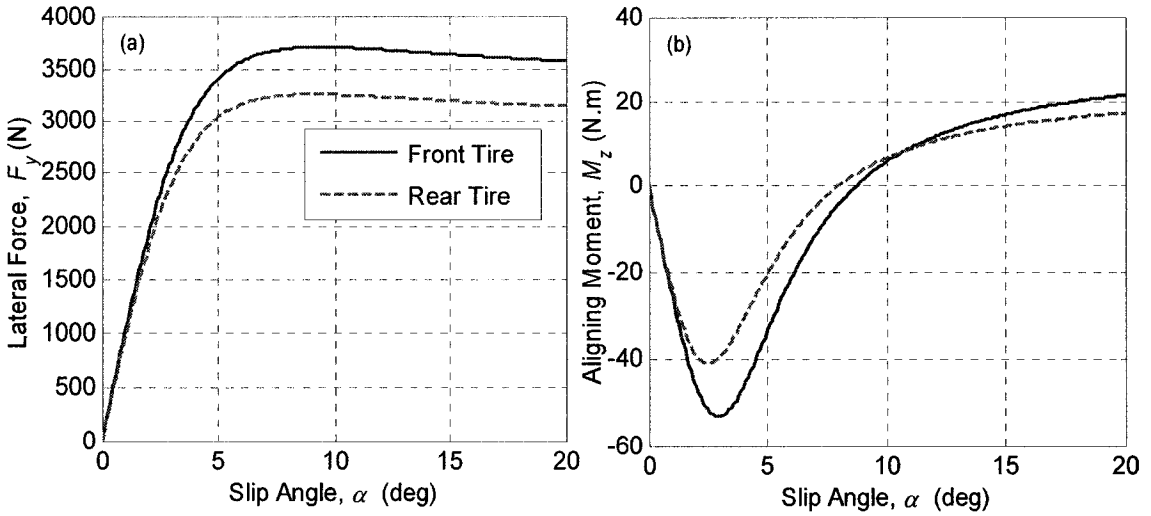

Figure 2.2: Lateral force and aligning moment vs. slip-angle using Magic formula

The linear tire model stiffness are compared with those established by Magic formula, and are found to be identical for $\alpha \leq 2^{\circ}$. The above tire properties along with the vehicle parameters presented in Table 2.2 are used in the following sections to carry out the steady-state and transient modeling. The physical parameters presented in Table 2.2 are typical for a medium size car [20, 67, 82, 83, 85] and are same as those used later for the 4-wheel model.

Table 2.2: Physical parameters for Bicycle model

Mass of the vehicle, m	1530 Kg
Wheel base, L	2.8 m
Distance of CG from front axle, b	1.3 m
Distance of CG from rear axle, c	1.5 m
Centroidal mass moment of inertia about z axis, I_{zz}	3500 Kg.m^2
Height of CG from ground, h_{cg}	0.4 m
Front axle weight, $W_f = (m.g.c)/L$	8035.7 N
Rear axle weight, $W_r = (m.g.b)/L$	6964.3 N

2.2 Steady State Model

Steady-state handling performance is concerned with the directional behavior of a vehicle during a turn under time-invariant conditions; such as vehicle traveling on a circular path with constant forward velocity. Such a model is useful for defining the steering characteristics of the vehicle, such as oversteer, understeer or neutral steer of the vehicle depending on the front and the rear tire stiffness. The steady state model is used to validate the transient response results. In case of a bicycle model steering input can be calculated as a function of turning radius R and wheel base L, as follows [16]:

$$\delta_{st} = \frac{L}{R} + \alpha_f - \alpha_r \tag{2.3}$$

where, α_f and α_r are the front and rear tire slip-angles, respectively. Using the relation between the slip-angles with cornering forces and tire stiffness, and replacing the force with normal load on each axle, the above equation takes the following form [16]

$$\delta_{st} = \frac{L}{R} + \left(\frac{W_f}{2C_{f,f}} - \frac{W_r}{2C_{f,r}} \right) \frac{V^2}{gR} = \frac{L}{R} + K_{us} \frac{V^2}{gR} \tag{2.4}$$

where $\boldsymbol{K_{us}}$ is the 'understeer coefficient' and found to be **0.3524 deg** for the vehicle parameters used. The positive value of K_{us} indicates the understeer nature of the vehicle for the given set of parameters. Hence, the model will show increase in the radius of curvature with increasing speed and vice-versa, at constant steering input. The steady-state handling Equation (2.4) can easily be extended to express steady-state yaw-rate, radius of curvature and lateral acceleration as [16]

$$\text{Yaw-rate Response, } \Omega = \frac{\delta_{st} V}{L + K_{us} V^2 / g} \tag{2.5}$$

$$\text{Curvature Response, } R = \frac{V}{\Omega} = \frac{L + K_{us} V^2 / g}{\delta_{st}} \tag{2.6}$$

$$\text{Lateral Acceleration Response, } a_y = \frac{V^2}{R} = \frac{g \delta_{st} V^2}{gL + K_{us} V^2} \tag{2.7}$$

These simple steady-state response expressions can be used to validate response of a transient model. However, a transient model with longitudinal degree-of-freedom, may not reach steady-state even for fixed steering angle. The speed may reduce with time due to work done by cornering forces. One must, therefore, be careful to ensure their validity when the responses from the two models are compared.

2.3 Transient Model

2.3.1 Equations of Motion

Transient analysis is typically carried out utilizing a 2-DOF model with lateral and yaw motions. The cornering forces are assumed to act perpendicular to the vehicle's direction of motion and hence, do not affect the forward velocity. The forward velocity is assumed to be constant, if no tractive or braking forces are applied, and hence the equation of motion in the longitudinal direction is neglected. As stated earlier, the transient model developed for this investigation also includes the longitudinal motion to be consistent with the 4-wheel model developed later in chapter 3.

During turning the reaction to centrifugal force acts on the vehicle through the tire-road contact patch. As discussed for tire model in Section 2.1, the lateral force leads to a deviation between wheel heading and direction of travel referred to as slip-angle. The path the vehicle follows is thus dictated by the steer angle and resulting slip-angles

developed at the front and rear wheels. The lateral forces acting on a bicycle model for radius of curvature R, are shown in Figure 2.3. The lateral forces on each tire act perpendicular to the direction of wheel heading and not wheel travel as shown in Figure 2.3.

The lateral force, $F_{y,f}$ makes an angle α_f with the perpendicular to the tire travel direction. This results in a component of the force in the direction of the tire travel as $F_{y,f}.\sin(\alpha_f)$. This component opposes the motion of the tire and hence, does a negative work causing deceleration of the vehicle. This force is known as 'induced drag' and has a significant effect on vehicle deceleration [64].

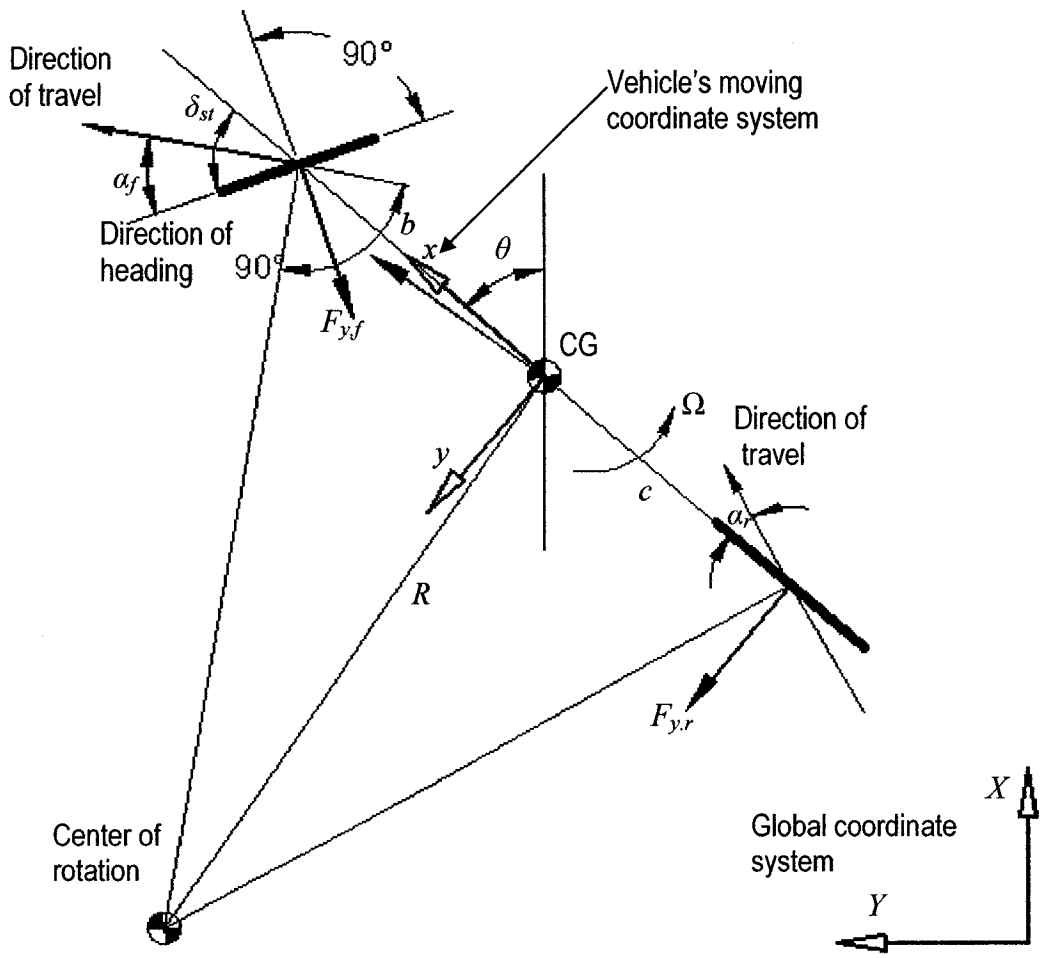

Figure 2.3: Direction of lateral forces acting on the bicycle model

Thus, though there is no braking or tractive effort, there is an opposing force during turning. Hence, it is suggested to use all the three equations of motion, including the longitudinal equation, during turning maneuver. The negative work done by the induced drag and the self aligning moment causes loss in energy, and hence deceleration of the vehicle, which is further discussed later in this chapter.

The three equations of motion, namely, longitudinal, lateral and yaw, can now be easily expressed in the form [16]:

$$\begin{aligned} m a_x &= -F_{y,f} \sin(\delta_{st}) \\ m a_y &= F_{y,f} \cos(\delta_{st}) + F_{y,r} \\ I_z \dot{\Omega} &= b \cdot F_{y,f} \cos(\delta_{st}) - c \cdot F_{y,r} - M_f - M_r \end{aligned} \tag{2.8}$$

where a_x and a_y are longitudinal and lateral accelerations, respectively. In Equation (2.8) $F_{y,i}$ and M_i ($i = f, r$) represent tire lateral force and self aligning moment, respectively. The steer angle is represented by δ_{st} and it is assumed that there is no tractive or braking effort. The longitudinal and lateral acceleration can further be expressed as [23]:

$$\begin{aligned} a_x &= \dot{V}_x - \Omega \cdot V_y \\ a_y &= \dot{V}_y + \Omega \cdot V_x \end{aligned} \tag{2.9}$$

where V_x and V_y are the longitudinal and lateral velocities of the vehicle's CG, and Ω is the angular velocity. The models for steering angle as well as the tire lateral forces and moments are derived separately in the following subsections.

2.3.2 Steering Model

The gear ratio between steering wheel and the road wheels is taken as 1 and hence, the driver steering command is used as the front steering angle directly. The steering

command for a circular motion is given as a step input. The sharp ends of the input are smoothened using sinusoidal function as shown in Figure 2.4. As shown, the steering input δ_{st} is initiated at $t = 2$ sec, and reaches 0.1 rad (5.73°) at $t = 4$ sec, with a period of 2 sec.

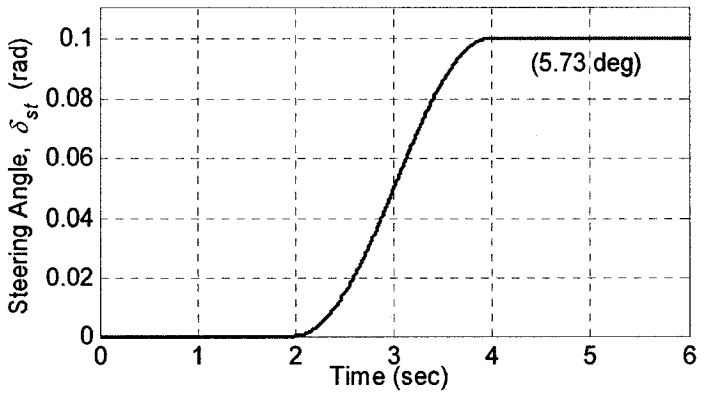

Figure 2.4: Steering input for the circular motion

The equation of the above steering command is given as follows:

$$\delta_{st} = \begin{cases} 0 \;\; ; \;\; 0 \le t < 2 \\ 0.05 \sin\left(\frac{\pi}{2} t - \frac{3\pi}{2}\right) + 0.05 \;\; ; \;\; 2 \le t \le 4 \\ 0.1 \;\; ; \;\; t > 4 \end{cases} \tag{2.10}$$

2.3.3 Slip-angle Model

The lateral force and self aligning moment developed at each tire are functions of slip-angle. The slip-angles for the front and rear tires can be calculated using the steering input and the direction of motion of the vehicle. Based on the vehicle longitudinal (V_x), lateral (V_y) and yaw (Ω) velocities, the slip-angles for the front and rear tires can be expressed as [16]:

$$\tan(\delta_{st} - \alpha_f) = \frac{V_y + \Omega \cdot b}{V_x} \quad \Rightarrow \alpha_f = \delta_{st} - \tan^{-1}\left(\frac{V_y + \Omega \cdot b}{V_x}\right)$$
$$\tan(\alpha_r) = \frac{\Omega \cdot c - V_y}{V_x} \quad \Rightarrow \alpha_r = \tan^{-1}\left(\frac{\Omega \cdot c - V_y}{V_x}\right) \tag{2.11}$$

Once the slip-angles are calculated, cornering forces and aligning moments acting on each axle can be calculated using linear tire model as:

$$F_{y,i} = 2C_{f,i} \cdot \alpha_i \; ; \; M_i = 2C_{m,i} \cdot \alpha_i, \quad (i = f, r) \tag{2.12}$$

2.4 Vehicle Handling Response

The above equations are combined together to create a Matlab-Simulink model and is run for 500 sec. The equations of motion represent the motion in vehicle local co-ordinate system. To find the response of the vehicle, a global co-ordinate system is required as shown in Figure 2.3. The relation between these two co-ordinate systems is given by [25]:

$$X(t) = \int_0^t \left(V_x \cos\theta - V_y \sin\theta\right) \cdot dt$$
$$Y(t) = \int_0^t \left(V_y \cos\theta + V_x \sin\theta\right) \cdot dt \tag{2.13}$$

where X and Y are the global co-ordinates and θ is the yaw angle.

The trajectory of the vehicle in global co-ordinate system obtained from above relation is shown in Figure 2.5 for a simulation carried out with step steering input and forward speed of 15 m/s for 500 sec. The vehicle parameters were presented in Table 2.2 for which the vehicle's understeer coefficient was found to be 0.35°.

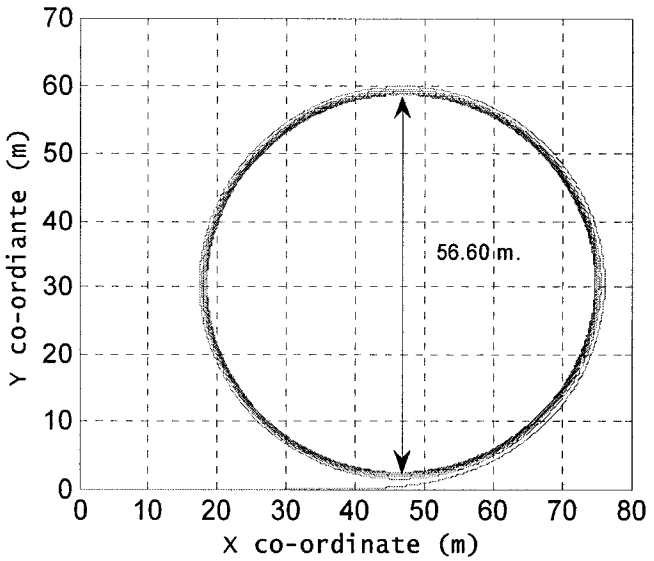

Figure 2.5: Vehicle trajectory for step steering input (bicycle model)

Figure 2.5 shows a band of vehicle trajectory with decreasing radius of curvature which is shown in Figure 2.6. From Figure 2.6 it is clearly noticed that the steady-state is not reached even after a long time. This can be attributed to the fact that the longitudinal velocity of the vehicle reduces with time due to the longitudinal component of the cornering force. The longitudinal velocity time history for the simulation is shown in Figure 2.7(a). As the results show, the velocity from its initial value of 15 m/s reduces significantly with time as the vehicle enters a curved path. This reduction is present even though there is no resistance due to rolling or air drag and is purely due to the energy loss in cornering. This reduction in speed leads to reduced radius of curvature for a fixed steering angle, since the vehicle simulated is understeer in nature. However, the radius of curvature R, is bounded by a lower limit of 28 m [$R = L/\tan(\delta_{st})$] and in 500 sec reaches a value of 28.3 m as can be seen from Figure 2.6. This value is with in 1% limit of the steady state value and the vehicle can be assumed to have reached steady state at this time. Hence other state parameters, such as velocities and forces would also be considered to have reached steady state at time $t = 500$ sec.

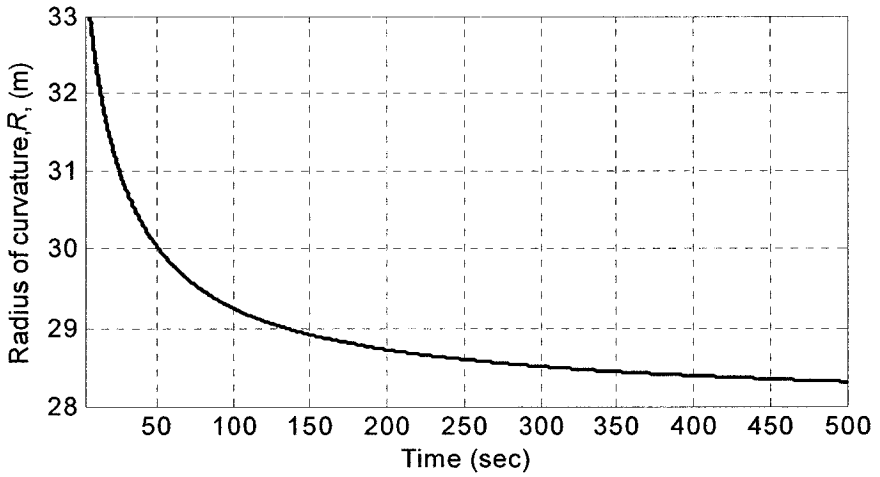

Figure 2.6: Radius of curvature for circular path (bicycle model)

The corresponding longitudinal acceleration is presented in Figure 2.7(b). From Figure 2.7 it is also evident that the rate of change of forward velocity diminishes after a long time. The lateral velocity and corresponding acceleration of the vehicle's CG are presented in Figures 2.7(c) and 2.7(d), respectively. The steady-state values for these two responses are 0.20 m/s and 0.00 m/s^2, respectively. Figures 2.7(e) and 2.7(f) show the yaw-rate and respective acceleration. The effect of continuously decreasing forward velocity can be seen in the yaw-rate response as the yaw-rate decreases with time and reaches a steady-state value of 0.1465 rad/s after 500 sec. The corresponding value of yaw acceleration is 0.00 rad/s^2.

Further, tire slip-angles, lateral forces and self-aligning moments are plotted in Figures 2.8 and 2.9. The slip-angles increase as the vehicle is steered during 2-4 sec and decrease thereafter due to vehicle deceleration. Though both tires on each axle are combined to form the bicycle model, slip-angles represent the average slip-angle of both tires on each axle, while the lateral forces and self-aligning moments are the total force and moment generated at each axle.

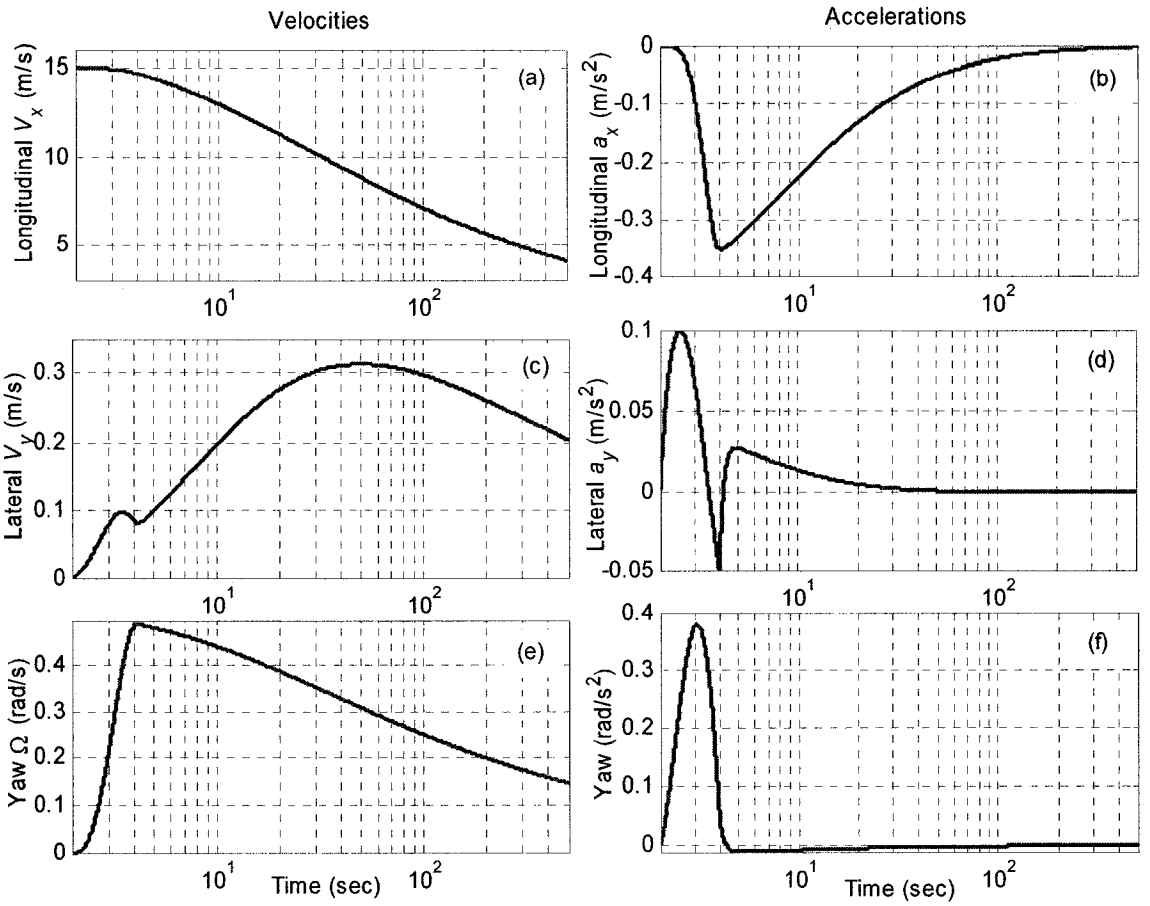

Figure 2.7: Velocities and accelerations for circular motion (bicycle model)

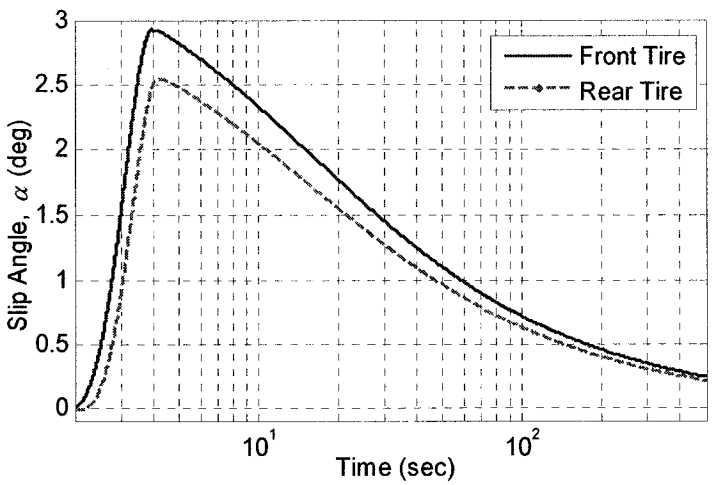

Figure 2.8: Slip-angles for circular motion (bicycle model)

This is consistent with the steady-state analysis since the vehicle CG is closer to the front axle (b = 1.3 m, c = 1.5 m) and the lateral forces are proportional to the weight on each axle, and self-aligning moments are result of the lateral forces [16].

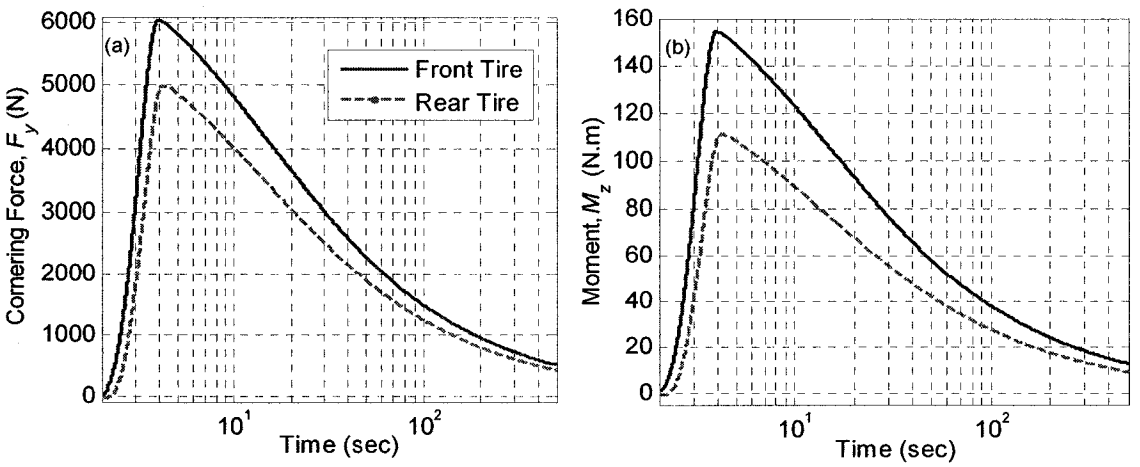

Figure 2.9: Lateral forces and aligning moments for circular motion (bicycle model)

2.5 Comparison between Transient & Steady State Models

It is observed that when the vehicle is traversing a curve, the velocity decreases continuously with time and never reaches steady-state. Hence, a comparison between the steady state and transient models can be done only under some common conditions. Such a common condition is the steady radius of curvature reached in the transient model. This condition is reached around 500 sec as seen in Figure 2.6. At t = 500 sec, the forward velocity is 4.1m/s as shown in Figure 2.7(a). This value is used for validation of the transient model with steady-state model. A comparison of selected performance measures obtained from two models is presented in Table 2.3.

Table 2.3: Comparison of transient bicycle model with steady state model

Performance Parameter	**Steady state**	**Transient Bicycle**
Yaw velocity, Ω	0.1459 rad/s	0.1465 rad/s
Radius of curvature, R	28.1 m	28.3 m
Lateral Acceleration, a_y	0.60 m/s^2	0.59 m/ s^2

It should be noted that the lateral acceleration presented in Table 2.3 is the centripetal acceleration of the vehicle as defined by the Equation (2.7) and can be represented as V^2/R for the transient response (V = 4.1 m/s, R = 28.3 m). The parameters follow the expected trend when compared with steady-state values. In view of incorporating linear tire model and neglecting the lateral load shift, the bicycle model has limited scope in vehicle dynamics studies. This model, however, helps in understanding the general behavior of the vehicle. The model developed in this section will be extended to include non-linearity and lateral load shift utilizing a 4-wheel system. Since, the change in longitudinal velocity in a transient model is attributed to the longitudinal component of the cornering force, it is interesting to examine and quantify the associated energy. The following section presents a closer look at the energy loss in a turning maneuver.

2.6 Loss of Energy in Turning Maneuver

As explained in section 2.3.1, the lateral forces acting on both tires oppose the motion in the form of an "induced drag". Similarly, the aligning moments also contribute to the negative work. The linear velocity for both tires is calculated using vehicle forward velocity and yaw velocity as:

$$\begin{aligned} V_f &= \sqrt{V_x^2 + \left(b \cdot \Omega + V_y\right)^2} \\ V_r &= \sqrt{V_x^2 + \left(c \cdot \Omega - V_y\right)^2} \end{aligned} \tag{2.14}$$

where, V_f and V_r are the front and rear tire velocities. The power loss due to the work done by the forces and moments is given as:

$$P = F_f \sin\left(\alpha_f\right) \cdot V_f + F_r \sin\left(\alpha_r\right) \cdot V_r + M_f \cdot \left(\Omega + \left(\dot{\delta}_{st} - \dot{\alpha}_f\right)\right) + M_r \cdot \left(\Omega - \dot{\alpha}_r\right) \tag{2.15}$$

which can be integrated to give the work done as:

$$W_d = \int_0^t P \cdot dt \tag{2.16}$$

The negative work causes loss in the kinetic energy of the vehicle. If V_o is the initial forward velocity of the vehicle, the total loss in kinetic energy at a given time can be calculated as:

$$\Delta E = \frac{1}{2}\left[m \cdot V_0^2 - \left\{ m \cdot \left(V_x^2 + V_y^2\right) + I_z \cdot \Omega^2 \right\}\right] \tag{2.17}$$

The negative work done and the loss in energy are calculated separately from Equations (2.16) and (2.17), respectively, and compared in Figure 2.10 as functions of time.

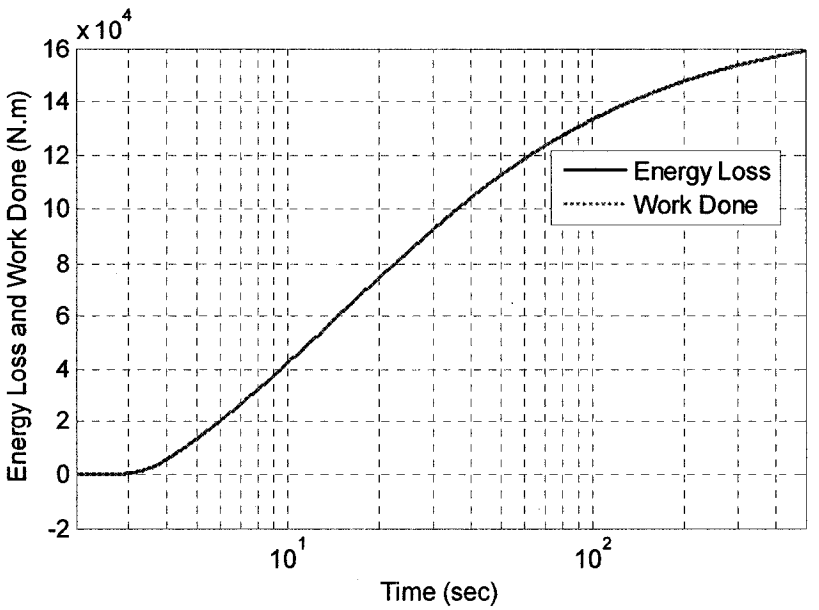

Figure 2.10: Energy loss and work done by external forces/moments

This energy loss can be attributed to the non-conservative component of the lateral force in Equation (2.8), $m a_x = -F_{y,f} \sin(\delta_{st})$. This can be explained as: when a side force acts on the wheel, the tire develops a slip-angle due to the deformation in its side walls as shown in Figure 2.1. The tire side wall is deformed from point 'a' to the maximum deformed shape at 'b', due to the tire-road contact forces. When this patch comes out of

the contact, the side wall regains its shape at 'c'. The work is done by the road contact force to deform the tire from 'a' to 'b' which is not re-gained when the tire comes back to the original shape. This hystersis in the tire accounts for the energy loss during turning. Similar explanation, relating the energy loss to the heat generated in tires is given in [118].

2.7 Summary

Steady-state and transient bicycle models have been formulated using the same physical parameters which will be used to formulate a 4-wheel handling model in the next chapter. Non-linear tire characteristics using Magic formula were analyzed. Linearized tire model was assumed for this section in order to compare the transient response with steady-state model. But as higher slip-angles are expected in active control, a non-linear tire model will be adopted later for 4-wheel model. The results from transient bicycle model are consistent with those from the steady state model. A bicycle model is good for analyzing the understeer nature of the vehicle and would be used later to realize given understeer characteristics of the vehicle. The transient model developed and studied in this section included the longitudinal DOF. The results show that in the absence of any tractive or braking effort, rolling resistance, and aerodynamic drag, the forward velocity decreases due to longitudinal component of tire lateral forces. Due to deceleration of the vehicle, it was found that significant time is required for the vehicle to reach a state when it can be compared with steady-state model. The deceleration of the vehicle was explained and the loss of energy during cornering was accounted for.

3 Four-Wheel Model

Bicycle model with linear tire characteristics for vehicle handling studies was developed in Chapter 2. Such a model is often used for its simplicity and closed form steady-state responses. The 2-wheel 3-DOF transient model developed in Chapter 2 demonstrates its effectiveness in predicting response to steering input. Many studies utilize such a model to investigate tire dynamics and active control. However, a bicycle model can not be used to study independent steering control and hence, a 4-wheel handling model must be developed. Prior to introducing the control, the model, however, can be validated against the one developed in Chapter 2.

The 4-wheel model developed in this chapter will include the provision to apply independent steering input to inner and outer wheels, lateral load shift and nonlinear tire characteristics. The model is compared for simple steering input by comparing responses with those presented in Chapter 2, and with responses from a commercial software "CarSim", utilizing same vehicle parameters.

3.1 Equations of Motion

As in the bicycle model developed in Chapter 2, the 4-wheel vehicle system is assigned lateral, longitudinal and yaw motions to describe handling response. For a steering input

δ_L and δ_R at the left and right wheel, respectively, the forces and moments developed at each tire-road contact patch are shown in Figure 3.1.

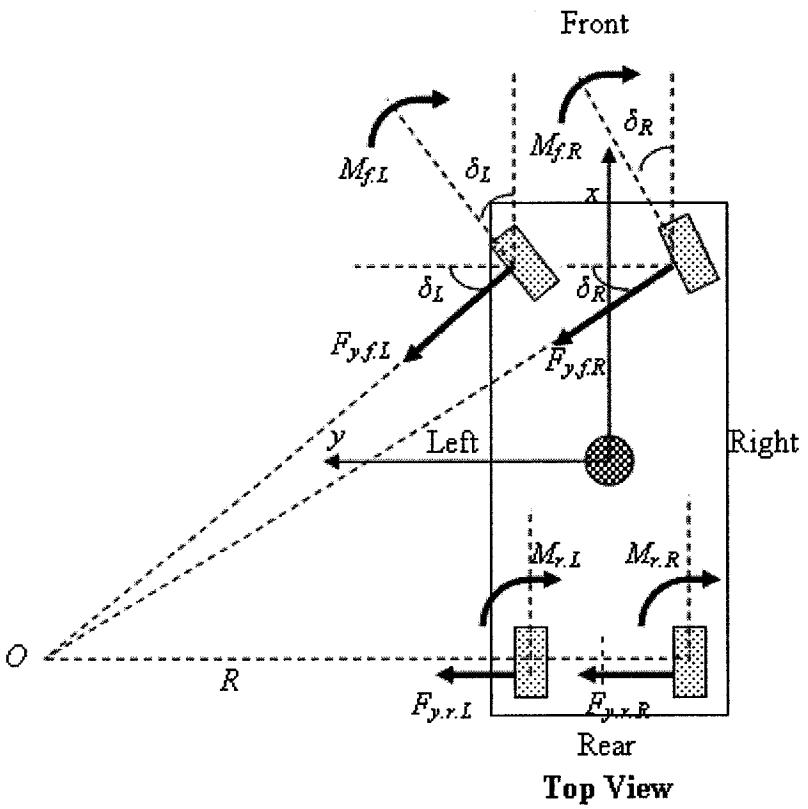

Figure 3.1: Forces and moments acting on the vehicle

The forces shown in Figure 3.1 are generated as a reaction to centrifugal force due to cornering, and are complex functions of normal load and slip-angle at each tire. In addition to the lateral force, each tire also develops self aligning moment which can also be established based on tire mechanics. In the absence of any longitudinal tire forces due to acceleration or braking, the longitudinal, lateral and yaw motions of the vehicle CG can be expressed as [21, 23, 25]:

$$m a_x = -\left[F_{y.f.R}\sin(\delta_R) + F_{y.f.L}\sin(\delta_L)\right]$$

$$m a_y = \left[F_{y.f.R}\cos(\delta_R) + F_{y.f.L}\cos(\delta_L)\right] + \left[F_{y.r.R} + F_{y.r.L}\right]$$

$$I_z \dot{\Omega} = -\left[\sum_1^4 M_i\right] + \left[F_{y.f.R}\left\{b\cos(\delta_R) - T_f \sin(\delta_R)\right\} + F_{y.f.L}\left\{b\cos(\delta_L) + T_f \sin(\delta_L)\right\}\right] - c\left[F_{y.r.R} + F_{y.r.L}\right] \tag{3.1}$$

where the longitudinal and lateral accelerations can be expressed as shown in Equation (2.9). The steer angles for the left and right front wheels in Equation (3.1) must be derived as a function of driver steering input. The Magic formula tire model presented in Chapter 2 is utilized to generate the tire forces and moments in Equation (3.1).

3.1.1 Steering Model

As discussed earlier, vehicle steering system is designed to minimize wheel scrub on a turn by providing different steer angles at the inner (left) and outer (right) wheels, such that all wheels will be in pure rolling. Such a geometry, known as Ackerman geometry based on pure rolling at low speeds, is shown in Figure 3.2. Defining radius of turn for rear axle centre as *R*, the steer angle for the right and left wheels can be expressed as:

$$\delta_R = \tan^{-1}\left(\frac{L}{R + T_f}\right)$$
$$\delta_L = \tan^{-1}\left(\frac{L}{R - T_f}\right) \tag{3.2}$$

The ratio between steer angle of left and right wheels can further be expressed in terms of vehicle wheel base and track width to yield:

$$\cot\delta_R - \cot\delta_L = \frac{2T_f}{L} \tag{3.3}$$

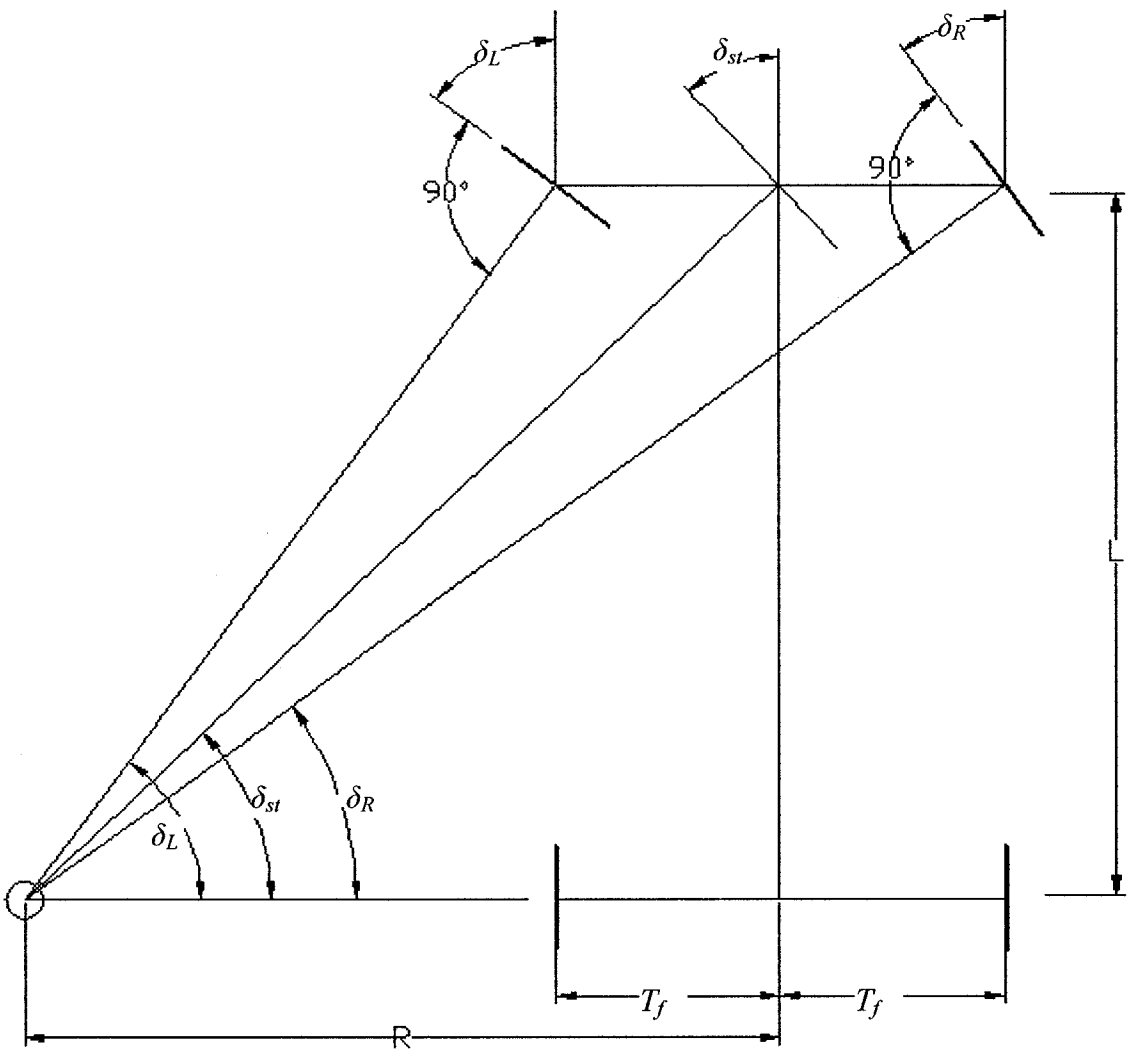

Figure 3.2: Ackerman geometry

Using above relation, the outer steering angle can be written in terms of the inner steering angle as

$$\delta_R = \cot^{-1}\left(K + \cot\delta_L\right) \tag{3.4}$$

where K is the ratio of the track width and the wheel base. The ideal steering geometry is simulated for different values of K and the results are shown in Figure 3.3. The results show that as the value of K increases, i.e. as the track width increases, the difference

between δ_L and δ_R increases. The steering angle for the inner and outer wheels would be derived using this ideal geometry for a given driver steering input.

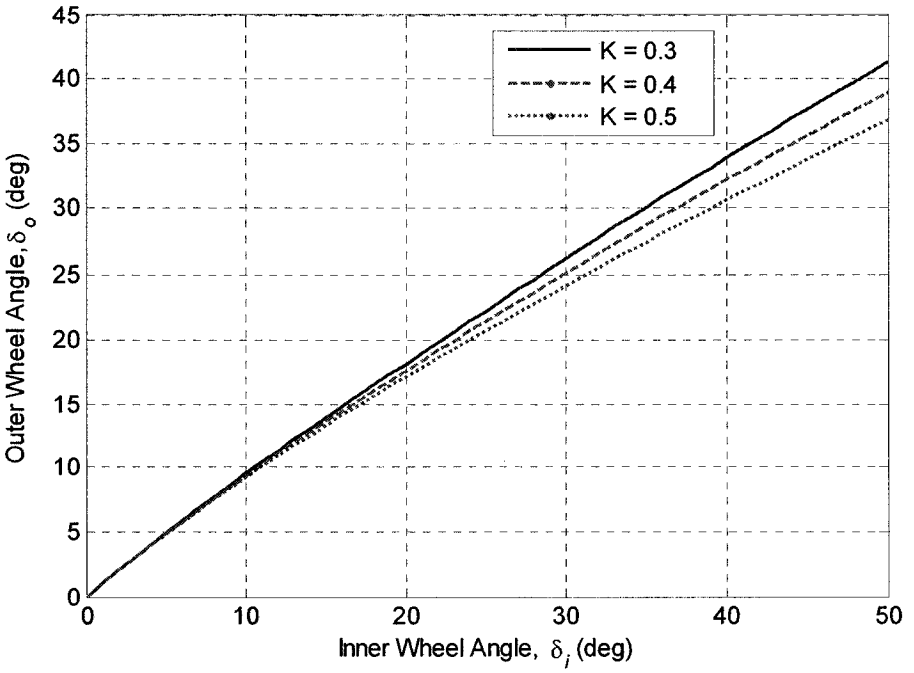

Figure 3.3: Ackerman steering relation for different K values

The average angle to be used as driver command can be taken as the angle required at mid front axle as shown in Figure 3.2:

$$\tan(\delta_{st}) = \frac{L}{R} \quad \text{or} \quad R = \frac{L}{\tan(\delta_{st})} \tag{3.5}$$

Substituting for R in Equation (3.2) the right and left steer angles as functions of δ_{st} are:

$$\delta_R = \tan^{-1}\left[\frac{\sin(\delta_{st})}{\cos(\delta_{st}) + \frac{T_f \sin(\delta_{st})}{L}}\right]; \quad \delta_L = \tan^{-1}\left[\frac{\sin(\delta_{st})}{\cos(\delta_{st}) - \frac{T_f \sin(\delta_{st})}{L}}\right] \tag{3.6}$$

The above equations are nonlinear and are not limited to small angles.

3.1.2 Tire Forces and Moments

The forces and moments generated at each tire shown in Figure 3.1 and Equation (3.1) are nonlinear functions of slip-angle and can be established using Magic formula. The Magic formula coefficients, as discussed, are dependent on the tire normal load. The tire normal load and slip-angle in turn are dependent on vehicle response.

The vehicle geometry and co-ordinate system used to establish tire vertical loads is shown in Figure 3.4. The position of the CG determines the load ratio on two axles. The acceleration of the vehicle in longitudinal direction (in traction or braking) causes a load shift between the front and the rear axles. Also, due to the lateral forces on the vehicle (during a turn, banking or due to wind gust) load shift takes place from the inner wheels to the outer wheels as illustrated in Figure 3.5. Since the vehicle is considered to be stable in vertical direction, i.e., bounce and pitch motion of the vehicle are neglected, the forces in vertical direction (z) can be established by taking sum of the forces along z, and sum of the moments about x and y axes.

The final expressions for vertical forces at each wheel as a function of longitudinal and lateral accelerations are [21, 23, 80]:

$$\begin{aligned}
&\text{Front, Right wheel}: \quad F_{z.f.R} = W_f - \frac{m a_x h_{cg}}{2L} + \frac{m a_y h_{cg} c}{2 T_f L} \\
&\text{Front, Left wheel}: \quad F_{z.f.L} = W_f - \frac{m a_x h_{cg}}{2L} - \frac{m a_y h_{cg} c}{2 T_f L} \\
&\text{Rear, Right wheel}: \quad F_{z.r.R} = W_r + \frac{m a_x h_{cg}}{2L} + \frac{m a_y h_{cg} b}{2 T_r L} \\
&\text{Rear, Left wheel}: \quad F_{z.r.L} = W_r + \frac{m a_x h_{cg}}{2L} - \frac{m a_y h_{cg} b}{2 T_r L}
\end{aligned} \tag{3.7}$$

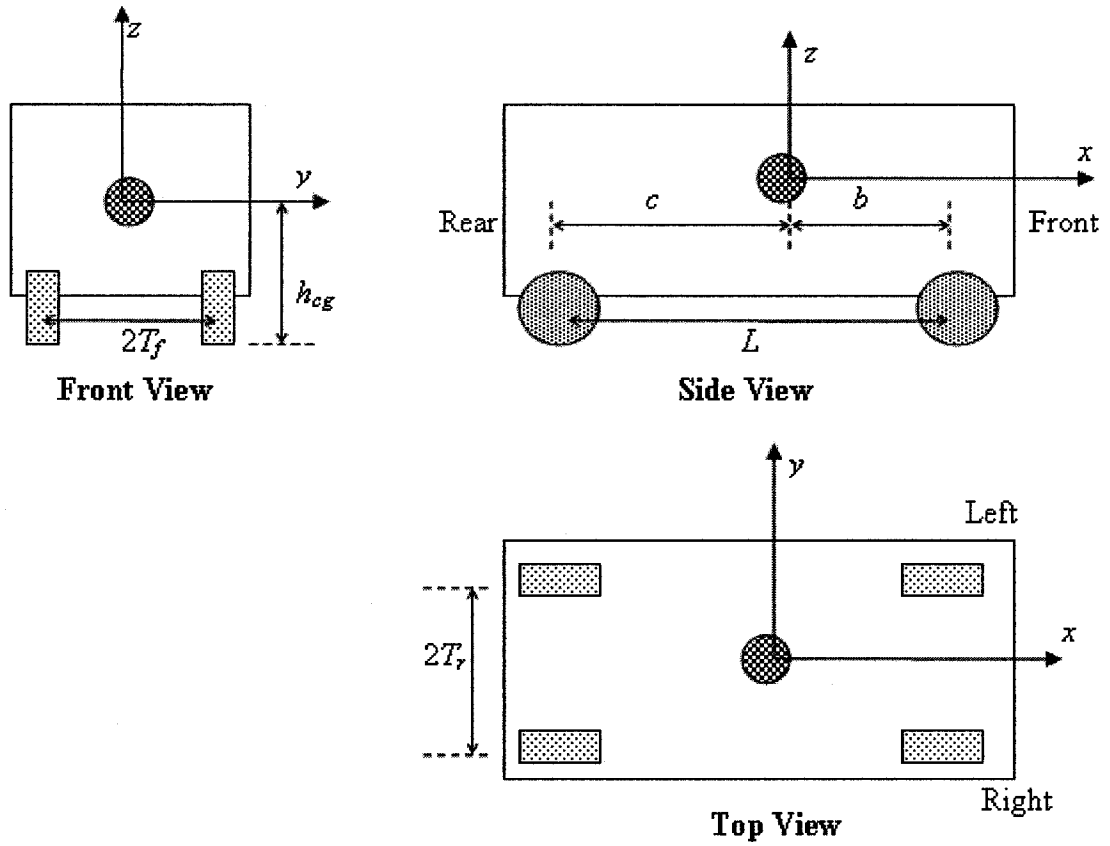

Figure 3.4: Vehicle co-ordinate axis system

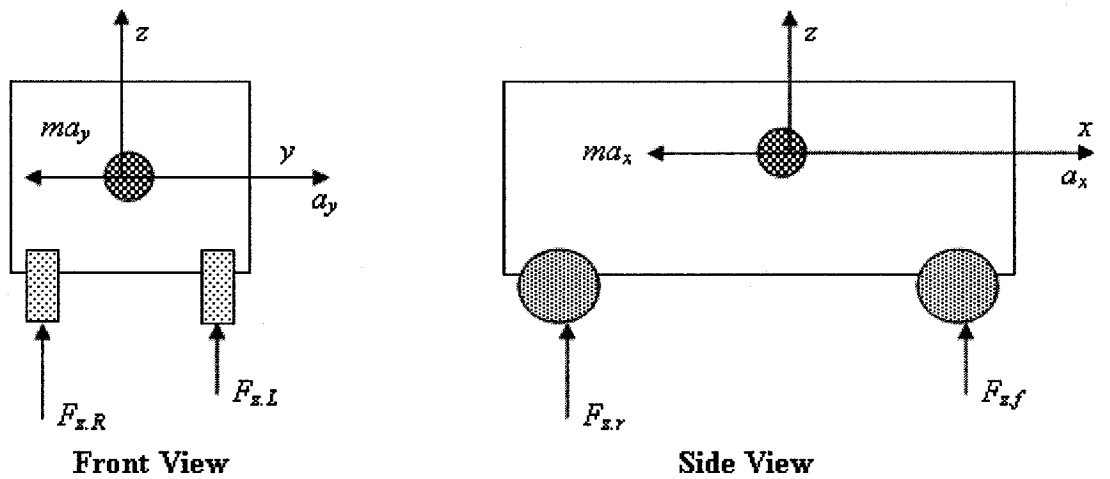

Figure 3.5: Longitudinal and lateral load shift

where, W_f and W_r are the static normal loads on *each* front and rear wheel. The required slip-angles at each tire can also be expressed in terms of vehicle responses (V_x, V_y, Ω).

Similar to Equation (2.11), the slip-angles for the 4-wheel system can be expressed as [23, 67, 76, 77]:

$$\alpha_{f\cdot R} = \delta_R - \tan^{-1}\left[\frac{b\cdot\Omega + V_y}{V_x + T_f\cdot\Omega}\right];\quad \alpha_{r\cdot R} = \tan^{-1}\left[\frac{c\cdot\Omega - V_y}{V_x + T_r\cdot\Omega}\right]$$
$$\alpha_{f\cdot L} = \delta_L - \tan^{-1}\left[\frac{b\cdot\Omega + V_y}{V_x - T_f\cdot\Omega}\right];\quad \alpha_{r\cdot L} = \tan^{-1}\left[\frac{c\cdot\Omega - V_y}{V_x - T_r\cdot\Omega}\right] \tag{3.8}$$

For a computed vertical load on a given tire and its slip-angle, the Magic formula is used to establish the tire forces. Due to the interdependence of these models, it is necessary to formulate a closed loop simulation scheme. For this, Matlab-Simulink is selected and the simulation steps are shown in Figure 3.6.

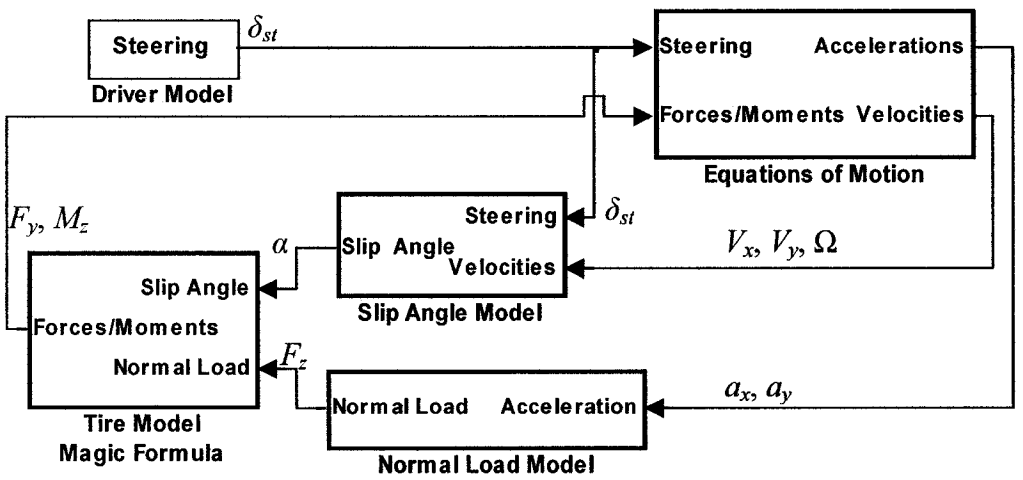

Figure 3.6: 4-Wheel vehicle Simulink model

The simulated results can now be readily compared with those derived in Chapter 2. For further validation of the results, a comparable model is also developed using CarSim.

3.2 CarSim Model

'CarSim Educational' edition 4.51, a vehicle dynamics simulation software from Mechanical Simulation Corporation (USA), is used for the verification of the Matlab model. Although, CarSim is not a precise tool for vehicle design purposes, it has been established as a robust tool for vehicle dynamics studies in auto industry. Vehicle parameters and tire properties along with different simulation conditions (braking/ throttle/steering input etc) can easily be defined in CarSim and hence, it proves to be an excellent means for validation purposes. The vehicle properties and simulation parameters for CarSim model are developed using comparable vehicle parameters.

The tire stiffness in CarSim is defined as the function of the normal load. For this purpose the Magic formula is used to find the stiffness values for variable load. The initial slope of the curve is used as the stiffness. These values are used to generate the stiffness characteristics of the tire model in CarSim as shown in Figure 3.7.

CarSim also supports the conventional control strategies and provides a platform for running tests such as constant radius, constant speed, constant steering input etc. It also provides the flexibility of changing design parameters such as camber, toe-in/out, suspension properties, tire model etc. A CarSim model can be integrated with Simulink to develop conventional control strategies. Despite all these facilities CarSim still does not provide the freedom to design a new variable-ratio steering mechanism, which limits its use to only verification purposes for uncontrolled vehicles or for comparison of active control with conventional control strategies. This justifies the development of the 4-wheel Matlab model.

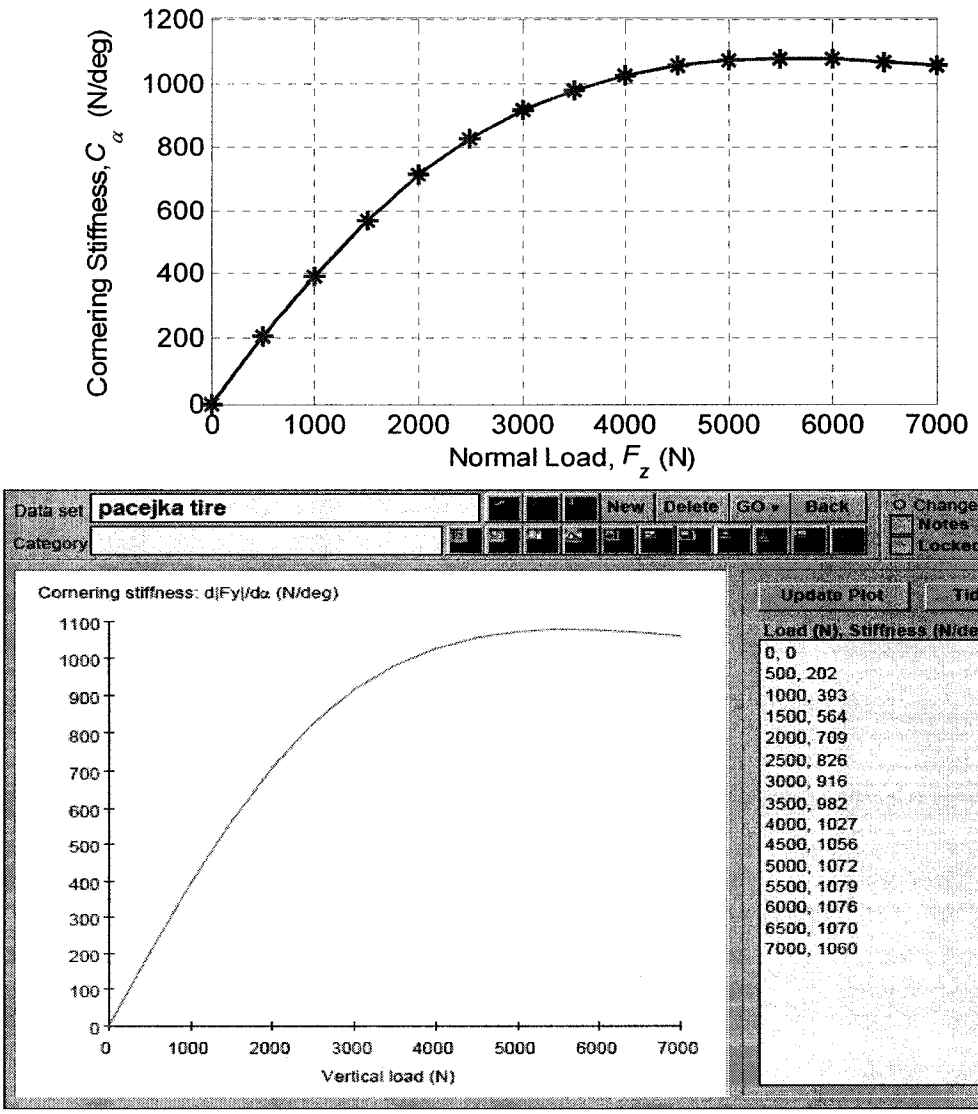

Figure 3.7: Cornering stiffness as a function of normal load; Matlab, CarSim

3.3 Simulation and Validation

Equations formulated in Section 3.1 are solved simultaneously using a Simulink program. The simulation process is shown in a flow chart in Figure 3.6. Driver command is given as input to the system. The output variables are displacement, velocity, acceleration, normal loads, lateral forces, self aligning moments, and slip-angles. Driver command for circular motion is chosen as a step input. Equation (2.10) with Equation (3.6) is used to

generate the driver input and outputs at both front wheels for circular motion as shown in Figure 3.8. The global trajectory can be derived from the body fixed co-ordinates as explained earlier in Equation 2.13.

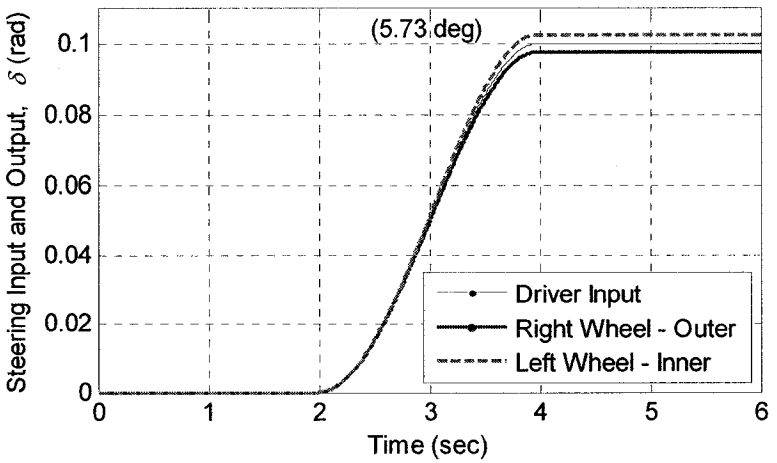

Figure 3.8: Steering input for circular motion

The vehicle parameters used for the simulation are same as those used for the simulation in Chapter 2. These parameters for the 4-wheel model are presented in Table 3.1. The initial velocity of the vehicle is 15 m/s (54 km/h). Since the vehicle slows down continuously in case of the circular motion, no steady state can be reached. Thus, the results at 500 sec when the radius of curvature reaches a steady state value are taken for the comparison with steady state bicycle model. The comparison of 4-wheel model with steady state and transient results of the bicycle model is shown in Table 3.2.

The transient results for other state and performance parameters such as displacement, velocity, acceleration, normal load, slip-angle, lateral force and self aligning moments are verified with the CarSim simulation for 25 sec.

Table 3.1: Physical parameters for 4-wheel model

Mass of the vehicle, m	1530 Kg
Centroidal moment of inertia about z axis, I_{zz}	3500 Kg.m^2
Wheel base, L	2.8 m
Distance of CG from front axle, b	1.3 m
Distance of CG from rear axle, c	1.5 m
Height of CG from ground, h_{cg}	0.4 m
Half Track Width - front axle, T_f	0.7 m
Half Track Width - rear axle, T_r	0.7 m

Table 3.2: Comparison of 4-wheel model

At 4.1 m/s forward velocity	**Transient analysis 4-wheel model**	**Steady state analysis- bicycle model**	**Transient analysis- bicycle model**
Yaw Velocity, Ω , rad/s	0.1459	0.1459	0.1465
Lateral Acceleration, a_y, m/s^2	0.60	0.60	0.59
Radius of Curvature, R, m	28.10	28.11	28.30

The effect of understeer drive is clearly seen on the vehicle trajectory as shown in Figure 3.9. The radius of the path decreases with the decrease in velocity. Due to negative longitudinal acceleration shown in Figure 3.10(b), the longitudinal velocity of the vehicle decreases continuously (Figure 3.10(a)). This trend matches with the transient bicycle model response in Figure 2.7. Steep rise in the lateral acceleration as the vehicle enters the turn and gradual decrease thereafter due to vehicle deceleration can be seen in Figure 3.11(b).

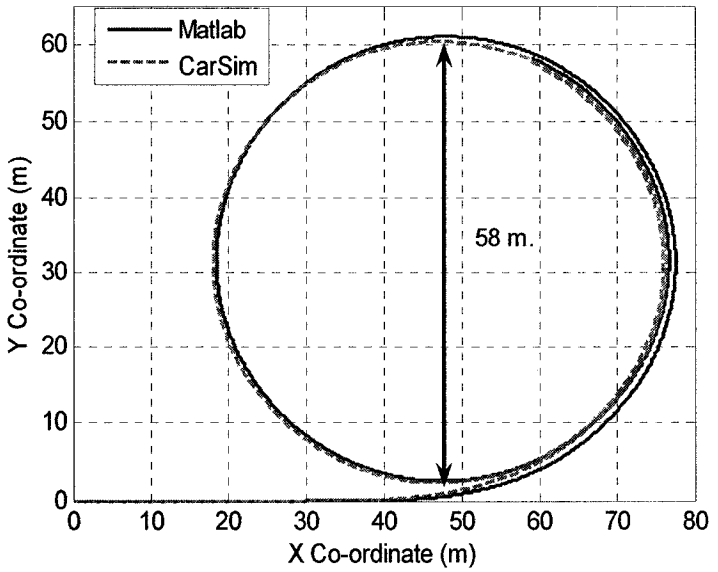

Figure 3.9: Vehicle path for circular motion

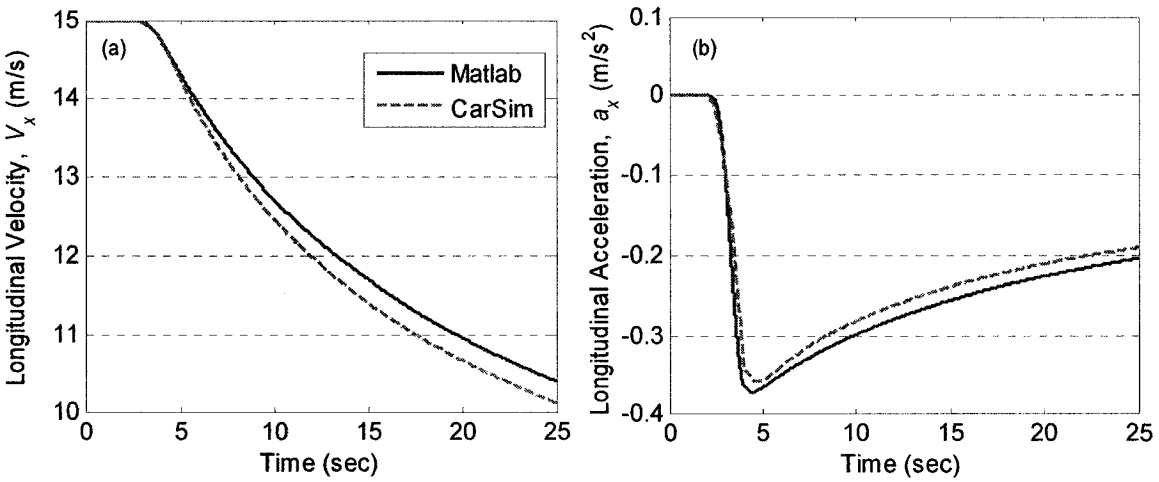

Figure 3.10: Longitudinal velocity and acceleration for circular motion

Similar trends are seen in the vehicle yaw response in Figure 3.12. From the transient vehicle response results, it is clear that the proposed 4-wheel model not only follows similar trend as of the simpler bicycle model, but it also matches well with the CarSim simulations. Vehicle response in terms of forces and moments are plotted further.

Figure 3.13 shows the effect of normal load shift in roll. Both tires on each axle start with equal normal loads, 4020 N on each front and 3480 N on each rear tire. As the vehicle enters the turn, the lateral acceleration causes a load shift from inner, i.e., left

wheel to the outer, i.e., right wheel. The normal load on each tire when maximum load shift takes place is found to be: $F_{z,f,R}$ = 5660 N, $F_{z,f,L}$ = 2460 N, $F_{z,r,R}$ = 4825 N, and $F_{z,r,L}$ = 2055 N. These results show that, the total load on the front axle increases from 8040 N to 8120 N and total load on rear axle decreases from an initial value of 6960 N to 6880 N, due to the longitudinal deceleration of the vehicle.

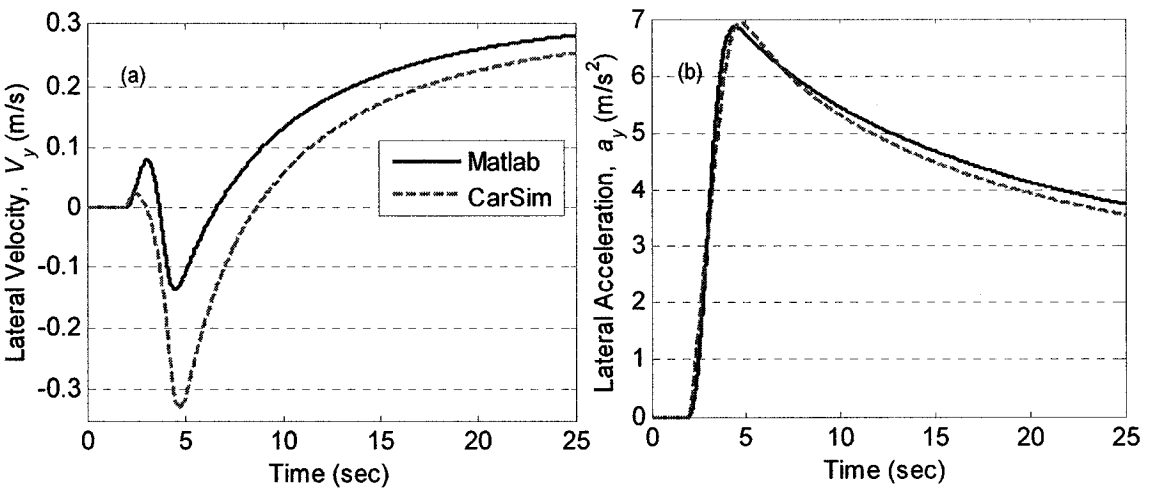

Figure 3.11: Lateral acceleration for circular motion

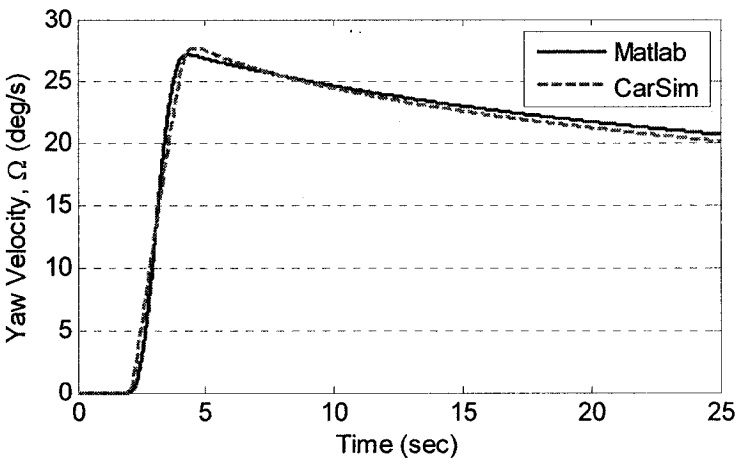

Figure 3.12: Yaw velocity for circular motion

Considering only lateral load shift, a significant normal load of 1600 N on the front axle and 1405 N on the rear axle takes place from left to right wheels, which is approximately 40% of the load on respective wheels. This load shift affects the lateral force generating

ability of the tires as stated by the Magic formula. The slip angles for both tires on each axle are approximately same as shown in Figure 3.14, but the lateral forces generated from both right tires are significantly higher than the left tires as shown in Figure 3.15. Higher lateral forces on right tires cause higher self aligning moments as shown in Figure 3.16.

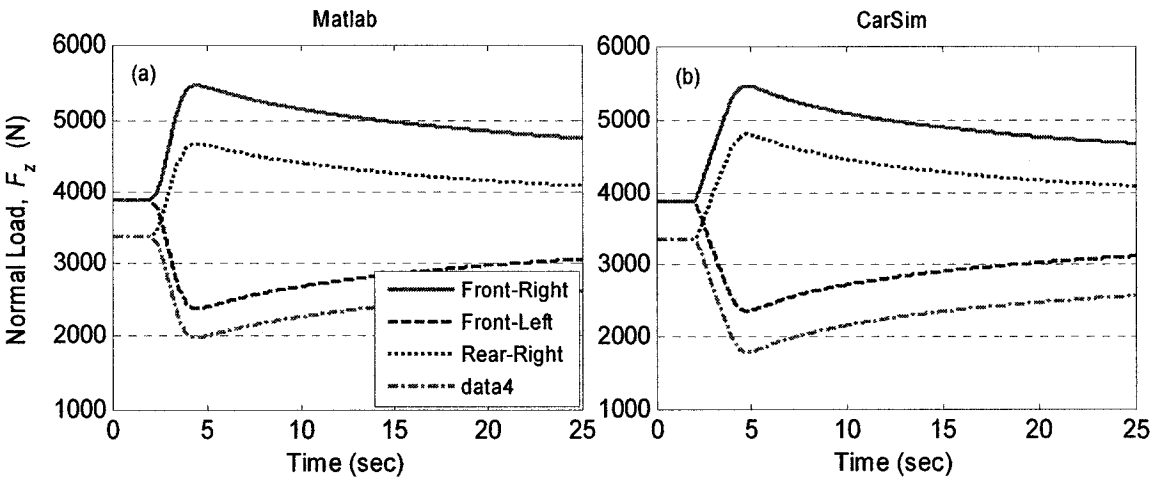

Figure 3.13: Normal load variation for circular motion

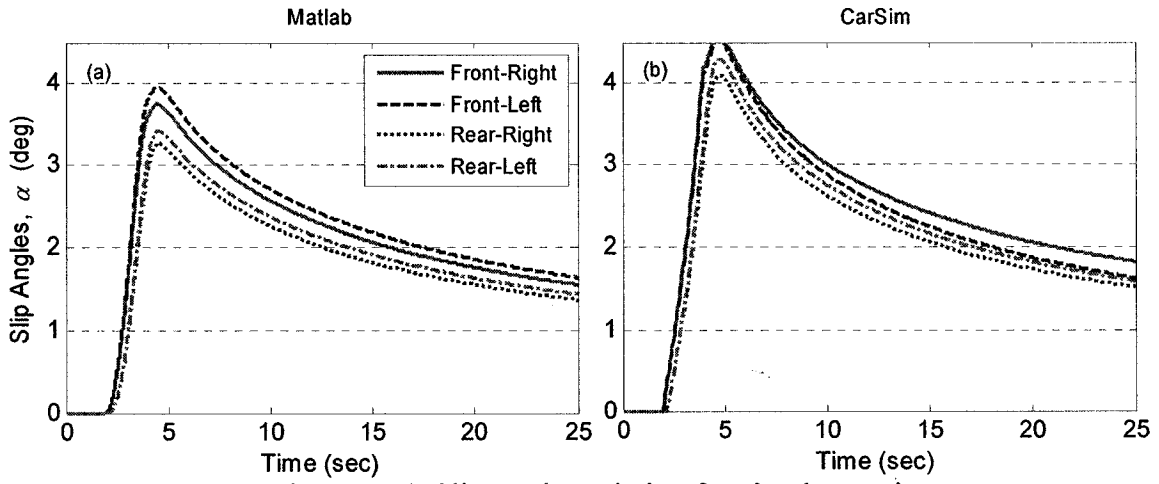

Figure 3.14: Slip-angle variation for circular motion

The CarSim model considers both, sprung and un-sprung mass of the vehicle, while the Matlab model is based on a single lumped mass system. This accounts for small

differences in the normal loads, and hence lateral forces and self-aligning moments in two models.

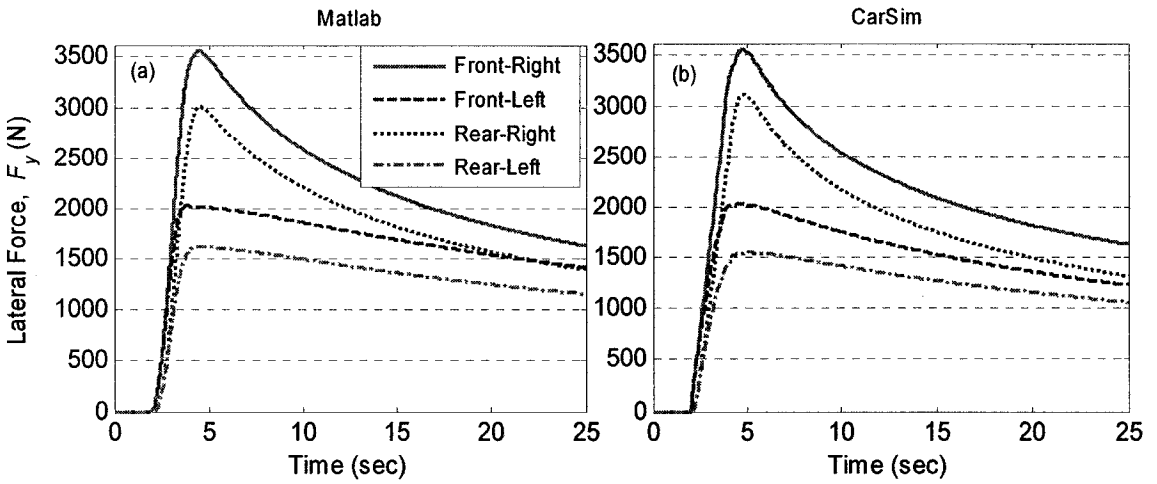

Figure 3.15: Cornering force variation for circular motion

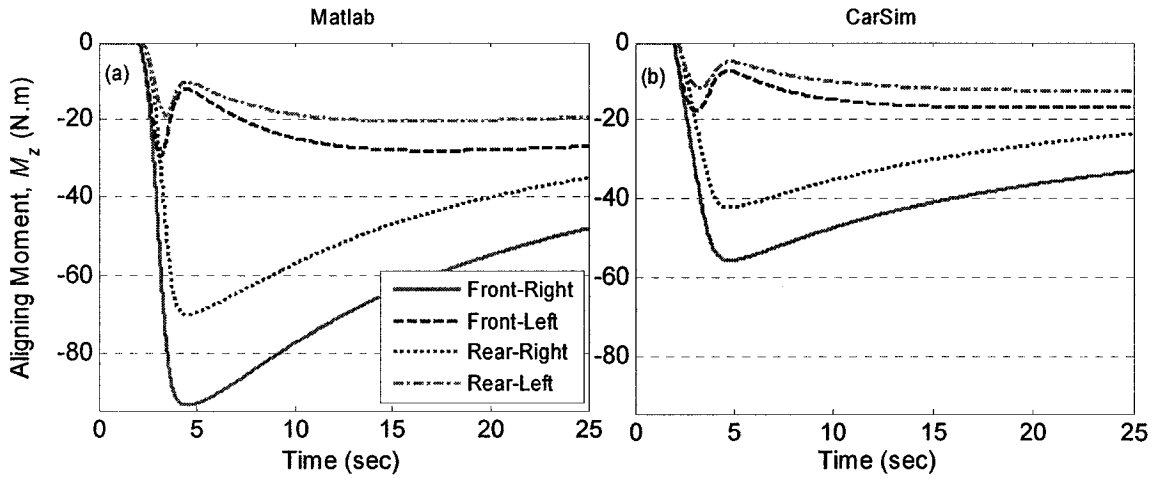

Figure 3.16: Self aligning moment variation for circular motion

3.4 Summary

For the circular motion the transient performance agrees well with the steady state bicycle model analysis. The vehicle follows the intended trajectory at lower speeds, but at higher speeds, the understeer characteristics come into picture, as the path radius increases with higher velocity. The significance of roll-load shift is seen clearly in the

normal load response (Figure 3.13) where both right tires (outer) have significantly higher loads than left tires (inner); though the difference decreases as the vehicle slows down. To calculate lateral forces and moments on the tires, Magic formula was incorporated which shows the effect of both, the slip-angle and normal load. Though the slip-angles at left tires (inner) are slightly greater (Figure 3.14), the higher normal loads on right tires account for higher lateral forces and moments (Figures 3.15, 3.16). This phenomenon will be used to generate higher lateral forces from outer tires later in the study. The analysis is not constrained to small angles and can be used for a wide range of input parameters. The response of the vehicle follows the expected trend when compared with CarSim model.

It is also observed that the effective tire stiffness for the 4-wheel model is less than that assumed in linear bicycle model, which results in higher slip-angles. This is a result of load shift and non-linear nature of the tire stiffness as a function of normal load. A bicycle model may thus overestimate the vehicle's ability to negotiate turns.

4 Development of AIFS Control Strategy

4.1 Introduction

A 4-wheel vehicle handling model developed in Chapter 3 was compared with steady-state and transient bicycle models. Although, bicycle model has been shown to be effective and widely used for handling analysis, it has severe limitation for this investigation as it neglects the effect of load shift and can not incorporate independent steering angle input. The 4-wheel vehicle model developed is capable of simulating handling responses which include tire nonlinearity, effect of lateral and longitudinal load shift and most importantly independent steering input to the left and right wheels.

The main objective of this chapter is to explore and develop a control strategy for independent steering input in order to improve handling performance. For this, it is first necessary to examine the forces that are developed at each tire-road interface and understand the existing control strategies. The 4-wheel model is utilized to simulate the responses with conventional steering as well as with existing active control strategy. The results are critically examined and shortcomings are identified. Based on the results in terms of ability of tires to generate forces during a handling maneuver, it is established that the concept of anti-Ackerman steering ratio can improve the handling by utilizing the available tire work-load. An adaptive front steering control strategy is then finally proposed in this chapter to adopt a differential front steering ratio based on a selected

response performance and vehicle handling characteristic. The vehicle's handling performance with the proposed control strategy is explored in the next chapter.

4.2 Longitudinal Vs. Lateral Force Control

One of the main focuses in current automotive research is vehicle chassis control which includes handling performance, ride quality improvement, and traction/braking performance. One such focus is on the handling performance via active front steering control. An extensive review of literature in the area presented in Chapter 1, showed that there are primarily two methods for control of tire-road interaction forces that are explored for the improvement of the handling performance. One deals with longitudinal force control in traction or braking and is the basis of ABS, DYC and TCS. On the other hand, AFS, ARS and 4WS systems are based on the control of lateral forces developed by the tires.

Both these methods utilize the friction force between the tire and the road. It has been shown that a combination of both methods is required for an ideal control. However, the cost, complexity and practicality play an important role in deciding which strategy to be used.

For pneumatic tire, it is well known that the lateral force that can be developed for a given slip-angle is dependent on whether any longitudinal force is also developed or not. The force developed by pneumatic tire in the x-y (longitudinal-lateral) plane represented by available friction in each direction can be represented by a friction ellipse as shown in Figure 4.1 [16, 67, 119].

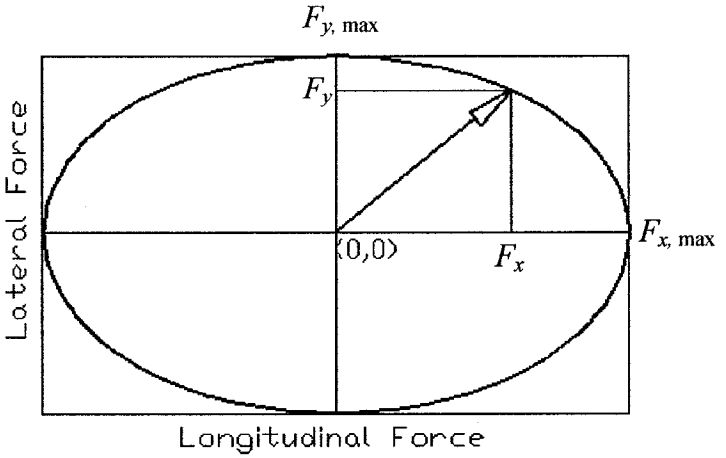

Figure 4.1: Friction ellipse for longitudinal and lateral tire forces

As seen in the above figure, the maximum lateral (y-axis) or longitudinal (x-axis) force is achieved only in the absence of the other force. For a combined longitudinal and lateral slip, the total available friction force has components in two directions. Also, the higher value of maximum longitudinal force shows that the lateral force saturates much faster than the longitudinal and hence, lateral force can not be used in extreme cases, such as wheel lockups.

For the purpose of introducing active control of vehicle yaw, it is easy to show that the lateral tire force, if introduced, can provide larger net counter moment than a longitudinal force alone. It can be visualized easily by the two control strategies presented in Figure 4.2 [17], where forces are generated only at the front tires to produce a counter-clockwise yaw-moment. As the figure shows, a longitudinal tire force $F_{\max}$ developed by introducing braking of the left wheel introduces a net moment of $F_{\max} \cdot T$. Whereas, if same lateral force is developed at each front tire (Figure 4.2, right), assuming $F_{y.\max} = F_{x.\max}$, a net moment of $2 \cdot F_{\max} \cdot 2T$ is realized.

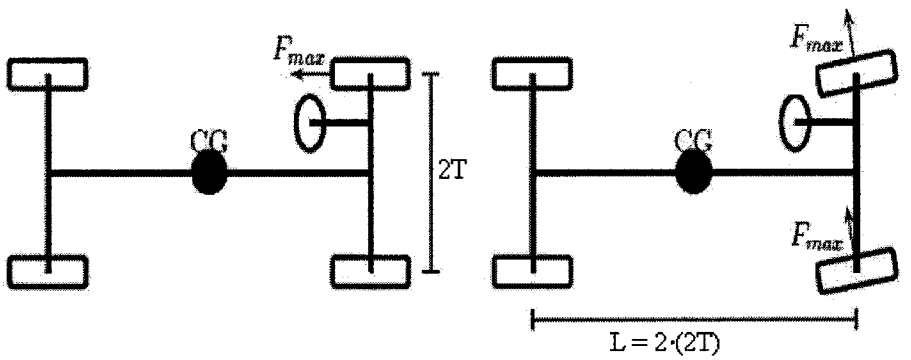

Figure 4.2: Maximum moment generated in front wheel braking and steering [17]

This shows that AFS utilizing lateral tire force can produce up to 4 times the stabilizing moment compared to active braking control or longitudinal tire force used in DYC. Even if active torque is implemented along with active braking in the first case (braking from left and traction from right tire), active steering would still generate twice the amount of moment.

Furthermore, in a split-μ case, the active steering can be shown as a very useful method to stabilize the vehicle, along with active braking. A typical split-μ case is shown in Figure 4.3, when there is a difference in friction coefficient between the right and left tires and the road. Both tires on right side experience a low friction surface and hence, can not generate enough force for traction/braking or cornering. In such a situation, if brakes are applied, the longitudinal force will be generated only on the left side, which will produce a net counter-clock-wise moment and hence, causes instability. Thus, active braking alone could prove to be dangerous in such cases. If active steering is implemented along with active braking, the lateral force from the front left tire can be used to generate a clock-wise moment, which would help in stabilizing the vehicle.

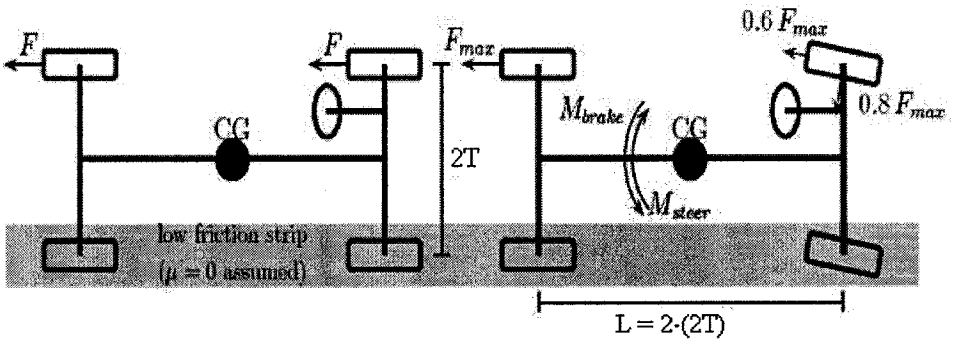

Figure 4.3: Effect of active steering control in split- μ condition [17]

In [81], it is further shown that the lateral force control can stabilize the vehicle in side wind-gust disturbance where longitudinal control fails. These arguments justify that given a choice, lateral control with active steering should be an integral part of any control system for improved handling and stability. Present investigation thus examines the potential of active steering control where the lateral forces developed at the left and right tires may be different. Vehicle behavior with conventional steering and conventional active front steering control is first thoroughly examined in the next section prior to establishing a control strategy.

4.3 Vehicle Behavior with Ackerman Steering - No Control

A theoretical steering mechanism based on Ackerman geometry is described in Section 3.1.1 and shown in Figure 3.2. Such a geometry is closely followed in road vehicles using a rack-pinion with 4-bar linkage mechanism. Ackerman geometry is necessary in road vehicles to avoid tire scrub at low speed turning [117]. The Ackerman geometry makes sure that all four wheels rotate about a common centre of rotation, thus avoiding unnecessary lateral scrub of the tires. However, as the speed increases slip-angles are generated in each tire as described in section 2.1. The slip-angles cause a shift in the centre of rotation as shown in Figure 4.4 [117].

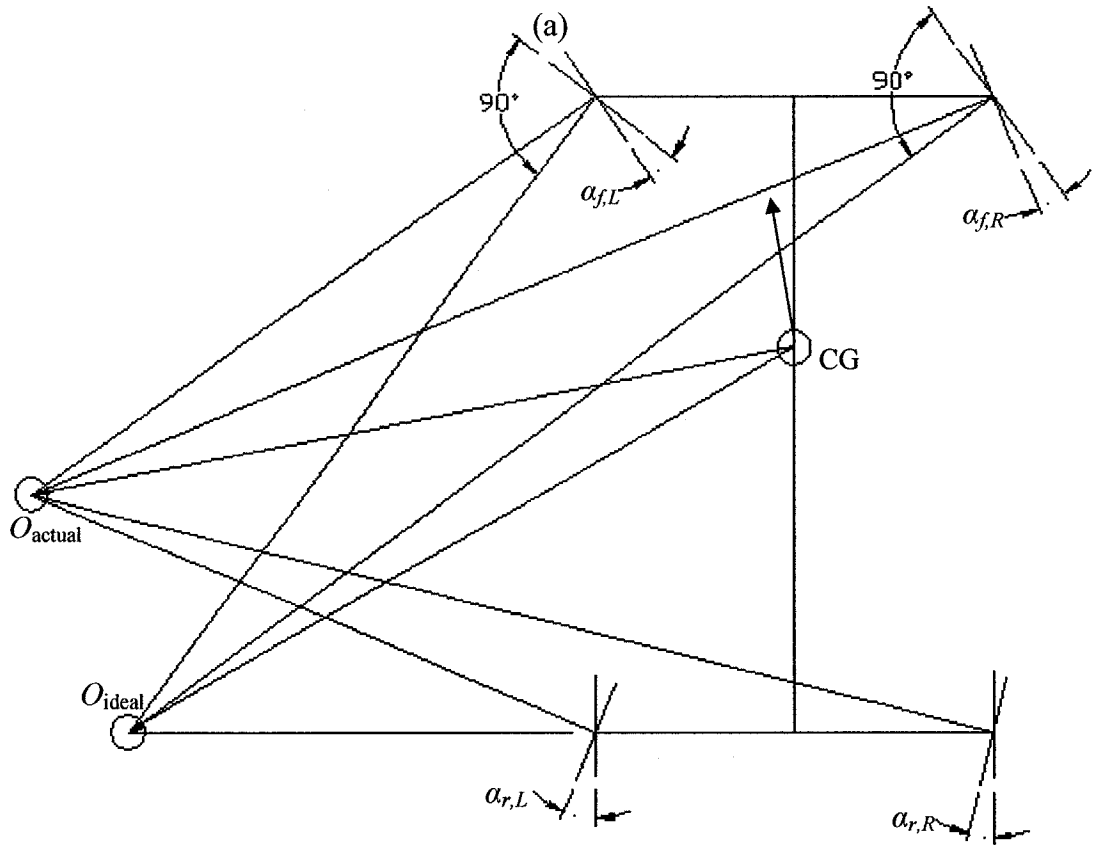

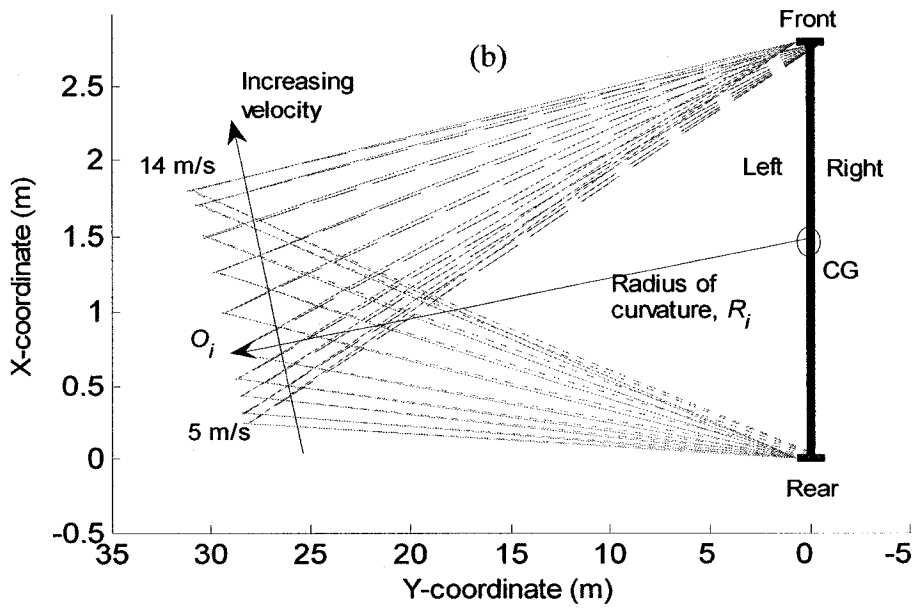

Figure 4.4: Position of centre of rotation
(a) Shift in centre of rotation due to slip-angle, (b) Centre of rotation position for different velocities

These results are obtained for candidate vehicle parameters presented in Table 3.1 by drawing perpendicular lines from each wheel's direction of motion. The centers of rotation are obtained for constant steering angle of 5.73°, as forward velocity is varied from 5 m/s to 14 m/s. The shift in the centre of rotation with increasing speed causes the vehicle to deviate from its desired path and yaw-rate. Depending on vehicle's handling characteristic, understeer or oversteer, the vehicle may follow a path of larger or smaller radius at high speed [16, 64]. Vehicles with different handling characteristics and different steering input are simulated in this section for an analysis of handling behavior.

4.3.1 Steering Input Command

A step steering input for circular motion was presented in Figure 3.8 in Section 3.3. Similar steering command is used for circular motion and another steering command with sinusoidal input for lane-change is developed in this section. For comparison purposes, vehicle's ideal path is required. It is assumed that the vehicle will follow the ideal path at close to zero forward velocity, since the slip-angles generated are nearly zero [119]. This ideal path can easily be established by simulating the vehicle response to a step steering input at low velocity. At higher velocity, however, the input period must be modified to obtain comparable response. A velocity dependent rounded step input is thus defined to generate vehicle's circular motion. A rounded step input function to reach 0.1 rad in 2 sec is selected for V = 15 m/s as:

$$\delta_{st} = \begin{cases} 0.05\sin\left(\frac{\pi}{2}t - \frac{\pi}{2}\right) + 0.05 & ; \quad 0 \le t \le 2 \\ 0.1 & ; \quad t > 2 \end{cases} \tag{4.1}$$

For an equivalent input at 1 m/s, the time period of the function is modified to yield:

$$\delta_{st} = \begin{Bmatrix} 0.05\sin\left(\frac{\pi}{30}t - \frac{\pi}{2}\right) + 0.05 & ; & 0 \le t \le 30 \\ 0.1 & ; & t > 30 \end{Bmatrix} \tag{4.2}$$

A time history plot of above input functions are presented in Figure 4.5.

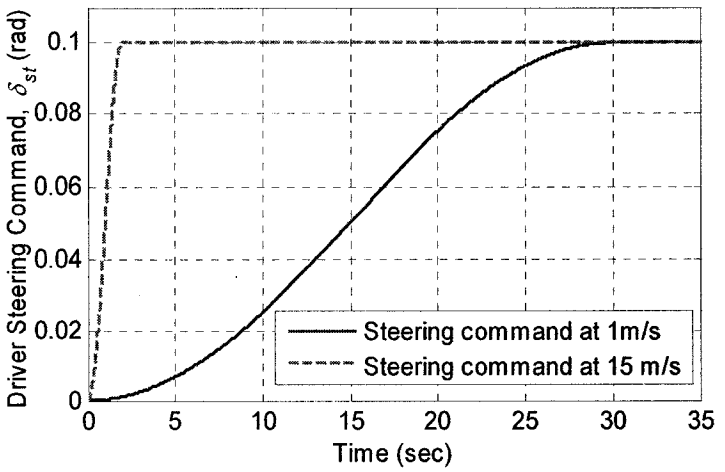

Figure 4.5: Steering input for ideal path for circular motion

A steering input for lane-change maneuver is modeled by a full period of a sine wave. The steering command for lane-change at 25 m/s forward velocity can be written as:

$$\delta_{st} = \begin{Bmatrix} 0.015\sin(t) & ; & 0 \le t \le 2\pi \\ 0 & ; & t > 2\pi \end{Bmatrix} \tag{4.3}$$

Again, an equivalent input at 1 m/s is obtained by changing the steering frequency to give:

$$\delta_{st} = \begin{Bmatrix} 0.015\sin\left(\frac{t}{25}\right) & ; & 0 \le t \le 50\pi \\ 0 & ; & t > 50\pi \end{Bmatrix} \tag{4.4}$$

The resulting time history of the steering input for lane-change at 1 m/s and 25 m/s are presented in Figure 4.6.

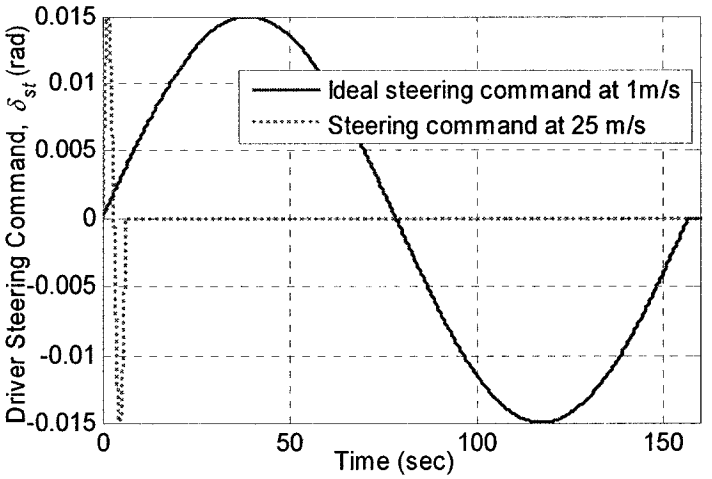

Figure 4.6: Steering input for ideal path for lane-change

The candidate vehicle with parameters presented in Table 3.1 is simulated for the above input. The parameters represent a vehicle with understeer characteristics as was established in Section 2.2. The characteristics can easily be changed to oversteer by modifying CG location. The following subsections present the circular motion and lane-change responses for both under and oversteer configurations of the vehicle.

4.3.2 Circular Motion - Understeer Vehicle

The 4-wheel vehicle system developed in Chapter 3 is used as the basic model for simulation in this section. The parameters in Table 3.1 with K_{us} = 0.35° represent an understeer vehicle. To examine possible parameters that can be used in control strategies, forward velocity is kept constant for all the simulations hereafter. For a given steering input at a given velocity, ideal radius of curvature and yaw-rate are taken as the reference response parameters. These reference values can be defined in terms of the steering angle, the forward velocity and the vehicle parameters as:

$$R_{ref} = \frac{L}{\tan(\delta_{st})}$$

$$\Omega_{ref} = \frac{V_x}{R_{ref}} = \frac{V_x \cdot \tan(\delta_{st})}{L} \tag{4.5}$$

where, R_{ref} is the ideal radius of curvature and Ω_{ref} is the ideal (reference) yaw-rate.

The circular motion is obtained from the *x-y* coordinates of CG at a constant forward velocity of 15 m/s and steering input as shown in Figure 4.5. The trajectory of the vehicle with understeer characteristics at low velocity (ideal path) is compared with that at 15 m/s in Figure 4.7(b).

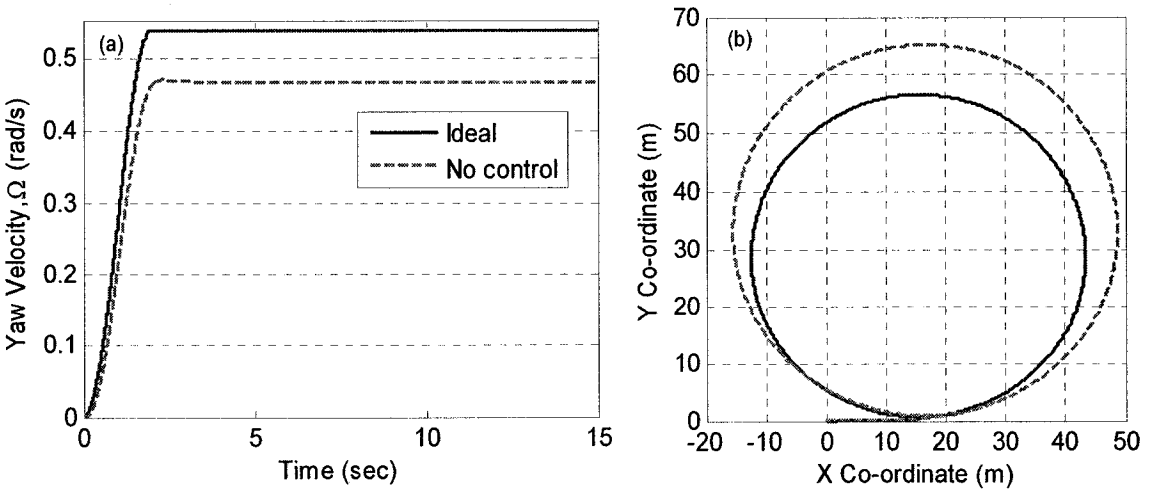

Figure 4.7: Yaw-rate and trajectory, understeer vehicle, no-control, circular motion

The results clearly show that the conventional Ackerman steering geometry will lead to deviation of trajectory with increasing velocity. Any attempt to conform to ideal path will require further driver-vehicle interaction.

The understeer vehicle generates higher slip-angles at the front tires compared to the rear and hence, follows a larger radius of curvature for the same steering input. With an increase in the radius of curvature, the yaw-rate of vehicle will reduce as the velocity increases. A comparison of resulting yaw-rate with that of reference yaw-rate (Equation

(4.5)) is presented in Figure 4.7(a). The results show that for an understeer vehicle, both transient and steady-state yaw-rate will be less than the reference yaw-rate for higher velocities.

The normal load experienced at each tire during the simulation is shown in Figure 4.8(a). The results show a very significant lateral load shift from the inner to the outer tires. The normal load on tires directly affects the lateral force generated at tires during the maneuver. Figure 4.8(b) shows the resulting lateral force at each tire for the circular motion at 15 m/s.

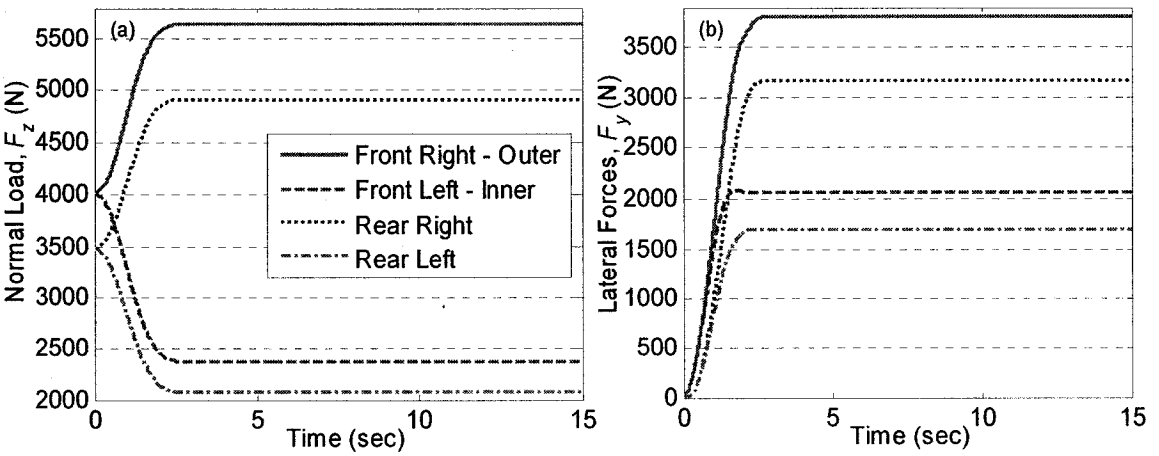

Figure 4.8: Normal and lateral forces, understeer vehicle, no-control, circular motion

4.3.3 Circular Motion - Oversteer Vehicle

The results presented in the previous section are for the candidate vehicle with understeer characteristics. The steering characteristics for the same vehicle can be modified to oversteer by moving the CG location closer to the rear axle. For this b = 1.7 m, c = 1.1 m. are used to establish the new characteristics. Using appropriate static tire load and cornering tire stiffness, the understeer coefficient (K_{us}) is established using Equation (2.4).

The new "understeer coefficient" for this model is found to be K_{us} = **-1.055°** (**-0.0184 rad**) resulting in oversteering. An oversteer vehicle is characterized by its *critical velocity*; a forward speed at which the vehicle will be unstable for any steering command [16]. This concept is valid only for a bicycle model and does not necessarily apply to a 4-wheel model. The critical velocity, V_{crit} for the new model is found to be:

$$V_{crit} = \sqrt{\frac{g.L}{-K_{us}}} = 38.6 \text{ m/s or } 139 \text{ km/h} \tag{4.6}$$

The oversteer vehicle tends to follow a smaller radius of curvature for a constant steering input with increasing speed due to higher slip-angles at rear tires. This results in higher yaw-rate when compared to the reference yaw-rate. The developed oversteer vehicle is simulated at 1 m/s and 15 m/s to obtain its response to rounded step inputs used in the previous section. Low speed trajectory considering as ideal path is compared with that at 15 m/s, and is presented in Figure 4.9(b).

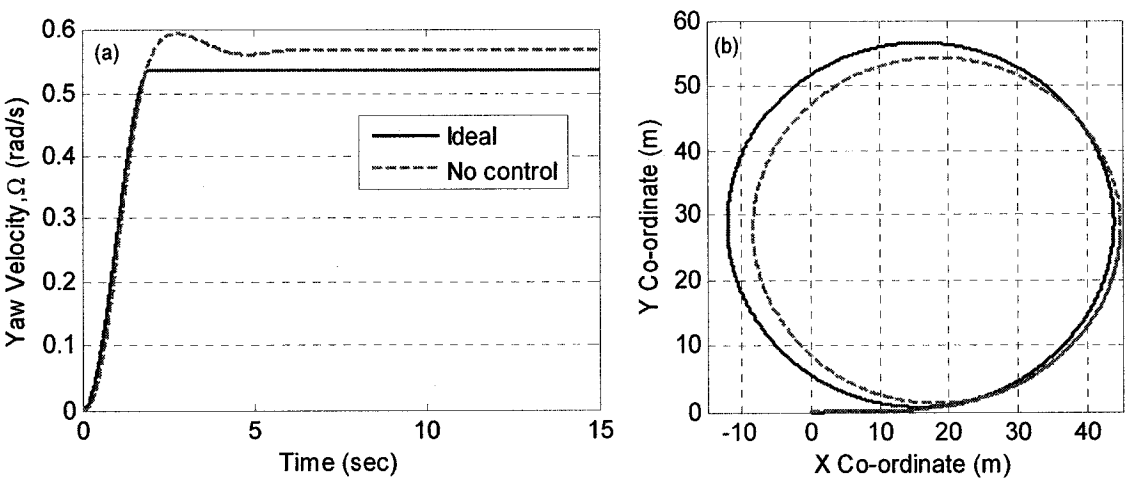

Figure 4.9: Yaw-rate and trajectory, oversteer vehicle, no-control, circular motion

The reduced radius of the trajectory shows the oversteer nature of the vehicle. The yaw-rate of this vehicle, when compared with the reference yaw-rate in Figure 4.9(a), shows comparable transient response, which settles at a higher value than the reference value.

The corresponding normal load at each tire during the maneuver is shown in Figure 4.10(a). This shows higher normal load on rear axle and a significant lateral load shift from inner to outer wheels as the vehicle negotiates the turn.

Finally, tire lateral forces are shown in Figure 4.10(b), where the effect of higher normal loads can again be seen on the lateral forces for both outer tires. Both of these under and oversteer vehicle models are simulated for lane-change maneuvers in the next subsections.

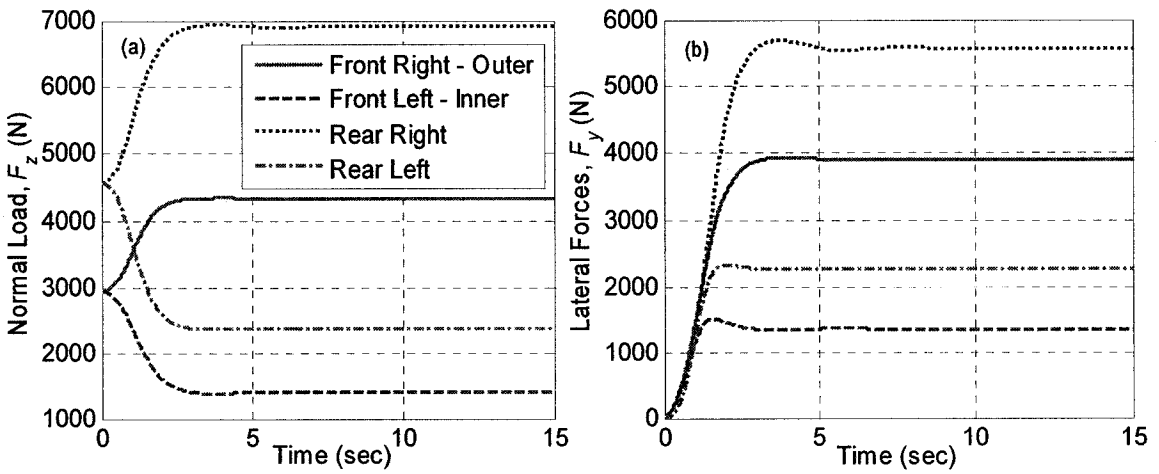

Figure 4.10: Normal and lateral forces, oversteer vehicle, no-control, circular motion

4.3.4 Lane Change - Understeer Vehicle

The vehicle model from subsection 4.3.2 is simulated for a lane-change maneuver using the sinusoidal steering input presented in Figure 4.6. The computed results in terms of vehicle trajectory at 1 m/s and 25 m/s are shown in Figure 4.11(b). The deviation of the vehicle path from the ideal path can be explained with understeer nature and low yaw-rate as shown in Figure 4.11(a). As seen in Section 4.3.2, low yaw-rate results in larger radius of curvature and hence, vehicle's actual path lags behind the ideal path.

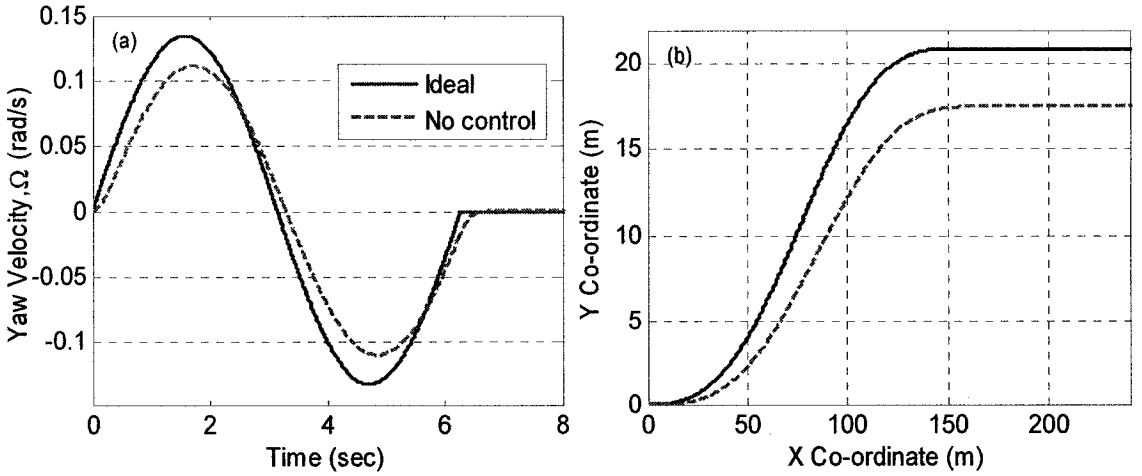

Figure 4.11: Yaw-rate and trajectory, understeer vehicle, no-control, lane-change

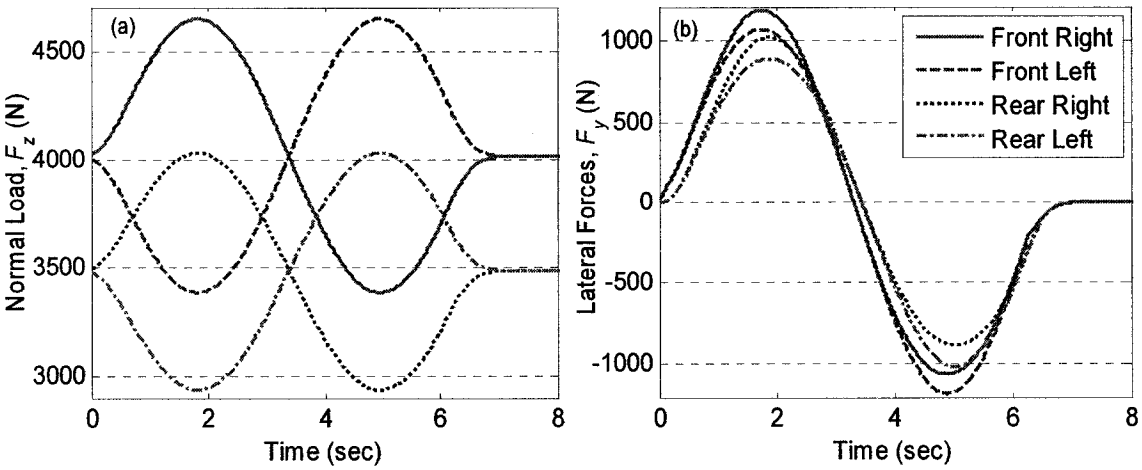

Figure 4.12: Normal and lateral forces, understeer vehicle, no-control, lane-change

In Figure 4.12(a) the effect of sinusoidal steering input can be seen as the right and left tires act as inner and outer for each half cycle and load shift takes place from left to right for the first half and from right to left for the latter. Finally, the effect of higher normal loads on lateral forces for each half cycle is presented in Figure 4.12(b), where right and left tires generate slightly higher forces for first and second half of the maneuver, respectively. Variation in both load shift and tire lateral force in this case are less severe than those found for circular motion due to less severity of the input used in a lane-change maneuver.

4.3.5 Lane Change - Oversteer Vehicle

Vehicle model with modified CG position as described in subsection 4.3.3 is simulated for lane-change maneuver at 1 m/s and 25 m/s. The oversteer vehicle is expected to follow a smaller radius of curvature when compared to the ideal curve for a given steering input. This effect can be seen in vehicle's trajectory in Figure 4.13(b) where the vehicle makes a sharper turn, as if it was given a larger steering angle.

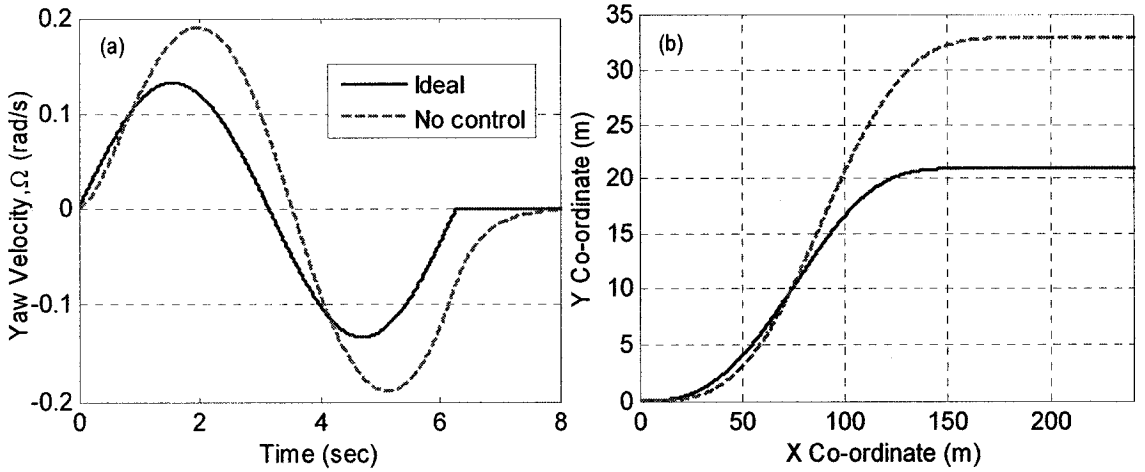

Figure 4.13: Yaw-rate and trajectory, oversteer vehicle, no-control, lane-change

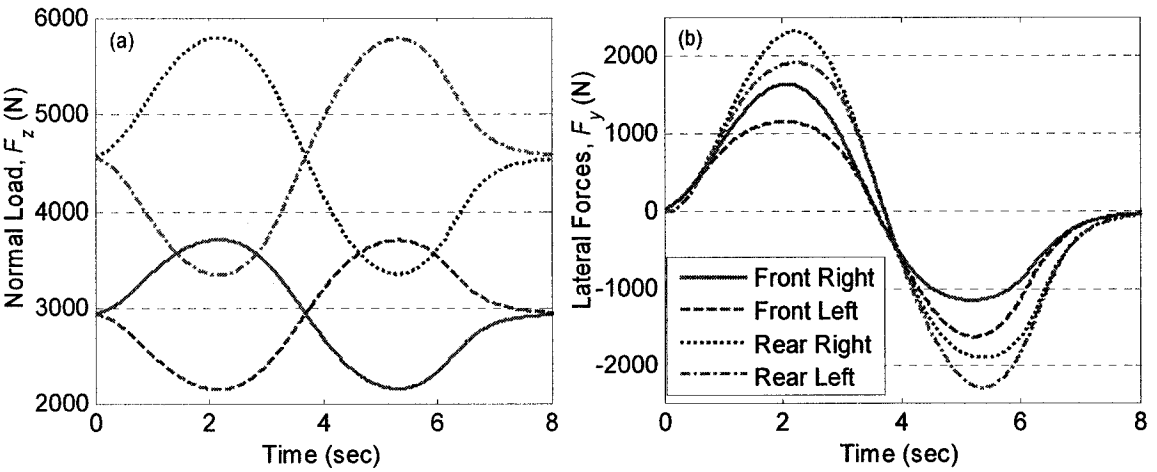

Figure 4.14: Normal and lateral forces, oversteer vehicle, no-control, lane-change

The higher yaw-velocity can be observed in Figure 4.13(a), which causes the deviation of vehicle from its ideal path. The CG position, being closer to the rear axle,

causes higher normal load on rear wheels. The normal load shifts from left to right and right to left for each half of the sinusoidal cycle, which results in load variation on four tires as shown in Figure 4.14(a). Again the higher normal load causes higher lateral forces to be generated at right and left tires for each half cycle as shown in Figure 4.14(b).

The results obtained in this section clearly indicate that the conventional steering system with fixed steering ratio based on low speed handling can not provide the response at higher speeds. Furthermore, the effect of speed is dependent on the vehicle's handling characteristic. It is also observed that there is a significant dynamic load shift which changes the tires ability to generate forces. In an uncontrolled system, therefore, the tire's ability to work is not maximized. Tire work-load and effect of steering ratio on tire work-load is next examined in the following section.

4.4 Tire Work Load and Anti-Ackerman Steering

In a handling maneuver there is significant load shift between left and right tires. Furthermore, longitudinal acceleration or braking causes load shift between front and rear axles as shown in Equation (3.7). If the location of CG is changed due to loading, the load on the wheels will also change. The load on a tire is thus a very dynamic parameter. Lateral forces using Magic formula at front and rear tires for static normal load for an understeer vehicle were compared in Figure 2.2. The higher normal load on front tire enables it to generate higher lateral force compared to the rear tire. Similar results were obtained in the previous section in Figures 4.8 and 4.12, where front tires with higher normal loads generate higher lateral forces compared to the respective rear tires, while

rear tires generate higher lateral forces in Figures 4.10 and 4.14 due to higher normal load for an oversteer vehicle. This ability to generate higher forces as a function of normal load can be clearly deduced from the Magic formula and is quantified in Figure 2.2.

Similar trend in lateral force generation from right and left tires on each axle can be noticed in each case in above section, as the vehicle negotiates a turn, which needs to be quantified. For this purpose the understeer vehicle discussed in section 4.3.2 and the similar circular motion condition would be used. Figure 4.8(a) shows the load shift due to the vehicle roll motion while negotiating a turn. Both outer tires (right tires in this case) show a significantly higher normal load than the inner (left) tires. For the front axle the normal load on the right tire is 5600 N while that on left tire is 2400 N, at 15 m/s, negotiating a 30 m radius turn. Using the Magic formula, lateral force generating ability as a function of slip-angle for both tires is drawn and shown in Figure 4.15.

Normal load on front outer tire, $F_{z,fL} = 5600$ N

Normal load on front inner tire, $F_{z,fR} = 2400$ N

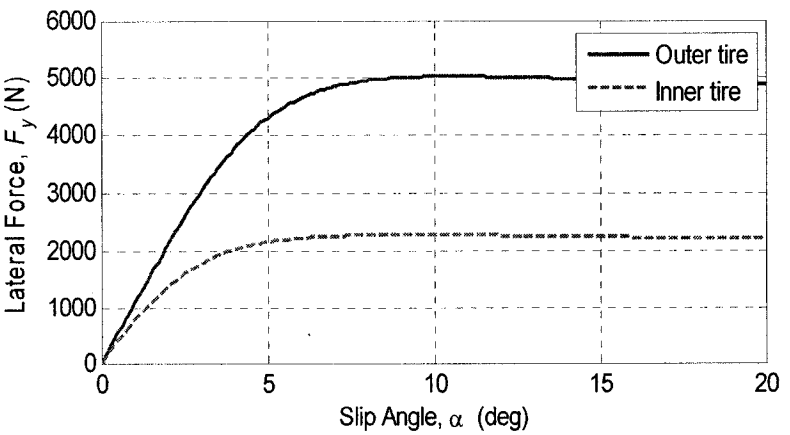

Figure 4.15: Lateral force generating ability for front tires

According to the Magic formula, the lateral force generated at a particular normal load reaches a maximum value at a particular slip-angle and decreases thereafter for any

further increase in slip-angle. Both, the value of maximum lateral force and corresponding slip-angle depend on the normal load. With increase in the normal load, both of these values increase [64, 117]. From Figure 4.15, it can be seen that the right (outer) tire with higher normal load generates a maximum of 5000 N at 11^{o} slip-angle while the left tire can generate maximum of 2300 N when slip-angle is 7^{o}.

The lateral forces generated at both front tires are shown in Figure 4.8(b). In this case, the left tire contributes 2100 N while the right tire generates 3800 N. The respective slip-angles for this maneuver are found to be 4.3^{o} and 4.1^{o} for left and right tires, respectively. From these results it can be deduced that the left tire, which acts as inner tire in the present case, is generating near saturation lateral force, while the right tire (outer) is capable of generating much higher force, which can be utilized for control purposes.

To compare the tire's ability of generating forces under given normal load, a performance parameter in terms of tire work-load is defined [19, 23]. Tire work-load is a measure of utilization of total frictional forces available and is defined as the ratio of total forces being generated by the tire to the maximum forces that the tires can generate at instantaneous normal load and can be expressed as:

$$\text{Tire work-load} = \frac{\sqrt{F_y^2 + F_x^2}}{\mu \cdot F_z} \tag{4.7}$$

where, F_y and F_x are the lateral and longitudinal forces, F_z is the normal load and μ is the average coefficient of the friction between the tire and the road. As the tire work-load reaches unity, i.e., the force reaches its maximum value, any further increase in slip or slip-angle decreases the force (Figures 2.2 and 4.15) [117]. In the current investigation, the longitudinal forces in traction or braking are neglected and the coefficient of friction

between the tire and the road is assumed to be same for all tires. Hence, the tire work-load can be simplified to:

$$\text{Tire work-load} = \frac{F_y}{F_z} \tag{4.8}$$

This definition of tire work-load will be used throughout this study as a performance parameter to compare different control strategies.

Using Equation (4.8) tire work-load for all four tires are calculated for the cases simulated in Section 4.3 and are presented in Figures 4.16 and 4.17. Figure 4.16(a) shows the tire work-load in circular motion for the vehicle with understeer characteristics for which tire lateral forces were presented in Figure 4.8(b). Comparison of these results show that although the front right (outer) tire generates almost twice as much lateral force as the left (inner) tire, it still operates at low work-load (< 0.7). The front left (inner) tire, on the other hand, operates at close to saturation value (~ 0.9). Thus, the inner tire may impose a limit over the amount of active control, as any further increase in steering angle, and hence slip-angle, will saturate the lateral forces at inner tire. This will in turn decrease the net forces generated from inner tire and hence, can cause instability in the vehicle. At the same time, the ability of outer tire to generate higher force remains unexploited.

For the oversteer vehicle, the tire work-load for both front tires are high as shown in Figure 4.16(b), since the vehicle is operating at higher yaw-rate compared to the reference value. In this case a controller would be desirable to reduce the steering angle to improve the relative stability of the vehicle. However, if the steer angles of both front wheels are reduced, it may decrease the tire work-load at the outer tire, but inner tire may still experience a relatively high work-load.

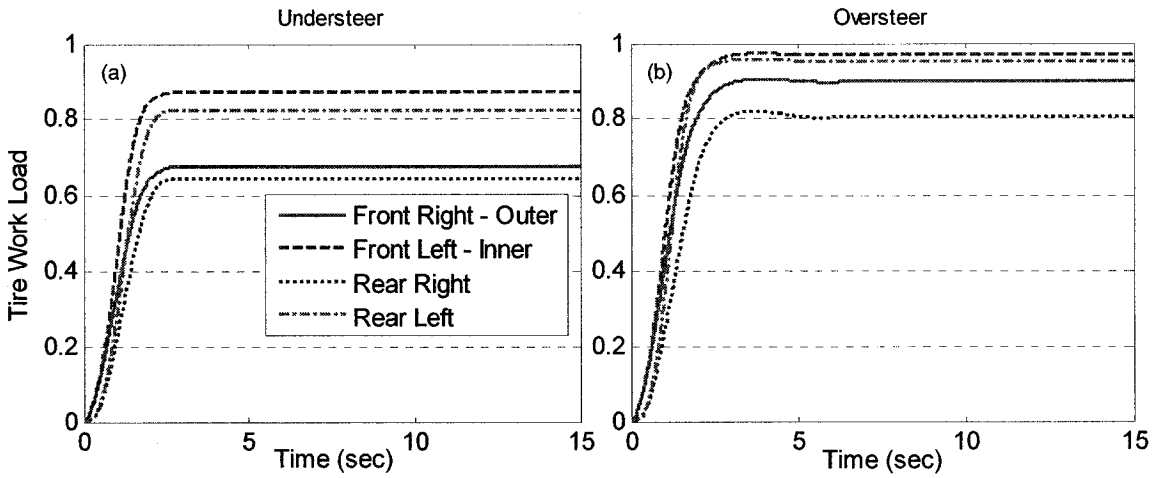

Figure 4.16: Tire work-load, no-control, circular motion

For lane-change maneuver, both front tires act as inner tire for half cycle and hence, show higher tire work-load for respective half cycles as shown in Figure 4.17. Again, the oversteer vehicle experiences higher work-load compared to the understeer vehicle due to higher yaw-rate.

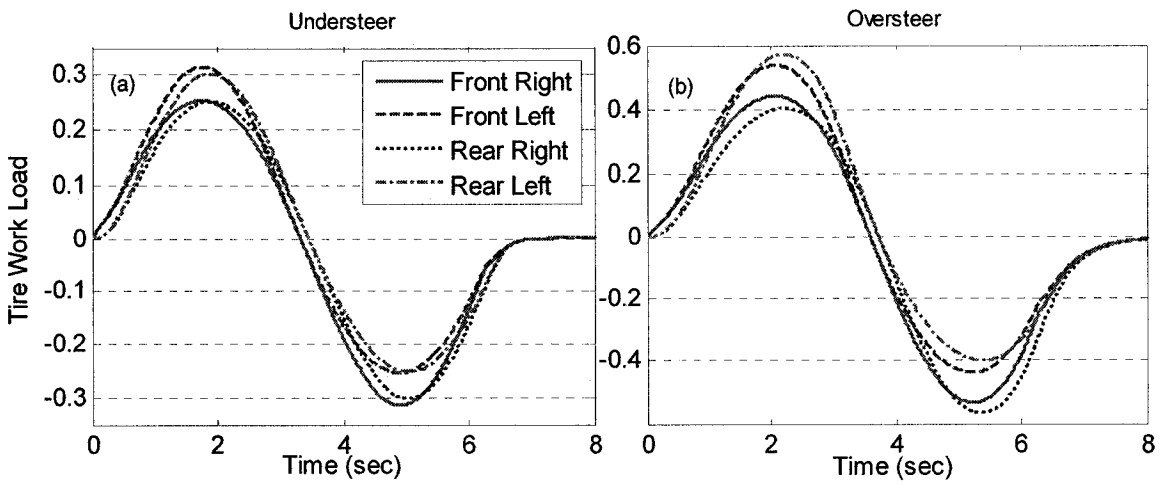

Figure 4.17: Tire work-load, no-control, lane-change

It can be clearly noticed from above discussion that the inner tire always experiences higher tire work-load irrespective of the vehicle handling characteristics or steering maneuver and is at the risk of saturation. To avoid such a situation and to utilize the higher lateral forces from the outer tire for better traction, certain vehicles such as race cars, utilize an anti-Ackerman geometry [64, 117, 118, 120, 121]. Anti-Ackerman

geometry requires outer wheel to be steered more than the inner wheel. It generates higher slip-angles and hence, higher lateral forces at outer tire as discussed in the next subsection.

4.4.1 Vehicle Behavior with Anti-Ackerman Steering

A steering mechanism can be designed in such a manner that the outer wheel is steered more than the inner wheel. This type of steering geometry is known as the anti-Ackerman geometry. The anti-Ackerman steering ratio helps in shifting the tire work-load from the inner tire to the outer tire and hence, avoids the inner tire from reaching its maximum capacity. This can generate higher total lateral forces in cornering and is often used in race car steering design [120]. A comparison of total lateral forces for Ackerman and anti-Ackerman steering is shown in Figure 4.18 for four different normal loads. These results show that for a given normal load anti-Ackerman generates significantly larger force. Such geometry, however, does not allow for pure rolling of the wheels at low speeds and makes it difficult to push the car around the pit [117].

The 4-wheel vehicle model is next examined for handling performance with anti-Ackerman geometry. A 10% anti-Ackerman geometry is realized by assigning:

$$\begin{aligned} \delta_o &= 1.1\delta_{st} \\ \delta_i &= 0.9\delta_{st} \end{aligned} \tag{4.9}$$

where outer wheel is steered more than the inner wheel. Such steering system is simulated for a step steering input for circular motion of the understeer vehicle. Vehicle trajectories for 10% and 20% anti-Ackerman and ideal path are compared in Figure 4.19.

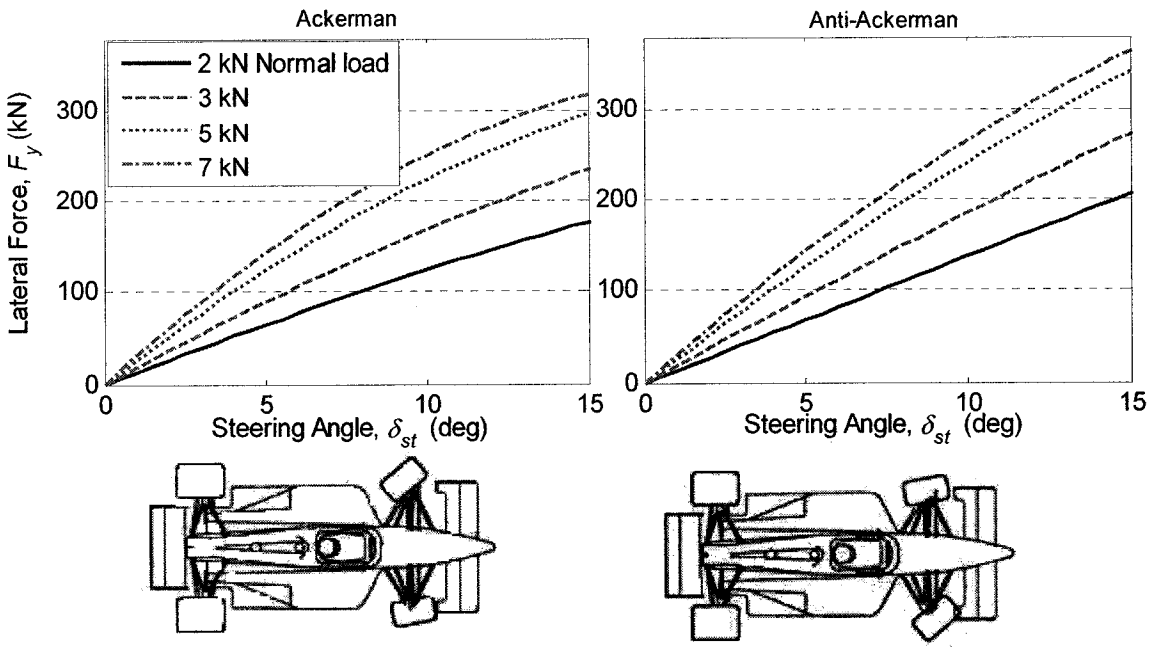

Figure 4.18: Anti-Ackerman geometry for the race cars

The results show that anti-Ackerman does not change the understeer characteristics by much and follows a similar path as that of the Ackerman geometry. The results in terms of tire work-load are presented for the three cases in Figure 4.20. These results show that with the increase in anti-Ackerman ratio the work-load is more equalized between front inner and outer tires. Thus, anti-Ackerman geometry proves to be a promising design for better lateral control at high speed operations, while it is desirable to have Ackerman geometry at low speeds.

A steering can be designed to follow Ackerman or Anti-Ackerman ratio by changing the physical parameters in the 4-bar steering linkage mechanism or by setting an initial toe-in [117]. Road vehicles are, however, designed for close-to-Ackerman geometry to avoid tire scrub, and the same ratio is maintained for all speeds. Even with conventional active control, Ackerman ratio is used for input at the left and right wheels while $\Delta\delta_{st}$ is introduced to improve handling. A typical active front steering (AFS) control system for the 4-wheel vehicle model is formulated in the following section.

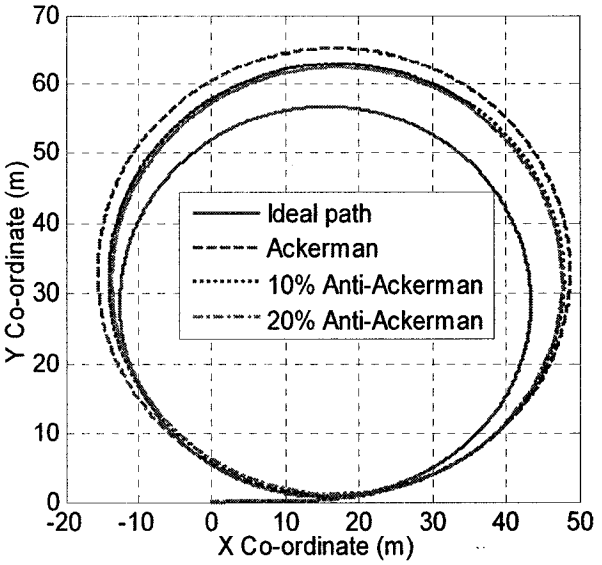

Figure 4.19: Vehicle trajectory for Ackerman and anti-Ackerman steering

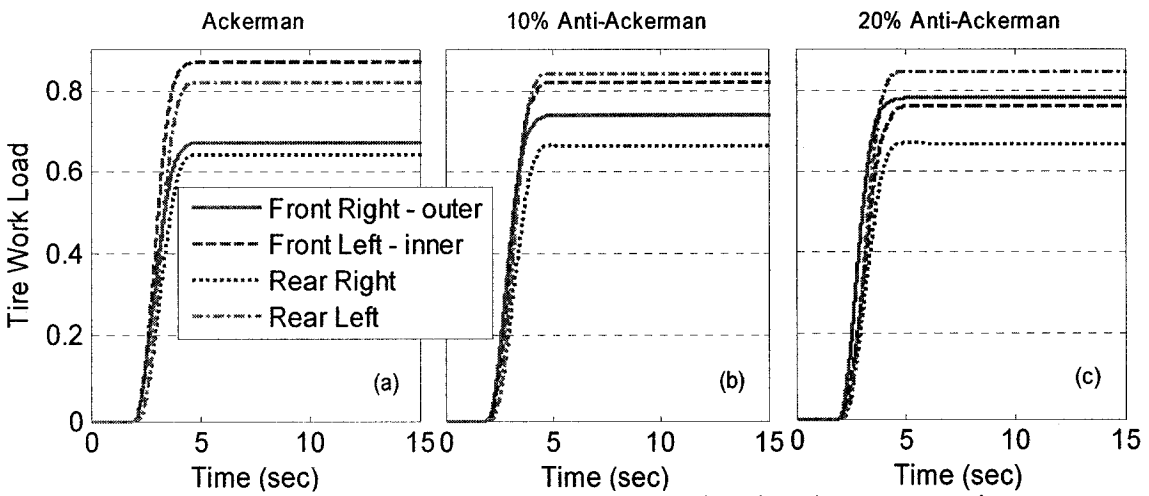

Figure 4.20: Tire work-load for Ackerman and anti-Ackerman steering

4.5 Vehicle Behavior with Conventional AFS

In order to achieve ideal state of a response, active feedback control is employed in road vehicles. The controller changes one of the input parameters to achieve one of the reference or set-point state parameters. In the present investigation, front steering input is controlled in order to achieve the reference yaw-rate. The conventional active front steering (AFS) controller, developed in this section is based on a simple feedback

proportional-integral (PI) control strategy [122]. A conventional controller, as discussed earlier, controls steering angle of both front wheels simultaneously following an Ackerman ratio between inner and outer wheels. The controller calculates the reference yaw-rate from forward velocity and the driver steering command as shown in Equation (4.5). The response can be used to define an error in the yaw-rate as:

$$\Delta\Omega = \Omega_{ref} - \Omega_{act} \tag{4.10}$$

To minimize this error an actively controlled additional steering command has to be added to the driver input. The amount of active steering command is proportional to the error in the yaw-rate. The steer gain factor, K_{st} can be defined as:

$$K_{st} = \frac{\delta_{st}}{\Omega_{ref}}$$

Substituting for Ω_{ref} from Equation (4.5), the gain can be written as:

$$K_{st} = \frac{\delta_{st} \cdot L}{V_x \tan(\delta_{st})}$$

For control purposes, for small δ_{st}, $\tan(\delta_{st})$ is assumed to be equal to δ_{st} and hence, the steer gain factor reduces to:

$$K_{st} = \frac{L}{V_x} \tag{4.11}$$

The corrective steering angle can be calculated from the gain factor and the yaw-rate error as:

$$\Delta\delta_{st} = K_{st} \cdot \Delta\Omega \tag{4.12}$$

and the actively controlled steering command with PI controller can finally be calculated as:

$$\delta_c = k_1 \Delta\delta_{st} + k_2 \int \Delta\delta_{st} \tag{4.13}$$

The first and second terms on the right hand side of the Equation (4.13) represent the proportional and integral part of the feed-back controller, and k_1 and k_2 are the weight assigned to proportional and integral parts. In the present study the weight for proportional and integral parts used, based on optimized overshoot and response time lag are: $k_1 = 4$, $k_2 = 6$.

The controlled steering command, δ_c, is added to the driver steering command and given as input to both front wheels. Since the controller is based on only proportional and integral parts and the differential part is not considered (PID controller), an overshoot in the response is expected. The controller is similar to the one shown in Figure 1.1 and is represented by block diagram in Figure 4.21.

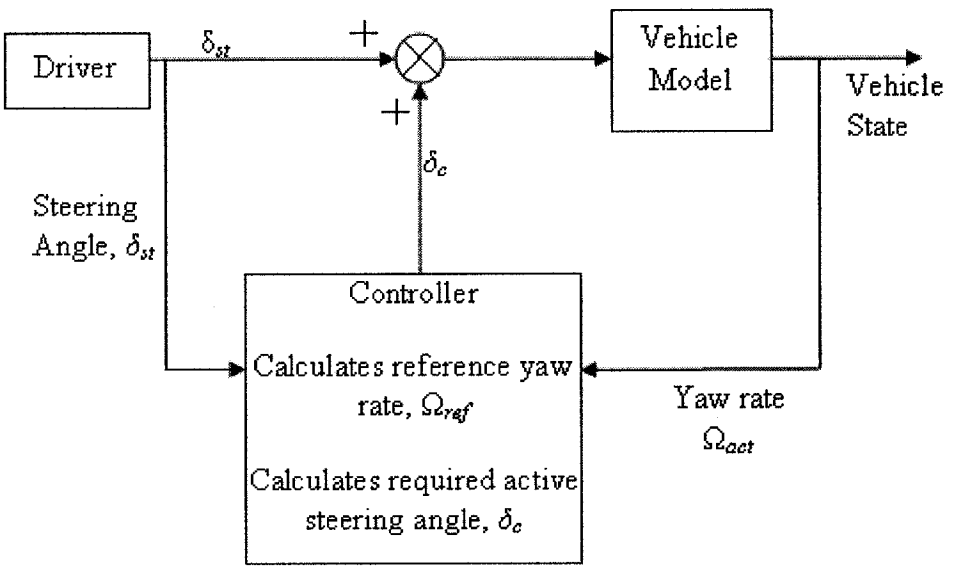

Figure 4.21: Schematic of the feed-back controller with vehicle model

This conventional AFS is applied to the circular motion of the understeer vehicle to achieve the reference yaw-rate. Maximum forward velocity at which the control can be applied depends on the total tire lateral force available during a maneuver. For the proposed simulation the maximum velocity can be established from:

$$\frac{mV_{\max}^2}{R} = F_{\max}$$

For a given steering angle (δ_{st}), reference radius being $R = (L/\delta_{st})$, the $F_{\max}$ can be calculated from Magic formula. For the vehicle parameters used, and $\delta_{st} = 0.1$ rad, the maximum forward velocity is found to be: 16.4 m/s. It is thus safe to use the same velocity as the previous section, which is 15 m/s.

At velocities higher than this, the vehicle can never reach the reference values and thus, the controller will become unstable. The understeer vehicle equipped with this conventional AFS controller is simulated for step steering input for circular motion. The total steering angles at the front wheels are result of driver steering command added with active controller command as shown in Figure 4.22.

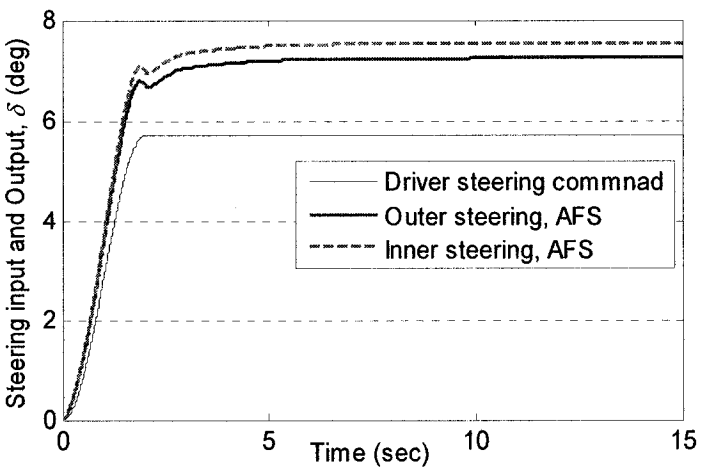

Figure 4.22: Steering angle with AFS

The results show that in order to meet the required reference yaw-rate, significantly larger steering angles are produced by the AFS controller. The ratio of inner to outer wheel, however, remained according to the Ackerman geometry. The resulting yaw-rate during the maneuver is shown in Figure 4.23(a). This result clearly shows the effectiveness of AFS in realizing the reference yaw-rate.

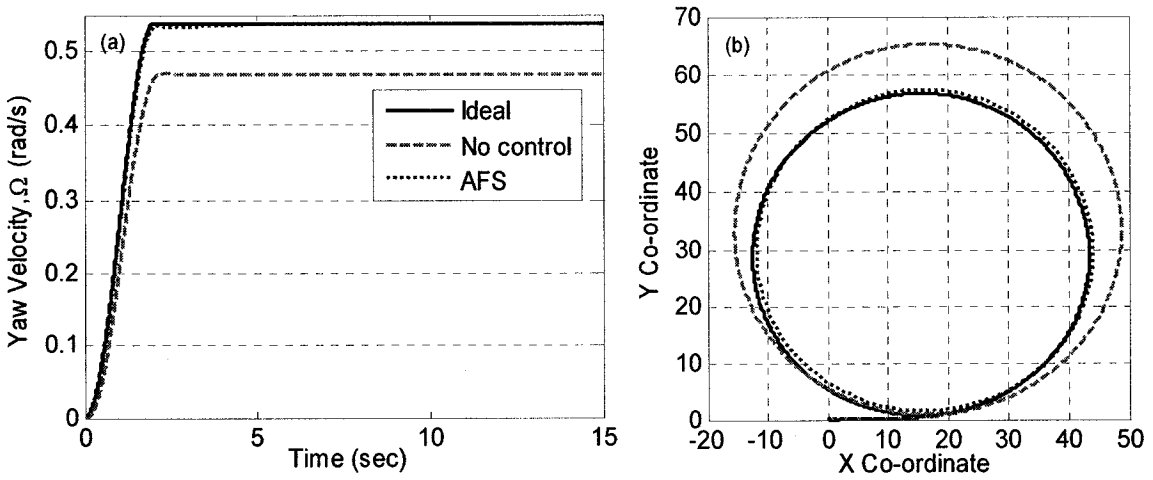

Figure 4.23: Yaw-rate and trajectory with AFS

Since the vehicle achieves the reference yaw-rate with AFS control, it follows close-to ideal path as shown in Figure 4.23(b). The radius of the path is same as the ideal path and the horizontal and vertical offset is due to the response-time delay of the controller. The response time delay can further be improved with robust control techniques.

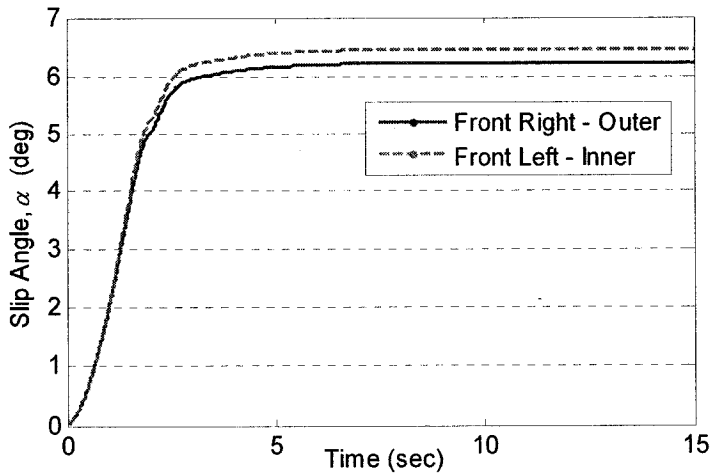

Figure 4.24: Slip-angles with AFS

The slip-angles developed at the front tires of vehicle with AFS shown in Figure 4.24 indicate that the maximum slip-angles developed by inner and outer tires are 6.5° and 6.2°, respectively. It would be interesting to compare the tires' ability to generate lateral force for the same operating conditions. For AFS control of the vehicle with

understeer characteristics it is noticed that the active control increases the steering angle to bring the vehicle yaw-rate towards the reference value. This causes further lateral load shift and the inner tire further loses its ability to generate lateral force. The normal loads on each front tire after implementing active control are found to be:

F_z, Right (outer) tire = 5900 N

F_z, Left (inner) tire = 2100 N

The ability of each tire to generate lateral force under above normal loads is calculated using Magic formula and is presented in Figure 4.25.

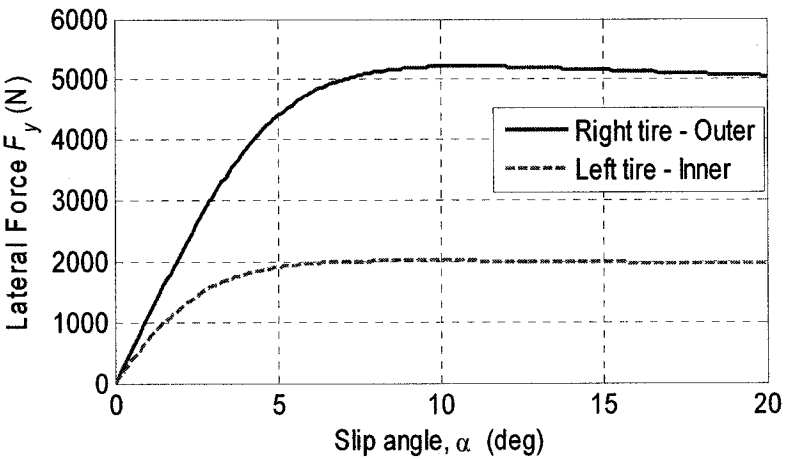

Figure 4.25: Lateral force generating capability for front tires in AFS

The maximum lateral force for each tire and corresponding slip-angle, in this case, are found to be:

$F_{y,max}$, Right (outer) tire = 5200 N, $\alpha = 11^o$

$F_{y,max}$, Left (inner) tire = 2000 N, $\alpha = 7^o$

which shows a decrease for inner tire and increase for outer when compared to no-control case presented earlier in Figure 4.15. Thus, the active control further reduces inner tire's ability to generate lateral force which may have a negative effect on the performance of the active control. This effect can be noticed in Figure 4.26, where the lateral force at the

inner tire reaches its maximum value of 2100 N, but as the active control keeps increasing the steering angle at the inner wheel, further load shift takes place and the lateral force drops to 2000 N rather than increasing any further.

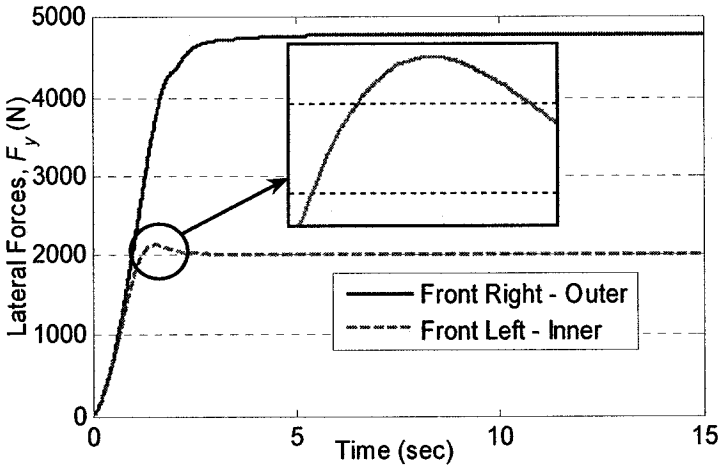

Figure 4.26: Lateral forces with AFS

The outer tire generates 4800 N and is still capable of generating up to 5200 N of lateral force. Finally, the tire work-loads for front tires are compared for AFS with no-control case in Figure 4.27. Since the coefficient of friction while calculating tire work-load in Equation (4.8) is taken as 1, the inner tire shows a work-load of 0.95, but it is actually operating at full work-load. The outer tire on the other hand, is not utilizing the maximum available frictional forces.

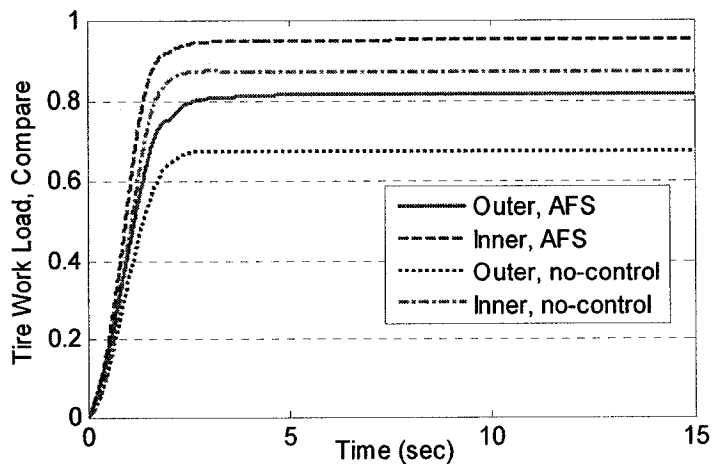

Figure 4.27: Tire work-load with AFS

From the results of step steering input and circular motion of the vehicle with AFS, it is observed that a conventional AFS may achieve the reference state in terms of yaw-rate. It is further found that in such control inner tire's force saturation may lead to vehicle instability as any further actively controlled steering command will reduce the forces at inner tire while outer tire may be further capable of generating forces. This is expected since the steering ratio remained unchanged and no attempt is made in maximizing the tire work-load. An improvement of AFS can thus be proposed by implementing an independent steering control for each front wheel. Such an Active Independent Front Steering (AIFS) is developed in the next section.

4.6 Active Independent Front Steering Control Technique

The results presented so far in this chapter provide insight into the important issues related to the vehicle handling performance and the potentials for improvement. It is obvious that Ackerman steering geometry is essential for passenger vehicles to minimize tire scrub and related noise and wear. On the other hand, anti-Ackerman ratio as used in race cars has its merits where the tire, capable of developing higher lateral force, is allowed to do so.

The control strategy available in literature, namely AFS, has been shown to improve handling response as it can match the yaw-rate to reference response. It may, however, saturate tire force prematurely and fail to utilize potential of each tire.

A new control strategy is therefore proposed in this investigation that utilizes Ackerman steering geometry with active independent front steering (AIFS) control. Such control strategy will allow anti-Ackerman ratio for high speeds when necessary to realize

the reference yaw-rate, while maximizing the tire work-load. Based on the observations of previous simulations, it is established that the proposed AIFS should:

- be able to identify the sign of steering command, i.e., turning left or right, to assign outer tire as right or left respectively.
- *add* the active command to the tire with low work-load, i.e., outer tire, in case of an understeer vehicle.
- *subtract* the active command from the tire with high work-load, i.e. inner tire, in case of an oversteer vehicle.

Based on the above rules a control algorithm is designed and is represented in form of a flow-chart in Figure 4.28.

In the algorithm shown in Figure 4.28 the driver steering command (δ_{st}) for a left turn is assigned positive and negative for right turn, thus making right tire as outer and left as inner for a positive steering command and vice-versa. The proposed technique changes the controller input from right to left wheel according to the direction of steering command for left and right turn. Also, it adds the controller command (δ_c) to the outer wheel in case of an understeer vehicle, while adding a negative command and hence, subtracts the controller command from inner wheel in case of an oversteer vehicle, thus maintaining an equalized tire work-load between front tires. The controller command (δ_c) can be established using the procedure outlined in Section 4.5 for AFS system. The controller table based on driver input and vehicle handling characteristic for the proposed AIFS is shown in Table 4.1.

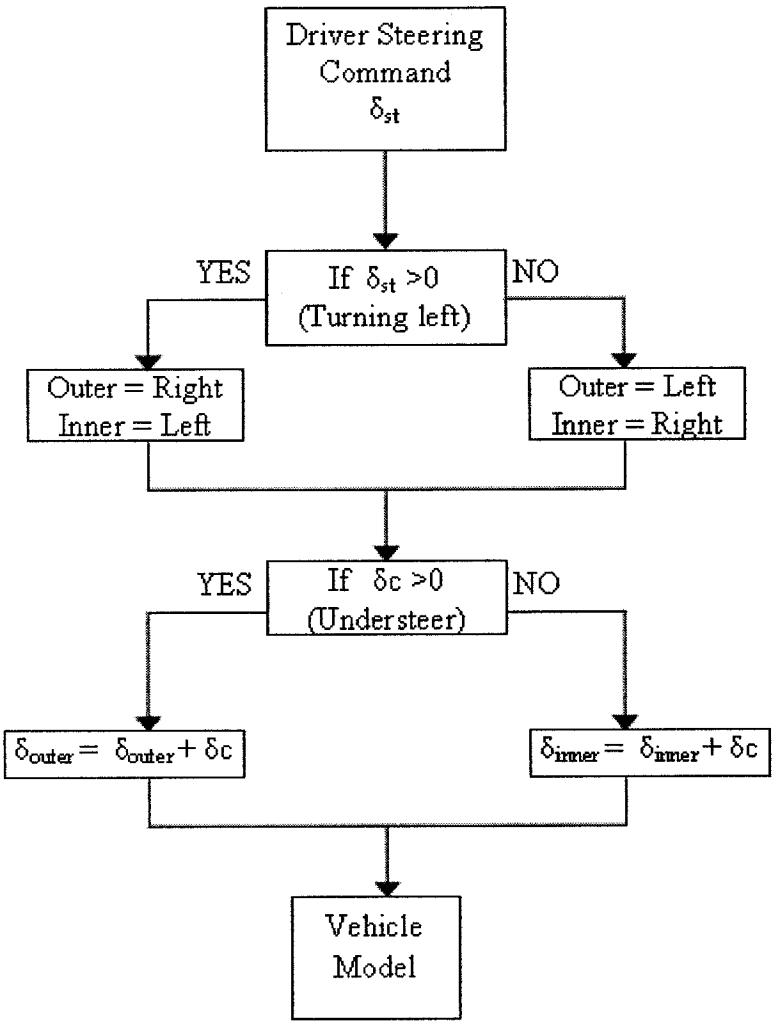

Figure 4.28: Flowchart for AIFS control technique

Table 4.1: Controller table for AIFS

Steering Angle / Handling Characteristics	+	−
Understeer	R	L
Oversteer	L	R

Above table shows the wheel to be controlled depending on the steering command and the vehicle handling characteristic. This gives a relation between active steering command and the wheel to be controlled as shown in Table 4.2.

Table 4.2: Decision table for AIFS

		Controlled wheel
Active command, δ_c	+	R
	–	L

This algorithm can be combined with a conventional AFS control technique developed in Section 4.5 (Equations 4.10 - 4.13) to give an AIFS control. Such a controller is designed and integrated with the vehicle model in the next chapter, where simulation results are also compared with those of no-control as well as conventional AFS.

4.7 Summary

Chapter 4 was devoted to in-depth understanding of vehicle handling response to a step input and lane-change maneuver. For this, simulations were carried out for Ackerman and anti-Ackerman steering geometries. The results were compared with those derived from AFS control. In each case results were examined with respect to various performance measures, namely ideal path, reference yaw-rate, tire vertical and lateral forces and most importantly, the tire work-load. From the results it was concluded that in order to obtain effective control at all speeds while maximizing the tire work-load, it is necessary to utilize a controller that can modify the left or right wheel steer angle independently based on vehicle's understeer characteristics, speed and driver steering command. A control strategy using active independent front steering (AIFS) is finally proposed in this chapter. The handling performance of the candidate vehicle with the proposed AIFS is examined in the next chapter.

5 Vehicle Behavior with AIFS Control

In Chapter 4 it was established that the front tire lateral forces provide practical and effective means to enhance vehicle stability. Front steering control was thus selected for the present investigation. Conventional AFS was also studied in Chapter 4 to examine its performance and to identify its limitations. A performance measure based on tire's ability to generate lateral force and actual lateral force developed was defined as tire work-load. Chapter 4 finally proposes an AIFS control strategy that can provide AFS performance with maximized tire work-load. This chapter presents a controller design for such an AIFS control algorithm.

An AIFS controller formulated in Simulink is integrated with the 4-wheel vehicle model developed in Chapter 3. The candidate vehicle with under and oversteer characteristics under different steering angles is simulated to observe the handling performance. The results are compared with no-control as well as conventional AFS control to demonstrate the effectiveness of the proposed AIFS control.

5.1 AIFS Controller Design

A controller based on the AIFS technique proposed in the previous chapter is developed in this section. The controller design is similar to the one designed for conventional AFS, using a PI-controller (Equations 4.5, 4.10-4.13), but the active command would be given to only one of the front wheels according to Tables 4.1 and 4.2. This decision is based on

the tire work-load for inner and outer tires on the front axle. The active command is added to the outer wheel, and subtracted from the inner when required.

The AIFS controller integrated with vehicle system is shown in Figure 5.1. The controller requires driver steering command and vehicle longitudinal velocity as inputs to calculate the reference yaw-rate as given by Equation (4.5). The active steering command is then calculated based on yaw-rate error using speed dependent gain as shown in Equations (4.10-4.13). The weights of the proportional and integral part of the controller are 4 and 6, respectively, which are same as those used in conventional AFS control in Section 4.5. When the active steering command is added to the driver steering command, the AIFS strategy is implemented. Based on the sign of the active command, positive or negative, it is either added to the right or left wheel, respectively, as given by Table 4.2.

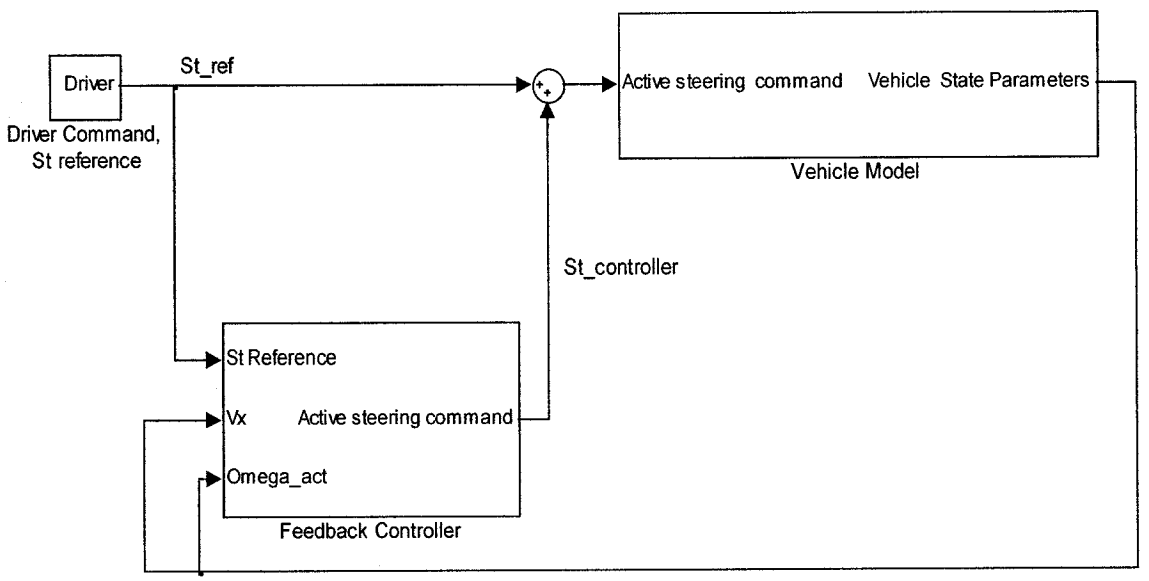

Figure 5.1: AIFS controller integrated with vehicle model

Selected vehicle configurations equipped with AIFS controller are simulated for different driver steering command in next section.

5.2 Vehicle Behavior with AIFS

Vehicle models, developed in Section 4.3 for circular motion and lane-change maneuver are simulated for AIFS control in this section. The steering commands for both maneuvers were presented in Section 4.3.1. The forward velocity for circular motion is taken as 15 m/s and for lane-change as 25 m/s. Vehicle behavior is observed and compared with conventional AFS control-equipped vehicle. Simulation results for circular motion are shown first in the next subsections, followed by lane-change maneuver.

5.2.1 Circular Motion - Understeer Vehicle

The understeer vehicle model is given a step steering input of 0.1 rad (5.73°) as driver command. As seen earlier in Sections 4.3.2, understeer vehicle's yaw-rate is less than the reference yaw-rate and hence, active control adds a control steering command to achieve the reference value. The resulting left and right wheel steer angle for AFS and AIFS are shown in Figure 5.2 along with the driver steering command. As was seen earlier, the AFS adds the control steering command to both wheels as it maintains the same ratio. The AIFS is designed to provide additional angle to one wheel only; in this case it adds the control steering command, δ_c, only to the outer (right) wheel to achieve the reference state, keeping the left wheel steering angle untouched.

From Figure 5.2 it can be further seen that the final outer wheel steering angle is greater in case of the AIFS control compared to the AFS, to compensate for not controlling the inner wheel. The slip-angles generated due to the active independent steering command are shown in Figure 5.3(a).

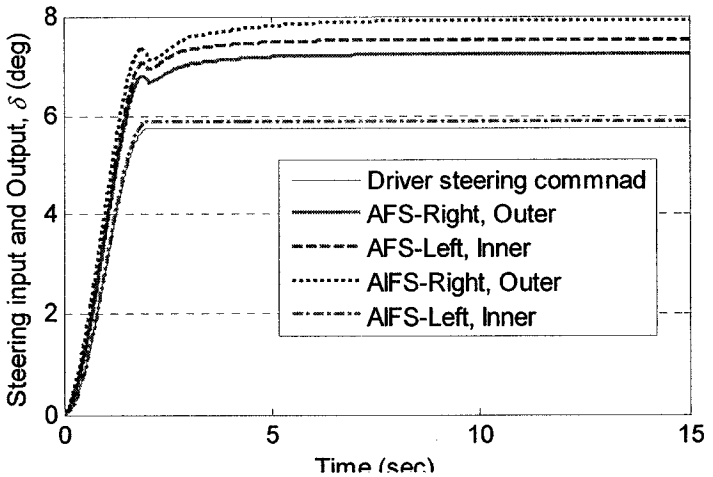

Figure 5.2: Steering output, understeer vehicle, circular motion

Again, the slip-angle at outer tire in AIFS is slightly greater than the one in AFS; however, a low slip-angle for inner tire is maintained in AIFS. These slip-angles cause different lateral forces at front tires when compared with conventional AFS as shown in Figure 5.3(b). The outer tire generates slightly higher lateral force in AIFS control compared to AFS. The inner tire generates low lateral force, which may be near saturation.

Vehicle yaw-rate as a result of these lateral forces in AIFS control is shown in Figure 5.4(a). The yaw-rate response shows similar result as that of conventional AFS and is very close to the reference yaw-rate. Since AIFS control is able to achieve the reference yaw-rate, vehicle is expected to follow a close-to-ideal trajectory, which is shown in Figure 5.4(b). The radius of the circular path followed by the vehicle is equal to the reference radius where the response time-delay causes the overall shift in the trajectory.

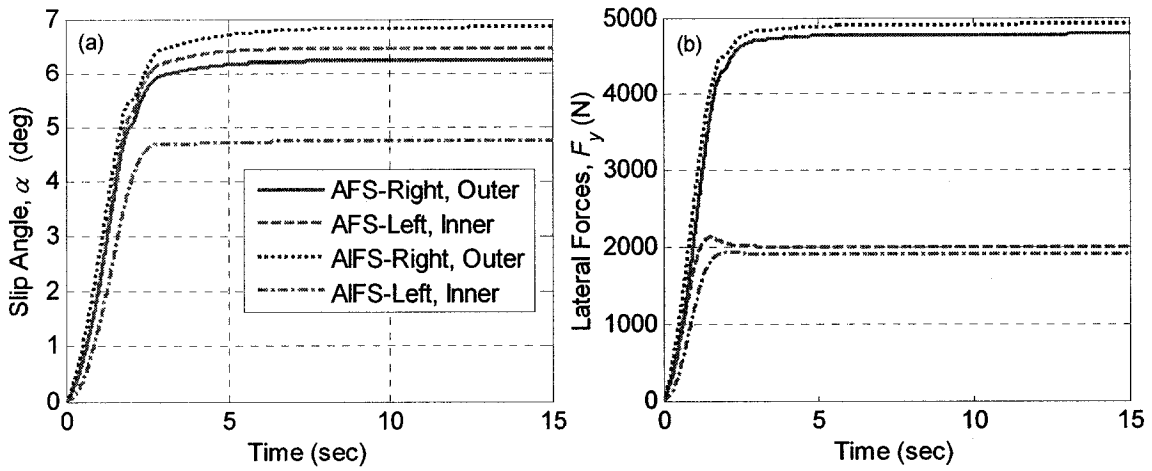

Figure 5.3: Slip-angles and lateral forces, understeer vehicle, circular motion

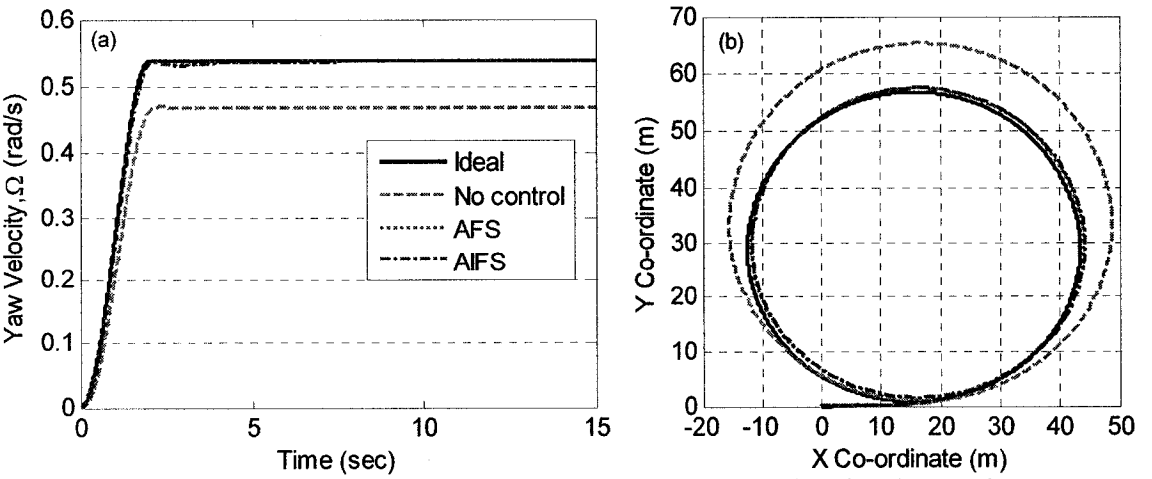

Figure 5.4: Yaw-rate and trajectory, understeer vehicle, circular motion

From Figures 5.3 it can be noticed that in AIFS:

- Outer tire generates a lateral force of 4950 N with a maximum ability to generate 5200 N and operates at a slip-angle of 6.85°.
- Inner tire generates a lateral force of 1900 N with a maximum ability to generate 2000 N and operates at a slip-angle of 4.75°.

When these results are compared with conventional AFS control in Section 4.5, it is clearly noticed that the tire work-load between front tires is equalized in AIFS which is shown in Figure 5.5. A slight increase in tire work-load for outer tire, from 0.82 for AFS

to 0.84 for AIFS, helps reduce tire work-load for inner tire from 0.95 in AFS to 0.90 in AIFS.

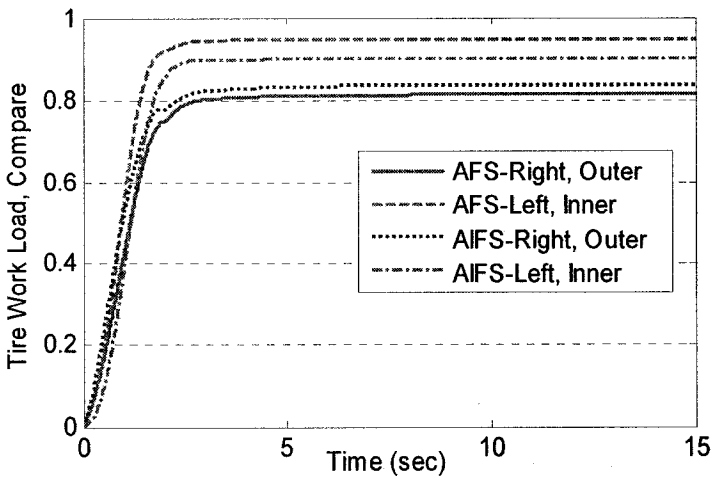

Figure 5.5: Tire work-load, understeer vehicle, circular motion

As shown in the above figures, the active independent control not only achieves the set point (reference) yaw-rate and ideal trajectory, but also equalizes the tire work-load between front inner and outer tires. The same control algorithm is now applied to an oversteer vehicle model.

5.2.2 Circular Motion - Oversteer Vehicle

The oversteer vehicle parameters used in Section 4.3.3 is simulated here for AFS and AIFS control. Since oversteer leads to higher yaw-rate with speed, the active control should reduce the steering angle in an attempt to achieve the reference yaw-rate. Though, a conventional AFS control will not increase the tire work-load of the inner tire in this case, since the steering angle is reduced, an AIFS can reduce the tire work-load of inner tire by a significant amount, thus bringing it closer to the work-load of the outer tire. For this purpose, AIFS controls only the inner wheel and leaves outer wheel uncontrolled. The steering output after active independent command is shown in Figure 5.6 along with those of driver command and AFS system. The AIFS, as designed, reduces the inner

wheel steer angle from 5.75° to 3.3° to achieve the target response. The resulting slip-angle time history for both AFS and AIFS system is shown in Figure 5.7(a).

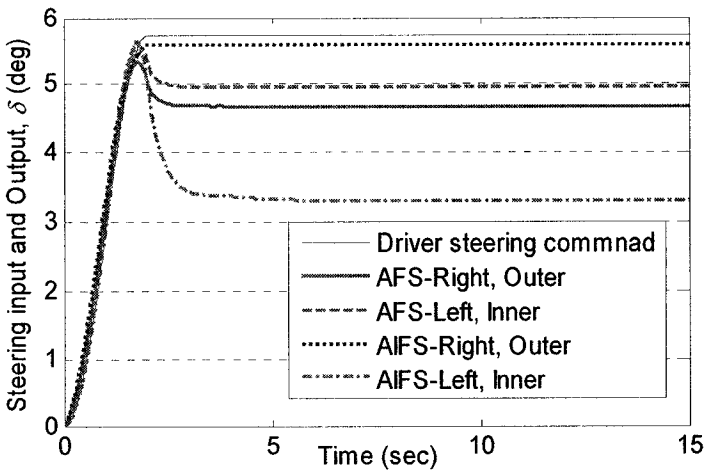

Figure 5.6: Steering output, oversteer vehicle, circular motion

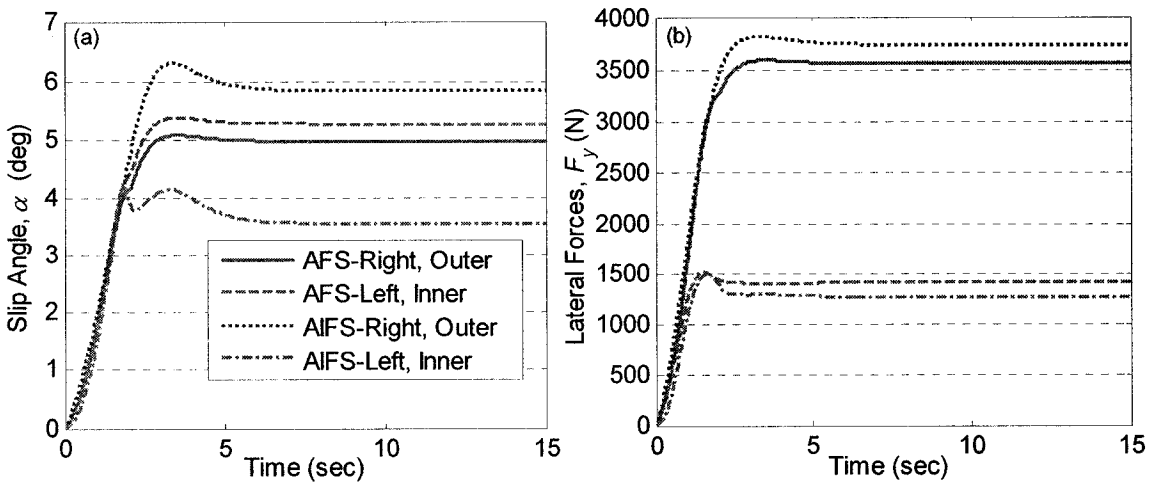

Figure 5.7: Slip-angles and lateral forces, oversteer vehicle, circular motion

These results show that AIFS requires slightly longer time to reach steady-state, and the slip-angle for outer wheel of AIFS is larger and for inner wheel is smaller than AFS. The corresponding lateral forces at both tires are shown in Figure 5.7(b). It can be seen that the outer tire generated much higher forces than the inner tire, but tire work-load results, plotted in Figure 5.8, show that both tires in case of AIFS generate equalized work-load (0.84 for inner and 0.87 for outer), which is not the case for AFS.

Above forces result in controlled yaw-rate and vehicle trajectory which are shown in Figure 5.9. Since the controller operates only on inner wheel, the value of active steering command is large and hence takes more time to be applied. This causes a higher overshoot in yaw-rate response when compared with AFS.

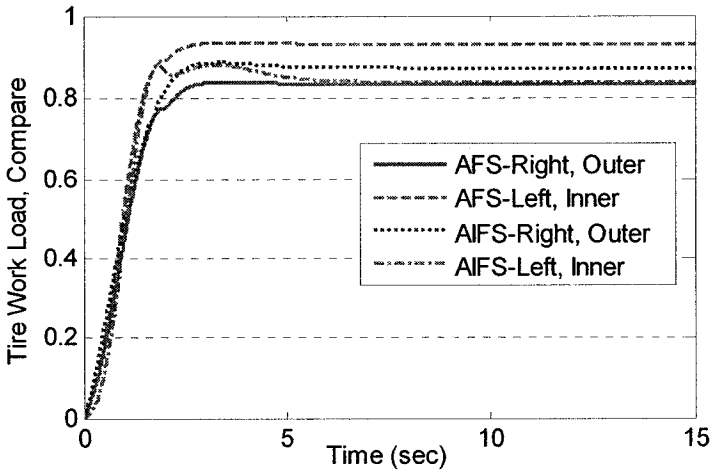

Figure 5.8: Tire work-load, oversteer vehicle, circular motion

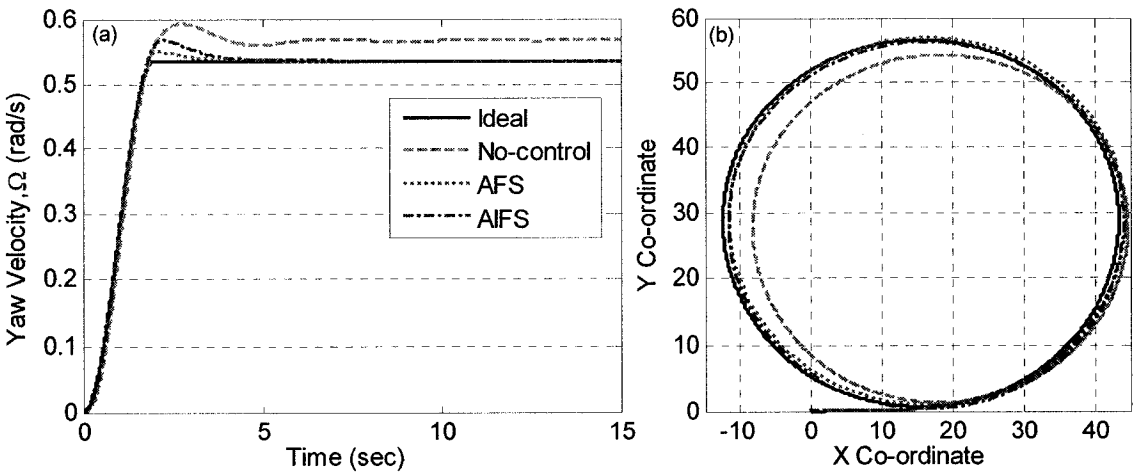

Figure 5.9: Yaw-rate and trajectory, oversteer vehicle, circular motion

This overshoot in yaw-rate, however, does not seem to affect the vehicle trajectory by large amount and the vehicle follows the ideal path closely.

The results presented in Section 5.2.1 and 5.2.2 for under and oversteer configurations, respectively, show that the AIFS algorithm is stable and is effective in providing required response, while improves the tire work-load significantly. To further

examine the applicability of AIFS control, it is applied to a lane-change maneuver which is discussed in the following subsections.

5.2.3 Lane Change - Understeer Vehicle

In line with the analysis presented in Chapter 4, the understeer vehicle with a forward velocity of 25 m/s is given the driver command for lane-change as shown in Figure 4.6. Due to the sinusoidal nature of the steering command each front tire acts as outer for each half cycle as discussed earlier. The AIFS hence changes the active command from right to left wheel after the half cycle. The steering output, after AIFS is applied, is shown in Figure 5.10 and is compared with conventional AFS results. While conventional AFS acts on both front wheels, AIFS controls only one wheel at a time and hence, maintains low slip-angle at respective inner tire for each half cycle as shown in Figure 5.11(a). The right wheel acts as outer wheel for first half of the cycle and left wheel acts as outer wheel for the other half cycle. Similar results for lateral forces generated at front tires can be seen in Figure 5.11(b).

The vehicle's response to lane-change input in terms of yaw-rate is shown in Figure 5.12(a) for AFS, AIFS and without control. The results when compared to reference yaw-rate show the effectiveness of both AFS and AIFS in achieving target response throughout the cycle. The corresponding vehicle trajectory is shown in Figure 5.12(b). Again, both AFS and AIFS performance are identical. In this case of lane-change of understeer vehicle, there is slight deviation from the ideal path during transient, however, the steady-state coordinate for the controlled cases are same as that defined as ideal.

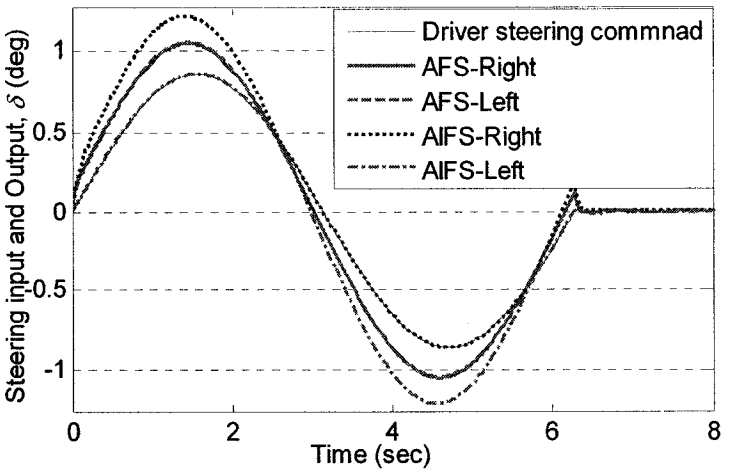

Figure 5.10: Steering output, understeer vehicle, lane-change

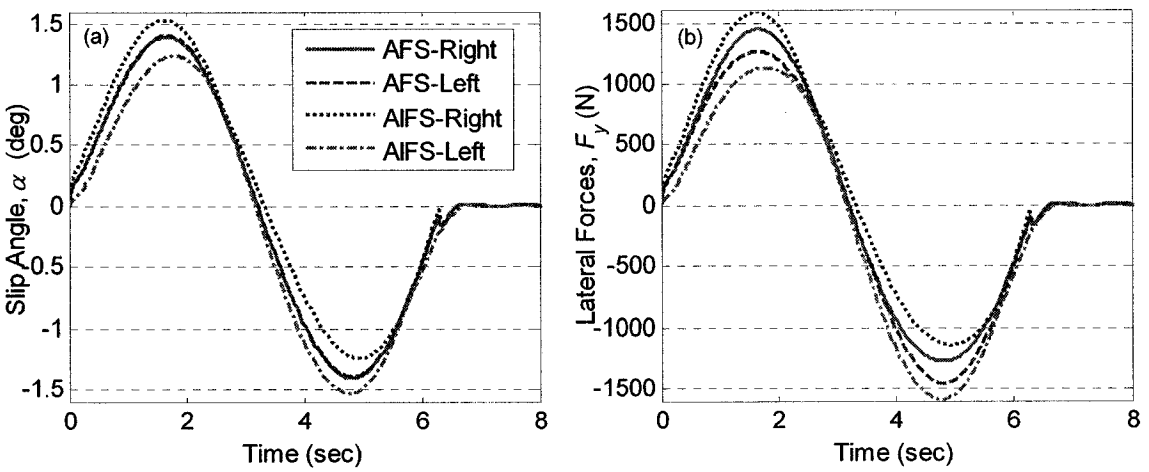

Figure 5.11: Slip-angles and lateral forces, understeer vehicle, lane-change

These results show that the similar performance can be achieved by actively controlling only one wheel at a time, since the contribution of the inner tire lateral force is not significant. Thus, AIFS control technique works as good as a conventional AFS control technique without risking the inner tire forces to saturate, which is evident from the tire work-load results presented in Figure 5.13. It is clearly noticed that both front tires operate at approximately same peak tire work-load of 0.34 in AIFS control, while there is a difference of 30% in the peak tire work-load values of inner and outer tires for a conventional AFS, with 0.3 tire work-load for outer and 0.4 for inner tire.

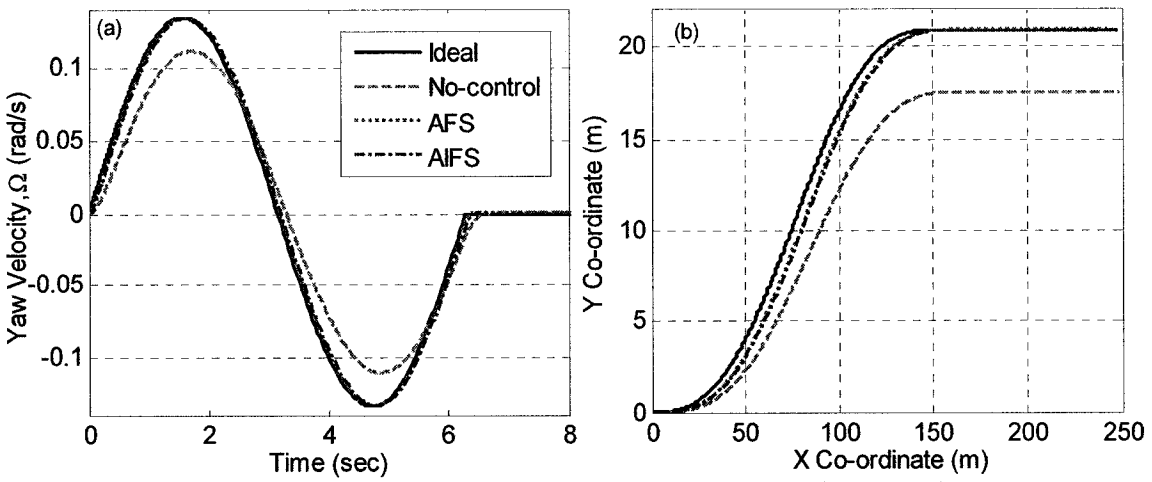

Figure 5.12: Yaw-rate and trajectory, understeer vehicle, lane-change

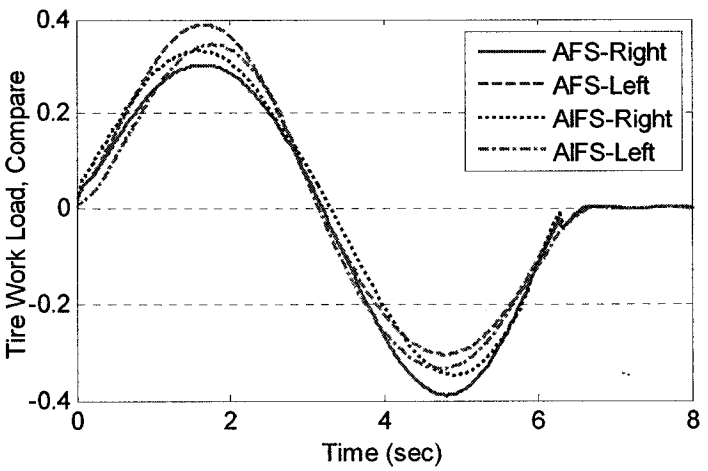

Figure 5.13: Tire work-load, understeer vehicle, lane-change

The AIFS technique is further applied to more complicated situation of lane-change maneuver of the oversteer vehicle in the next subsection.

5.2.4 Lane Change - Oversteer Vehicle

The vehicle model with oversteer characteristics due to modified CG position is simulated for similar steering command for lane-change as presented in the previous subsection. Two factors, namely, vehicle handling characteristic and sinusoidal steering command, both play their role in deciding the wheel to be controlled by AIFS. Since the vehicle yaw-rate is expected to be higher than the reference value due to oversteer nature,

the active steering command will be subtracted from the inner wheel for each half cycle. The driver steering command and resulting steer angles of left and right wheels for AIFS and AFS control are shown in Figure 5.14.

Due to the presence of an integral term in the PI controller as shown in Equation (4.13), $\delta_c = k_1 \Delta\delta_{st} + k_2 \int \Delta\delta_{st}$, the active control command δ_c does not change sign in phase with steering command δ_{st}, but before or after δ_{st}, governed by both 'P' and 'I' terms. This causes differential command to be applied to right or left wheel not for exact half cycle but changes within each half cycle as illustrated in Figure 5.14.

Tire slip-angles and respective lateral forces are shown in Figures 5.15. Since lateral force from only one tire at a time is controlled, an overshoot in yaw-rate response can be seen in Figure 5.16(a), compared to the conventional AFS. The vehicle, nevertheless, follows the ideal trajectory closely in this case as well which is demonstrated in the trajectory plot presented in Figure 5.16(b).

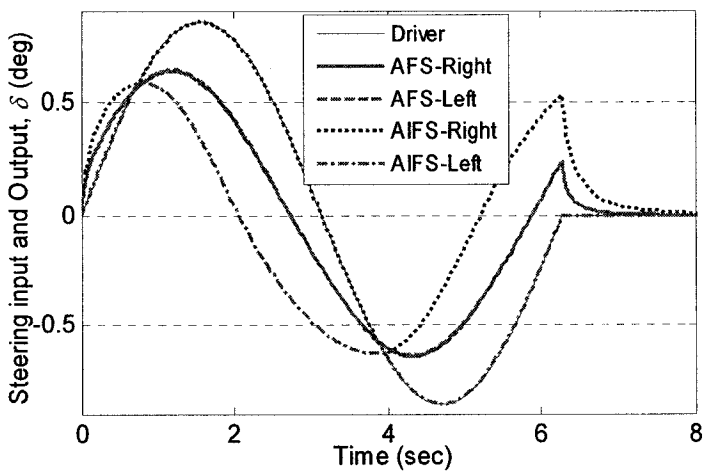

Figure 5.14: Steering output, oversteer vehicle, lane-change

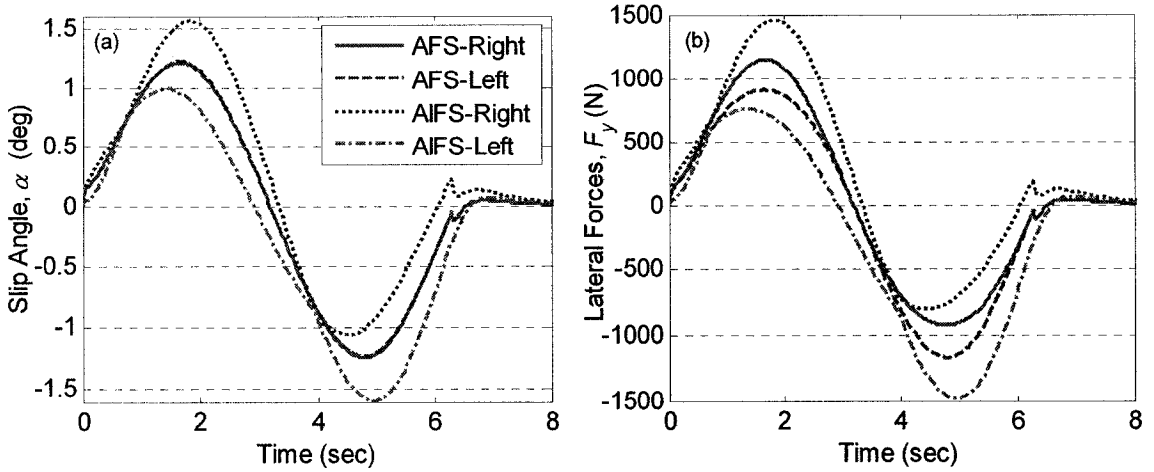

Figure 5.15: Slip-angles and lateral forces, oversteer vehicle, lane-change

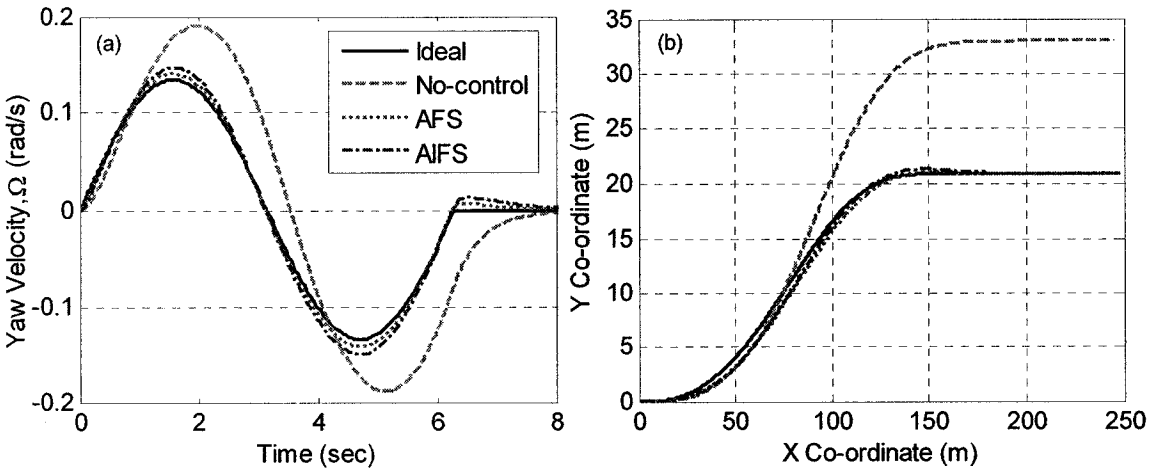

Figure 5.16: Yaw-rate and trajectory, oversteer vehicle, lane-change

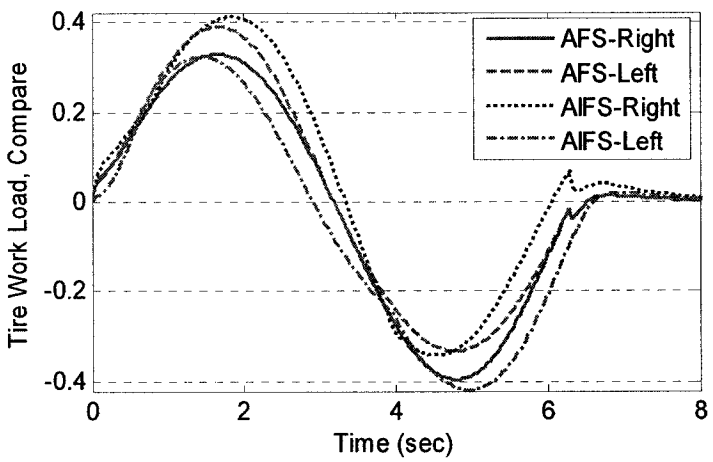

Figure 5.17: Tire work-load, oversteer vehicle, lane-change

Since the sign of controller command does not change in phase with steering command as explained earlier in this section, tire work-load is not equalized as shown in Figure 5.17. This would require further improvement in the control algorithm, and is likely that it can be realized by controlling both wheels, rather than only one at a time. Since the present control is based on one wheel, it is identified as a limitation where the proposed controller fails to equalize the tire work-load in case of lane-change of an oversteer vehicle. Although, an oversteer vehicle is not designed for road vehicles, an attempt to equalize tire work-load in this case is made by distributing the active steering command to both front wheels.

For an AIFS to operate on both front wheels simultaneously, it is suggested to distribute the active command on both wheels, by controlling the previously uncontrolled wheel in proportion to the controlled wheel. For the current case of lane-change of an oversteer vehicle, the other wheel is given a 40% controlled steering angle of the controlled wheel, which can be represented as:

$$\delta_i = \delta_{st} + \delta_c$$

$$\delta_o = \delta_{st} + 0.4\delta_c \tag{5.1}$$

Due to the oversteer nature, inner wheel is considered as the controlled wheel and only 40% of the controller command is added to the outer wheel. The results for tire work-load and resulting yaw-rate with distributed AIFS are shown in Figure 5.18 and are compared with AFS controlled vehicle. It is clearly noticed that the distributed AIFS is able to equalize the tire work-load better than the conventional AFS control. Although conventional AFS reduces the tire work-load for both front tires compared to no-control vehicle, it is incapable of equalizing them.

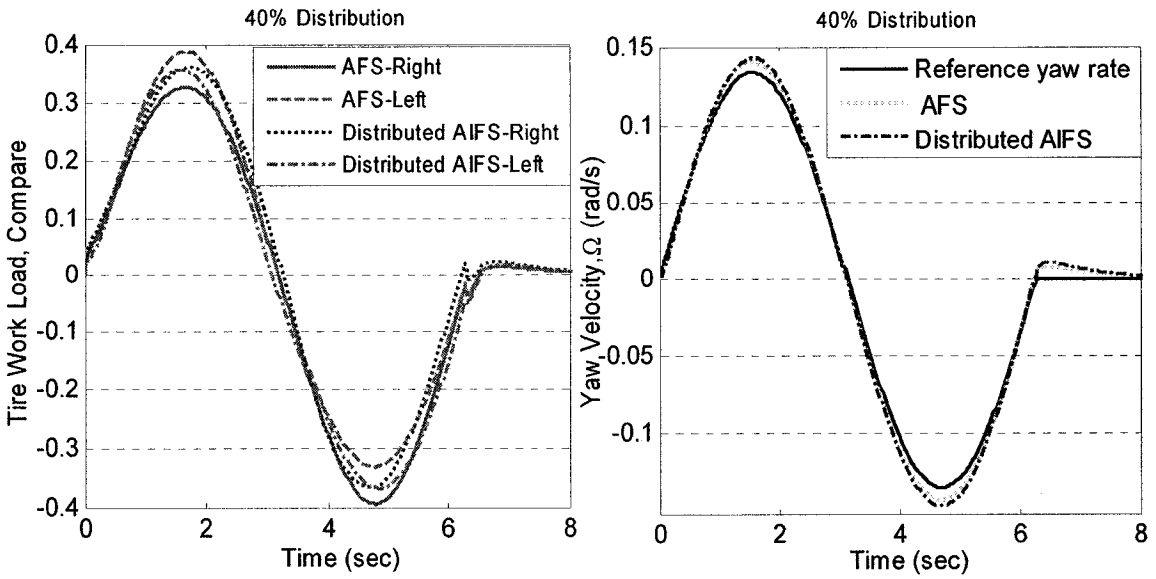

Figure 5.18: Tire work-load and yaw-rate, Distributed AIFS

From the results presented in this chapter so far it is seen that the proposed algorithm has the ability to control the vehicle with both under and oversteer characteristics. In each case, under step as well as sinusoidal inputs, the controller provides ideal responses at higher velocities. At the same time it equalizes the tire work-load between the left and the right tires in all cases except for lane-change of an oversteer vehicle, for which further improvements have been suggested. This equalization of work-load by AIFS will in turn prevent lateral force saturation and improve the stability limit of a vehicle.

Since AIFS can perform as well as AFS while providing important equalization of tire work-load, it may be interesting to examine the tire work-load characteristics reported in the literature for other control techniques. Figure 5.19 [23] presents the tire work-load time history for two different 4WS based controllers.

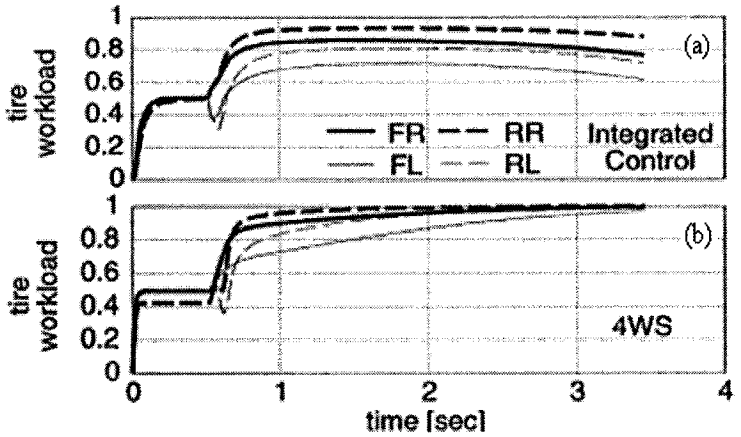

Figure 5.19: Tire work-load, conventional active controls, circular motion
a) Integrated 4WS+4 wheel torque, b) 4WS [23]

These tire work-loads were generated for a circular motion using 4WS+4 wheel active torque control and 4WS alone. In both cases a 4-wheel model is simulated for a step steering input of 6^{o} steering angle towards right, making the right wheel as the inner wheel. It can be seen that both right (inner) tires experience higher tire work-loads. The outer tire (left in this case) is not exploited to its limit to generate lateral forces and work under low tire work-loads.

In another study [19], vehicle handling is improved with integrated controls (DYC+AFS and DYC+4WS). The vehicle is simulated for a lane-change maneuver and tire work-loads were presented as shown in Figure 5.20 [19]. It is again observed that there is a significant difference in the tire work-loads developed at the inner and outer tires for all the control strategies. This shortcoming of available control strategies puts a limit on the control that can be exercised by active systems. This limitation of active controller can be overcome by the proposed AIFS system. The AIFS system can be easily integrated with DYC to provide improved handling and stability. It is easy to see that the proposed AIFS system will allow the integrated DYC system to generate required lateral force for stability even under the most extreme handling maneuvers.

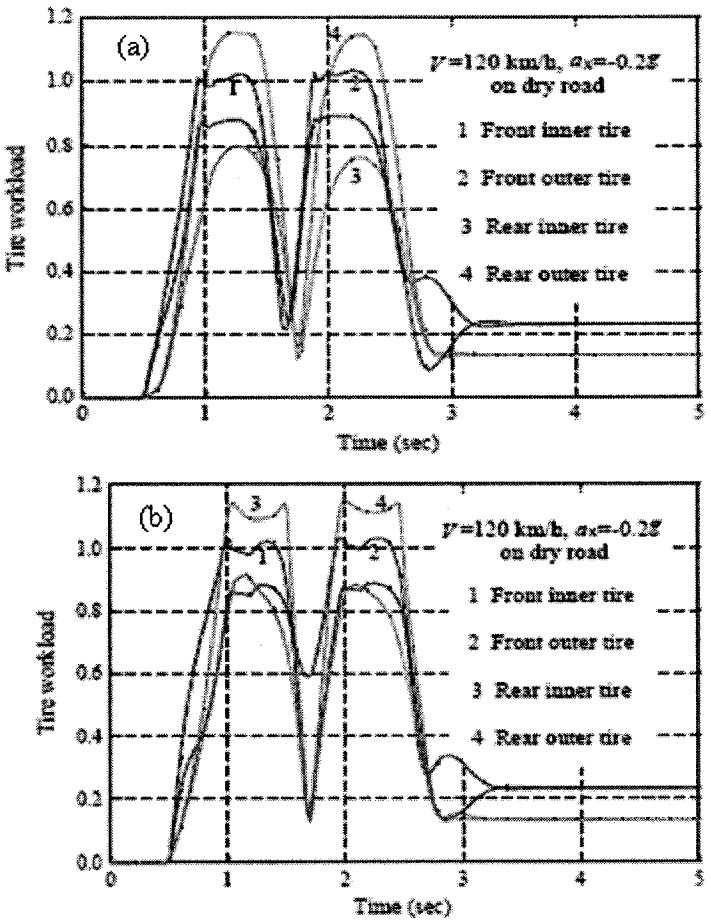

Figure 5.20: Tire work-load, conventional active controls, lane-change
a) DYC+AFS b) DYC+4WS [19]

5.3 Summary

An AIFS controller was developed based on the AIFS algorithm presented in the previous chapter. The controller proved to be stable for different vehicle models and steering commands. The AIFS controller when compared with conventional AFS control, showed significant improvement in tire work-load while giving similar handling response. Such AIFS control proves to be a promising control technique since higher forces can be generated from the same vehicle model. For further improvement of vehicle handling response, AIFS technique may be integrated with other control techniques.

Though, AIFS technique developed in this investigation did not show tire work-load improvements in an oversteer vehicle for lane-change maneuver, it is not of critical importance to improve the algorithm, since most of the road vehicles are designed to be understeer in nature. Further exploration of this is proposed in the future studies. Even though a control algorithm for AIFS is formulated, a control system is designed and vehicle response is analyzed, the most important question remains as how to implement such a control strategy in road vehicles without a 'drive-by-wire' system. For this purpose a steering mechanism with mechanical linkages is proposed in the next chapter.

6 Steering Mechanism for AIFS

The most important part of any control strategy is to implement it practically within given constraints. Without a suitable hardware to install a controlled steering mechanism, any proposed control technique is not of practical use at present. Due to issues such as electronic component failure risk, regulations require a mechanical linkage between the driver steering wheel and the road wheels. These regulations impede the use of electronically controlled 'drive-by-wire' system in road vehicles and physical constraints inside the car body and cost effectiveness make it difficult to design appropriate mechanical hardware. Due to such limitations most of the active steering control techniques could never be applied in road vehicles.

Only after BMW applied an active steering strategy [115, 116] using a planetary gear, discussed later in this chapter, it is now possible to fully implement an active front steering control in road vehicles. Unlike earlier active steering control techniques [17], BMW's active steering is not constrained to 3-4° steering angle. The proposed active independent steering technique is based on the similar principal of using planetary gear, but the independent command to both front wheels requires an unconventional steering rack design. Such a design for independent steering mechanism is conceptualized and presented in this chapter.

First, kinematics of conventional steering mechanism is discussed. Alternate steering mechanism is suggested. Then, BMW's active steering mechanism is analyzed. Finally, steering mechanism for active independent control is discussed.

6.1 Conventional Steering Geometry

As discussed earlier road vehicles must follow Ackerman ratio for the front wheels for a scrub free low speed turning. The theoretical relation between steering angle of inner and outer wheel is defined by Equation (3.4). A mechanism is required which allows the front wheels to be steered in this ratio for the given driver steering command. A mechanism with 4-bar linkage can be employed for this purpose. The mechanism used in road vehicles is based on a double slider-crank mechanism; one slider-crank pair for each wheel.

6.1.1 Slider-Crank Mechanism

A slider-crank mechanism consists of 4 linkages; 3 moving and 1 fixed. There are 3 rotary pairs and 1 sliding pair of joints. Gruebler's equation [123] is used to calculate the degrees of freedom of planar, closed linkages. The number of degrees of freedom of a linkage, also called its mobility, is:

$$m = 3(n - 1) - 2f \tag{6.1}$$

where, m = mobility = degrees of freedom

n = number of links (including a single ground link)

f = number of one degree of freedom joints (pin or slider joints)

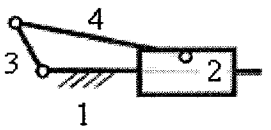

Figure 6.1: Slider-crank mechanism

A 4-bar slider-crank mechanism is shown in Figure 6.1. This mechanism according to the Equation (6.1) with $n = 4$ and $f = 4$, is a 1-DOF system. The slider (link 2) or crank (link 3), both can act as input to the mechanism and the other acts as output link, while the connecting rod (link 4) relates the motion between the two. Using this mechanism and changing different parameters such as linkage length, slider offset and initial angle of the crank, a steering mechanism can be designed to follow the Ackerman geometry closely. Two such mechanisms are joined together to form a steering mechanism. The steering rack acts as the slider for both mechanisms as input. The wheels are connected on cranks on each side. A half steering mechanism is shown in Figure 6.2 and the kinematical analysis is carried out to find the relation between the inner and outer wheel steering angle for a given input to the rack.

As seen in Figure 6.2, the relation between the inner and the outer steer angle depends on the length of linkages, l_1, l_2, the initial angle θ and the slider offset height h. The equation relating these parameters is derived as:

$$l_2 \sin(\theta - \delta_o) + \sqrt{l_1^2 - [l_2 \cos(\theta - \delta_o) - h]^2} = l_2[\,2\sin(\theta) - \sin(\theta + \delta_i)] + 2\sqrt{l_1^2 - [l_2 \cos(\theta) - h]^2} - \sqrt{l_1^2 - [l_2 \cos(\theta + \delta_i) - h]^2} \quad (6.2)$$

Above equation gives a relation between δ_o and δ_i, the inner and outer steering angles. By varying other parameters, one can achieve different ratio of inner and outer wheel steering for a given slider motion, i.e., for a given driver input. The parameters used in Equation (6.2), namely, l_1, l_2, θ and h are optimized to achieve the Ackerman ratio as

closely as possible in road vehicles, while it may be set to follow anti-Ackerman ratio for race-cars. This mechanism is also popularly used in industrial application to convert a sliding motion into a rotary motion or vice-versa due to least number of sliding pairs present and hence, avoiding unnecessary friction.

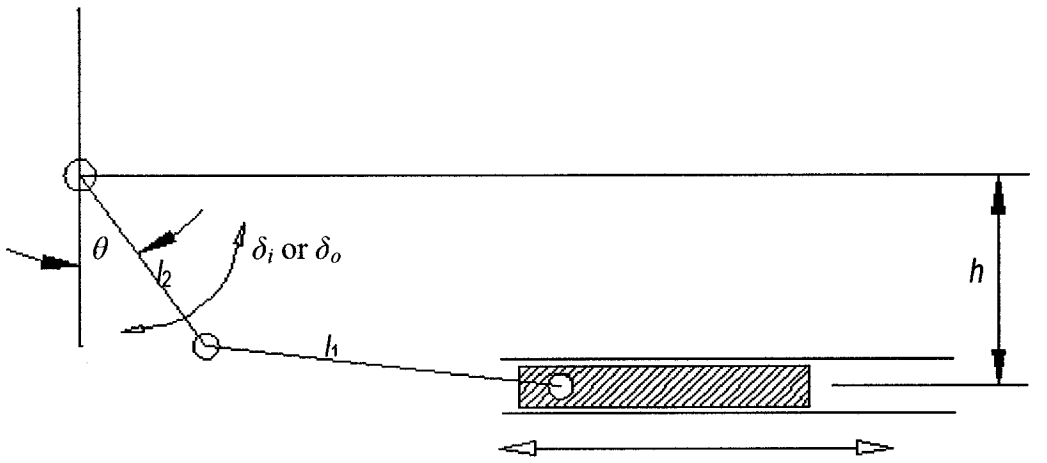

Figure 6.2: Half steering mechanism using Slider-crank

A slight modification to the slider-crank mechanism can convert it into what is known as Scotch-yoke mechanism which is discussed in the next subsection.

6.1.2 Scotch-Yoke Mechanism

By changing one more rotary-pair joint to a sliding-pair joint, a slider-crank mechanism can be converted to a scotch-yoke mechanism. Thus, a scotch-yoke mechanism consists of 2 rotary and 2 sliding pairs of joint as shown in Figure 6.3. According to Gruebler's relation (Equation 6.1), this mechanism can be shown to have 1-DOF. This setup is most commonly used in control valve actuators in high pressure oil and gas pipelines and has some distinct advantages over slider-crank mechanism, namely high torque output; fewer moving parts; smoother operation. As shown in Figure 6.3, the crank (link b), acts as a driving or driven link. Link c, the connecting link, acts as a slider inside the link d, which

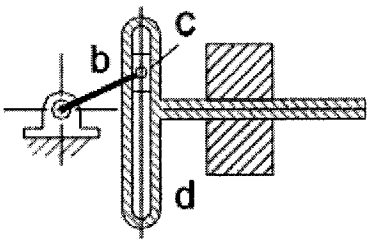

Figure 6.3: Scotch-yoke mechanism

is in turn a slider in the fixed link and works as a driven or driving link. A scotch-yoke mechanism is suggested as another possibility to be used in steering mechanism. Scotch-yoke mechanism gives freedom to vary the radius of curvature of the second slider, link d, and hence, the relation between inner and outer wheel steering angles can be manipulated precisely. A scotch-yoke mechanism with a finite radius of curvature for link d is shown in Figure 6.4 and the kinematical analysis is carried out.

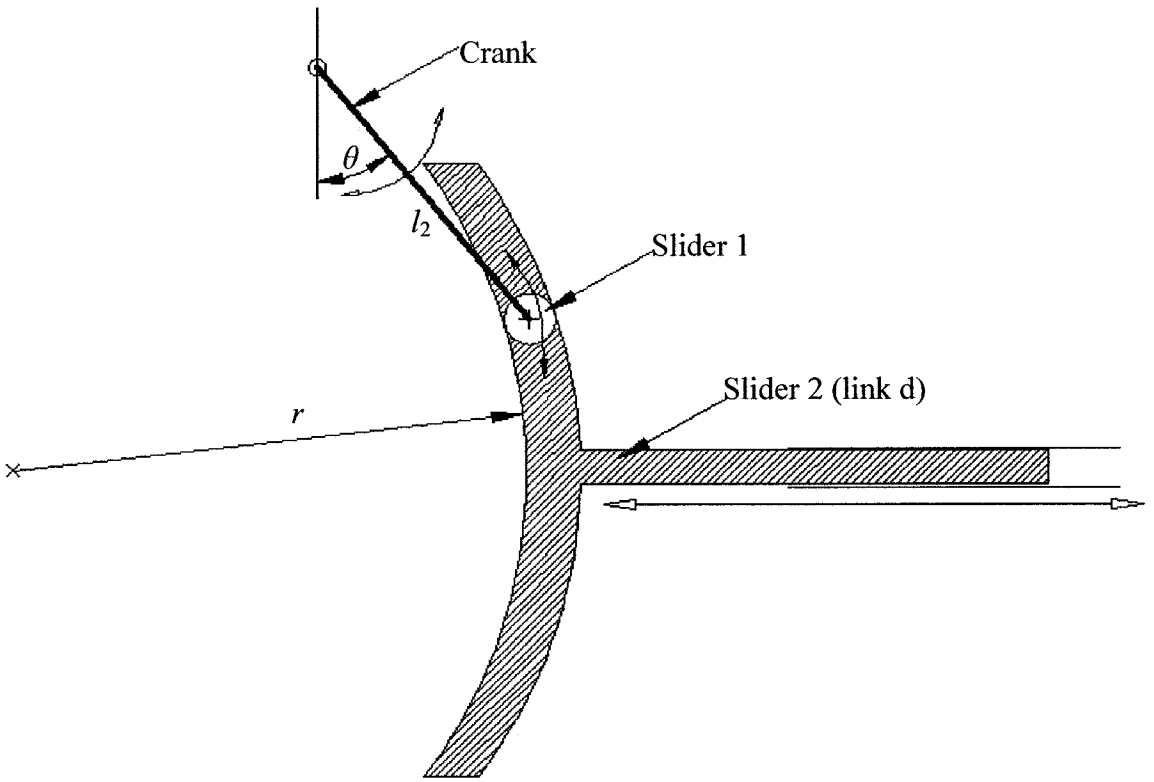

Figure 6.4: Half steering mechanism using Scotch-yoke

In the above figure a half steering mechanism using a scotch-yoke is presented. Depending on various parameters, such as, crank length l_2, crank initial-angle θ and radius of curvature r of link d, the relation between δ_i and δ_o, inner and outer wheel steering angles, can be derived and is given by the following equation:

$$l_2[\sin(\theta+\delta_i)-\sin(\theta)]+2r-\sqrt{r^2-l_2^2[\cos(\theta)-\cos(\theta+\delta_i)]^2} = l_2[\sin(\theta)-\sin(\theta-\delta_o)]+\sqrt{r^2-l_2^2[\cos(\theta-\delta_o)-\cos(\theta)]^2} \quad (6.3)$$

By varying different parameters the relation between δ_i and δ_o is plotted and compared with the ideal Ackerman curve in Figure 6.5:

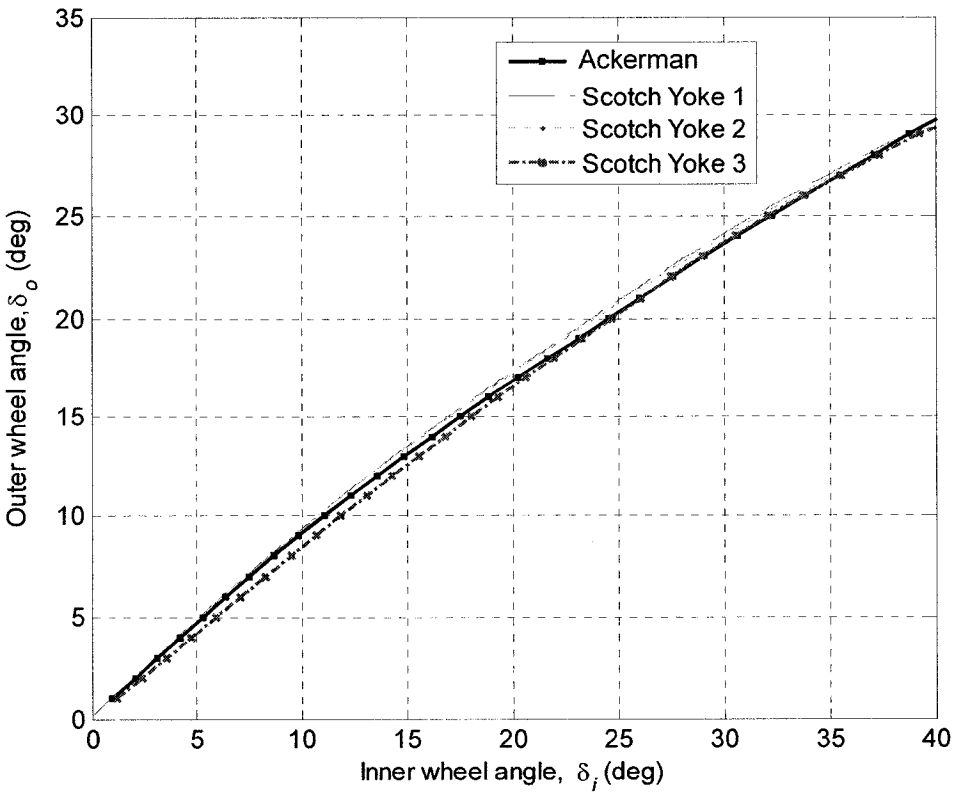

Figure 6.5: Ackerman vs. scotch-yoke mechanism

It is seen that the scotch-yoke mechanism follows the ideal curve very closely and can be optimized for better results. In the above mechanism a constant radius of curvature

for link d is used. The deviations from the ideal curve in different regions can be eliminated by changing the radius of curvature of link d at various points. Thus, a scotch-yoke mechanism provides flexibility of changing the relation between input and output within given constraints. However, due to continuous sliding of link c in the grove of link d, rapid wear of the slot in the yoke (link d) takes place, which prevents scotch-yoke to be a popular choice in industrial applications.

6.2 BMW's Active Steering

In recent years, there has been renewed interest on drive-by-wire, where the mechanical linkages in the steering assembly are replaced with torque/angle sensors and electric/hydraulic actuators to transmit the steering command from driver to the wheels. Sometimes, a single motor is used to steer the rack, while sometimes two motors are used to steer each wheel independently. But the applications of such mechanisms are very limited, as the government regulations impede the use of 'drive-by-wire' in road vehicles, and it is mandatory to use a mechanical linkage between steering wheel and the road wheels.

Within this constraint, BMW has designed a semi-mechanical steering mechanism using a 2-DOF planetary gear train. The system that BMW uses has a speed dependent variable steering ratio and also the ability to adjust for disturbances during driver reaction time via Dynamic Stability Control (DSC) [116]. This is achieved with a planetary gear with two inputs and one output and a fast transmission of information (100 Hz) from different sensors. The planetary gear is able to add or subtract a signal from the response

of the steering wheel that controls the road wheel angle. The planetary gear is situated between the steering column and the conventional steering rack as shown in Figure 6.6.

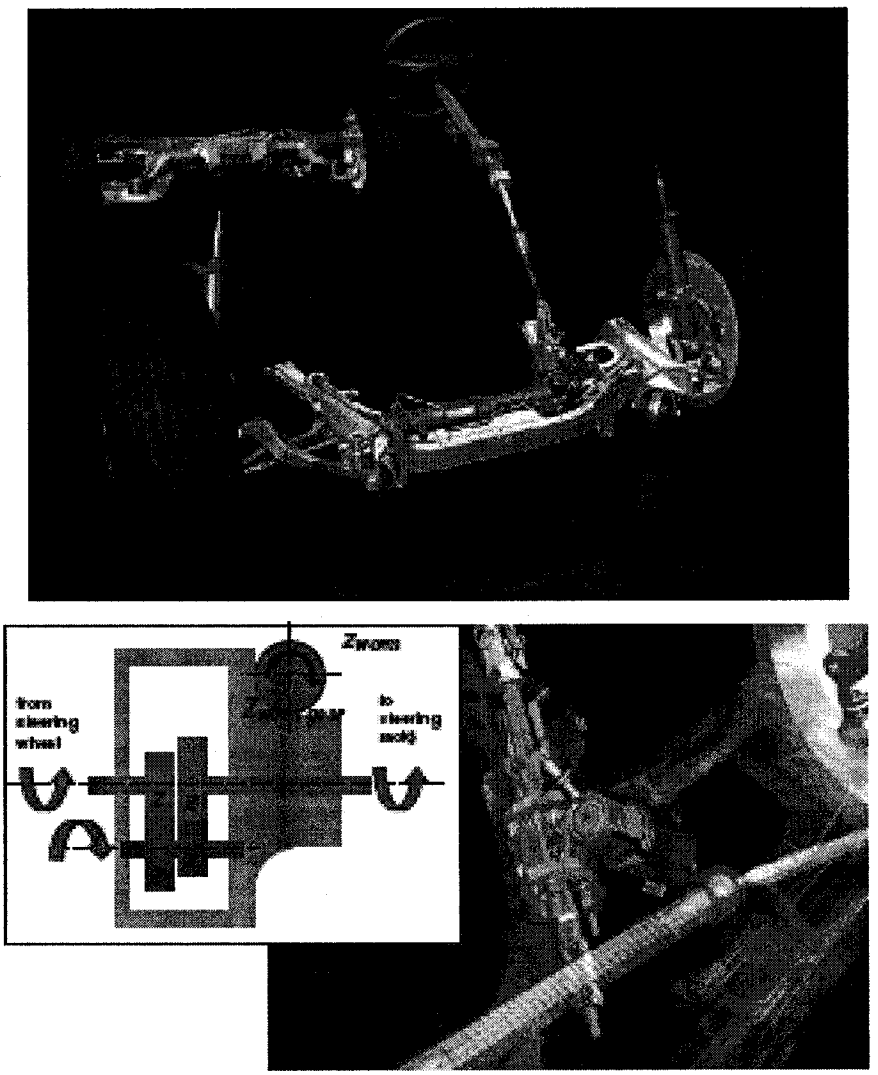

Figure 6.6: The placement of the planetary gear and the electric motor [116]

The planetary gear, also known as epicyclic gear is a gear system that consists of one or more outer gears, or *planet* gears, rotating about a central, or *sun* gear. Typically, the planet gears are mounted on a movable arm or *carrier* which itself may rotate relative to the sun gear. Planetary gearing systems may also incorporate the use of an outer ring gear or *annulus*, which meshes with the planet gears through its inner teeth. A typical planet gear system is shown in Figure 6.7.

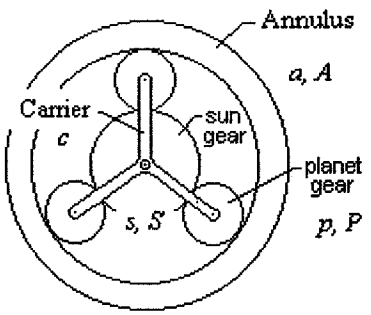

Figure 6.7: Planetary gear system

In many planetary gearing systems, one of these three basic components (sun, planet carrier or annulus) is held stationary; one of the two remaining components is an *input*, providing power to the system, while the last component is an *output*, receiving power from the system. The ratio of input rotation to output rotation is dependent upon the number of teeth in each gear, and upon which component is held stationary. One situation is when the planet carrier is held stationary, and the sun gear is used as input. In this case, the planetary gears simply rotate about their own axes at a rate determined by the number of teeth in each gear. If the sun gear has S teeth, and each planet gear has P teeth, then the ratio is equal to $-S/P$. This rotation of the planet gears can in turn drive the annulus, in a corresponding ratio. If the annulus has A teeth, then the annulus will rotate by P/A turns for each turn of the planet gears. Hence, for the planet carrier being 'locked':

- One turn of the sun gear results in $-S/P$ turns of the planets
- One turn of a planet gear results in P/A turns of the annulus

So, with the planetary carrier locked, one turn of the sun gear results in $-S/A$ turns of the annulus.

In other case, the annulus can be held stationary and the sun gear is used as the input, the planet carrier will be the output. The gear ratio in this case will be $1/(1+A/S)$.

This is the lowest gear ratio attainable with a planetary gear train. However, if input is given to both, sun and annulus, the output at planet carrier will be a linear superposition of these two inputs. Based on above two special cases, relation between the gear ratio of sun, annulus and carrier can be derived which is discussed further.

As discussed above, let the number of teeth in sun, each planet and annulus are *S*, *P*, and *A*, respectively. Let the angular velocity of each part is *s*, *p*, *a* and *c* for the sun, planet, annulus and carrier, respectively. The angular velocity of sun (*s*) and the carrier (*c*) is assumed to be in clock-wise direction and taken as positive, while the angular velocity of planet (*p*) and the annulus (*a*) is in the counter-clock-wise direction and is taken as negative. The clock-wise velocity would be represented with a '+' sign while the counter-clock-wise velocity is represented with a '-' sign. For the first case of fixed carrier, the relation can be written as:

$$s^{+}S = p^{-}P = a^{-}A \tag{6.4}$$

If the carrier is not restricted and allowed to rotate, the effect of rotation of carrier would come into the picture. For this case, if the system is observed from the carrier rotating frame of reference, above relation would still hold good for the relative velocities of each part with respect to the carrier. Hence, the absolute velocities of each part would follow:

$$(s^{+} - c^{+})S = (p^{-} + c^{+})P = (a^{-} + c^{+})A \tag{6.5}$$

The values of *s*, *p*, *a* and *c* are taken as the absolute values and hence, the carrier velocity is added to the planet and annulus velocities and not subtracted. From the first and last term of Equation (6.5) a relation between *s*, *c* and *a* can be derived as:

$$(s^{+} - c^{+})S = (a^{-} + c^{+})A \quad \Rightarrow \quad c^{+} = \frac{s^{+}S - a^{-}A}{S + A}$$

For the annulus velocity in the same direction as of the sun, one can write from the above equation:

$$c^{+} = \frac{s^{+}S + a^{+}A}{S + A} \quad \text{or} \quad c = \frac{s \cdot S + a \cdot A}{S + A} \tag{6.6}$$

Thus, the carrier velocity can be calculated as a linear superposition of known sun and annulus velocities. It can be observed that both special cases of fixed carrier and fixed annulus discussed earlier are satisfied by the above equation. According to the Equation (6.6) a planet gear system can have two independent input variables, from sun and annulus, and gives one combined output from the carrier.

In the BMW Active Steering system the sun gear is the input and the planet carrier is the output. The annulus is used for controller input by an electric motor steered by a computer. If the annulus is held fixed, then the steering ratio is constant and only dependent on the steering wheel. This way the active steering acts as a conventional rack and pinion steering mechanism. But if the annulus is in motion at the same time as the steering wheel, a variable steering ratio is attained. In some situations the annulus increases the response of the steering wheel, while in other situations the response is decreased.

At low vehicle velocities the planetary gear adds a contribution to the steering angle by rotating the annulus in the same direction as the steering angle, which makes the steering wheel lock-to-lock positions less than two rounds on the steering wheel. This is advantageous in parking situations and other 'slow moving - sharp turn' situations, since the driver can maintain the grip on the steering wheel. On the other hand, at high vehicle velocities the planetary gear subtracts a contribution to the driver steering angle by

rotating the annulus in opposite direction. This increases the safety for evasive maneuvers on the steering wheel and it provides an increased precision at highway driving.

This planetary gear system is not only used for changing the steering gear ratio between the driver steering wheel and the road wheels dependent on speed but also is used for actively controlling the vehicle yaw-rate by DSC. The active steering control calculates the vehicles desired path from the driver steering command and vehicle's ideal yaw-rate from vehicle forward velocity. If the vehicle shows a higher or lower yaw-rate than the desired yaw-rate due to its understeer characteristics, the active steering control reduces or increases the front steering angle by a small amount in order to achieve the desired or reference yaw-rate; keeping the driver steering wheel undisturbed. A detailed analysis of control technique using this active front steering control can be found in [124].

Although, such an active system can prove to be an excellent control strategy as all of the present AFS control techniques can be implemented using this 2-DOF steering system, yet, the use of planetary gear is limited to change the steer ratio between the steering wheel and both road wheels simultaneously, and not individually for each front wheel. If two of these planetary gears are used, one for each wheel, both front wheels can be steered independently for a given driver input. Such a steering mechanism is discussed in the next section.

6.3 Active Independent Steering Mechanism

An active steering for conventional steering mechanism was discussed in the previous section. The present investigation, however, is focused on an unconventional active independent steering technique and therefore requires an unconventional active steering mechanism to perform this task. An independent steering mechanism using 2 half racks and 2 planetary gear systems is developed in this section. The practical constraints under which the mechanism should be developed are:

- The mechanism should be symmetrical for right and left wheels.
- It should be fail safe and should be backed up by a conventional mechanical steering mechanism.
- It should be compatible with present road vehicles' physical constraints and should not require major changes in the chassis/suspension design.
- It should give the same feel to the driver as that of a conventional steering/active steering system.
- The cost should be reasonable.

Keeping all of the above constraints in mind, a design based on the available BMW's active steering mechanism is proposed. The independent steering mechanism employs 2 independent rack and pinion mechanisms for each wheel, driven by individual planetary gear systems. Each 'planetary gear - rack/pinion' mechanism works in the similar manner as the BMW's active steering [116]. The sun gears of both planet gears are directly driven by the steering column. The planet carrier of each gear system acts as the pinion for each rack. The annulus of each gear system is controlled by an individual

computer controlled electronic motor, which makes it possible to control each planet gear system individually. A schematic of this mechanism is shown in Figure 6.8.

The planet gear systems and the racks used for both wheels have same design parameters which makes this mechanism symmetrical for both front wheels. The mechanical connection between the steering wheel and the road wheels is maintained through the planet gear, thus making it safe. In case of any electronic failure, the annulus of both planet gear systems can be 'locked' as in the BMW's active steering [116], converting it into a conventional steering system. The only extra hardware added in this mechanism compared to the BMW's active steering are a half rack and another planet gear system with electronic motor, keeping rest of the mechanical linkages similar. This way, the proposed mechanism seems to be easily installable within the present vehicles without major changes in the chassis design. For the driver, the proposed steering mechanism would be similar to BMW's active steering mechanism in operation, since the proposed mechanism can also include the active steer ratio for slow and fast vehicle velocities. Finally, due to most of the hardware already present in the market and being implemented in the road vehicles, the proposed mechanism is expected not to impose a high cost from the manufacturing point.

A 3D model of the proposed mechanism is developed in graphics design software, Maya. The model only represents the mechanical connections between various parts and is not precise from the kinematical analysis. Screen shots of the model are shown in Figures 6.9-6.11. As seen in these figures, the input from the steering column goes to the sun gear of the first planetary gear system and then goes *through* the planet carriers to connect to the sun gear of the second planetary gear system. The planet carriers of both

gear systems are attached to individual pinion gears which run the racks for each wheel. Each rack acts as the slider for the slider-crank mechanism on either side, crank of which turns the road wheel on either side. The annulus of each gear system is also meshed with an electronic motor. Both of these motors are controlled independently by the computer. This way, for a given driver command, only outer or inner wheel can be controlled as required. Thus, perfect Ackerman or anti-Ackerman ratio can be attained when required.

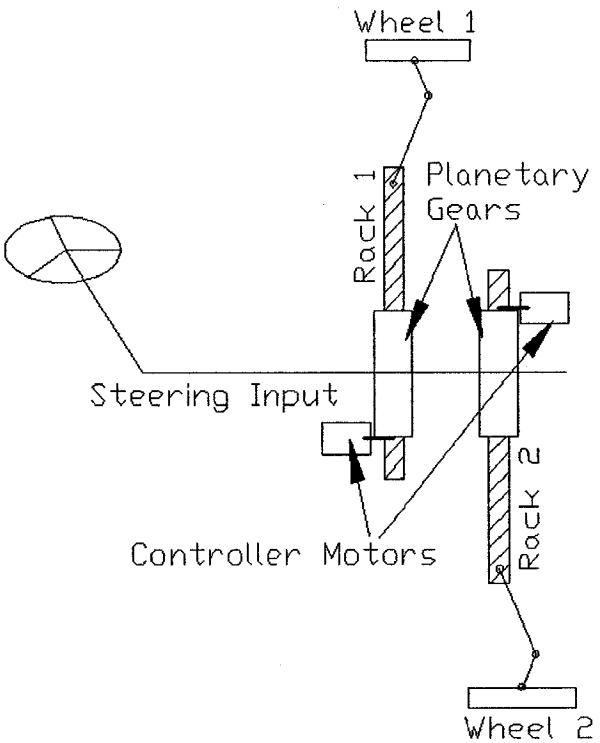

Figure 6.8: Mechanism with dual planetary gears for independent steering

Furthermore, through controller design, same system can be extended to provide independent input to selected wheel regardless of any driver command. Such input can generate a lateral force at the selected tire for enhancement of stability.

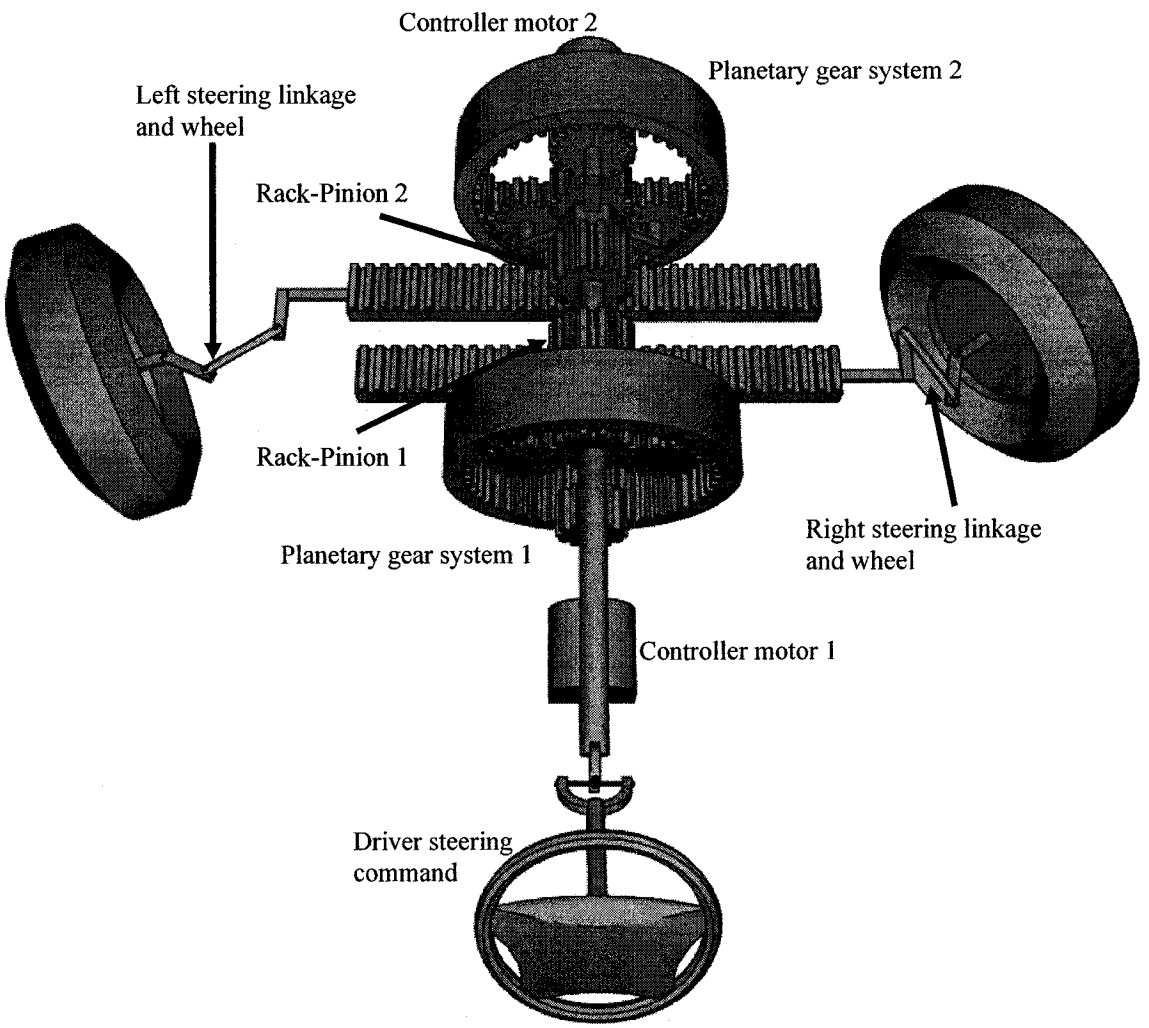

Figure 6.9: AIFS mechanism, full view

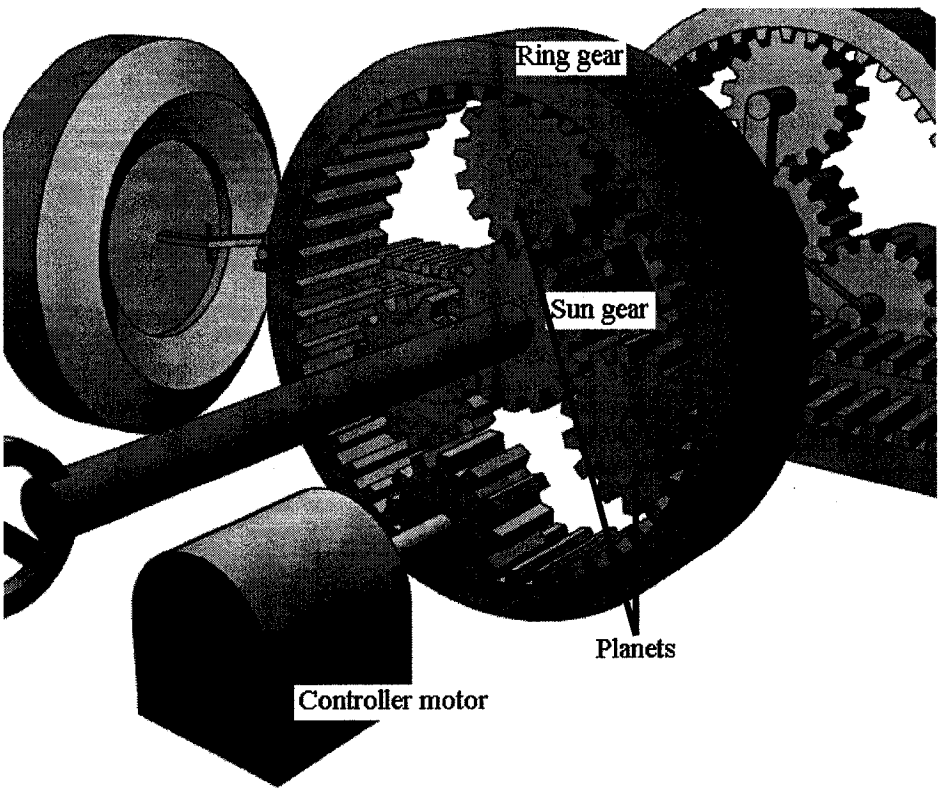

Figure 6.10: AIFS mechanism, planetary gear and controller motor

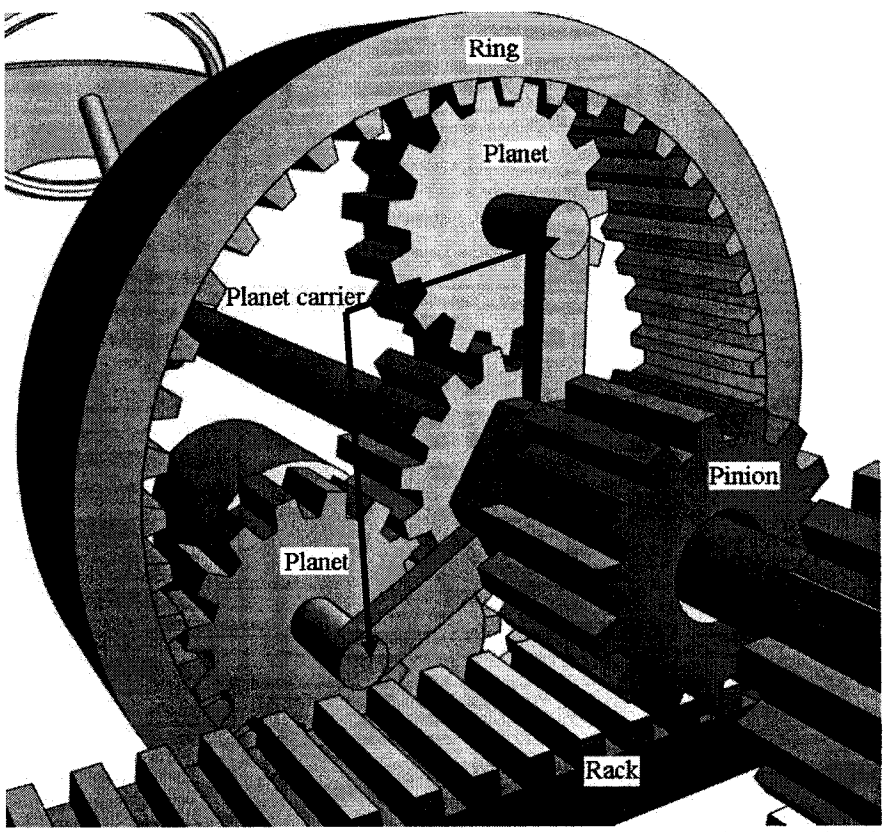

Figure 6.11: AIFS mechanism, planetary gear and rack-pinion mechanism

6.4 Summary

This chapter presented the kinematical analysis of a conventional steering system. It was shown that the similar relation for inner and outer wheel steering angles can be obtained by using a scotch-yoke mechanism in place of a slider-crank mechanism. Though, the scotch-yoke mechanism provides a higher torque output for the given input compared to the slider-crank mechanism, this deficiency of slider-crank is overcome by the power-steering system, installed in almost every vehicle currently. Yet, the scotch-yoke mechanism showed more flexibility in terms of the kinematical relation between inner and outer steer angle and hence, can be looked further into.

The active steering system developed by BMW was discussed. This mechanism opens doors to the existing AFS techniques and variable steer ratio, making driving easier and safer. The planetary gear system has been used in various industrial and auto applications, such as bicycle hub, construction equipment to provide high torque to drive wheels, automatic transmissions and other applications requiring large gear ratio of high torque transmission and velocity reduction. It has finally found its way in active steering control; an area which was incomplete due to physical constraints and could not be implemented.

The proposed mechanism takes the BMW's active steering one step further, controlling both front wheels individually, thus making proposed AIFS technique a practical approach to enhance handling performance and to introduce added stability and controllability. Only the mechanical concept for the system is presented here. A kinematical synthesis of the proposed independent steering mechanism and final design needs further study.

7 Conclusions & Future Recommendations

7.1 Highlights of the Study

The present investigation employed a 4-wheel vehicle model to study handling performance of road vehicles. The model developed was based on various nonlinearities encountered in vehicle dynamics studies and was compared with simpler bicycle model as well as professionally used CarSim simulations. Most other investigations in the field of vehicle handling utilize an approximate approach of a 4-wheel model in the form of a linear bicycle model. Therefore, use of a 4-wheel model in the present investigation gives more conservative and hence, safer results when compared to the other studies. For comparative study, performance measures were defined as target path, yaw-rate and resulting tire work-load. Target yaw-rate at any given speed is defined as V/R, where R is the radius of curvature of a neutral steer vehicle given by $L/\tan(\delta_{st})$. Ideal path is defined as the path that would be followed by a neutral steer vehicle. Vehicle behavior for understeer and oversteer handling characteristics was examined and compared with those of a neutral steer vehicle.

Various control strategies for handling performance improvement were studied and the importance of active front steering control was established. After comparing various control strategies, yaw-rate control using AFS proved to be an excellent choice. Vehicle behavior under a closed loop AFS control was examined. Effect of vehicle

handling characteristics on vehicle behavior and hence, on performance of the AFS control was observed. Shortcomings of the conventional control strategies in terms of possible vehicle instability were discussed. Comparing performance of road vehicles and race cars, anti-Ackerman steering mechanism certainly proved to be a better choice for handling improvements at high speeds. A conventional AFS control based on Ackerman steering, though could control vehicle yaw-rate, but failed to utilize the maximum available friction. On the other hand, a passive anti-Ackerman steering geometry showed not only improved vehicle path compared to the passive Ackerman steering, but also improved tire work-load.

Tire work-load was shown to be an important performance parameter and hence, should be optimized while applying any control strategy. Based on these experiences, a control strategy with independent control for both front wheels was suggested and implemented in the 4-wheel vehicle system. A mechanical steering mechanism based on a dual epicyclic gear system was proposed to realize a fail safe independent front steering input that can be adopted for AIFS system investigated in this work. Specific conclusions drawn from this investigation and a list of recommendations for future work are presented in the following sub-sections.

7.2 Specific Conclusions

The present investigation covered various aspects of vehicle dynamics study, including vehicle modeling, handling performance, active control and steering design. Based on the results of this investigation, following conclusions can be drawn:

- Similar handling performance results in terms of vehicle yaw-rate and target path were obtained with a single wheel control in AIFS when compared with a conventional 2-wheel control AFS system.

- Based on the theory of tire mechanics to generate forces, the proposed AIFS technique utilizes the maximum ability of the outer front tire to generate lateral forces. This strategy showed significant improvements in the tire work-load when compared with the conventional AFS.

- The logical yet simple algorithm, developed for AIFS technique, was able to control vehicle with understeer as well as oversteer characteristics under various steering maneuvers. The qualitative analysis of the proposed technique showed its contribution in stabilizing the vehicle, by maximizing the lateral force output.

- The only limitation observed for the proposed AIFS is its inability to equalize the tire work-load when the vehicle is strongly oversteer. In this case, in fact, a very large corrective steer angle is required. This deficiency, as illustrated, can be overcome by distributing the control to both front wheels.

- To implement the proposed AIFS control technique, a fail-safe steering mechanism, based on BMW's active steering, was proposed. The kinematical study of the mechanism was carried out; however, an accurate model design is required to finalize the mechanism.

7.3 Recommendations for Future Work

The present investigation can be considered the first step in exploring the concept of independent front wheel steering system. The potential of the concept was explored using a 4-wheel handling model and simple control system. As stated earlier, present investigation covers different aspects of vehicle dynamics study, further improvements in all of these areas is required before such an independent control technique can be implemented in the production vehicles. To this end, further study in the following areas can be carried out:

Vehicle Model

Although the vehicle model used in this study was a 4-wheel nonlinear model, it can further be improved by introducing the effects of aerodynamic drag, rolling resistance and suspension stiffness. These parameters will affect the normal load on tires and the friction forces acting on them. Also, combined slip during braking or accelerating while negotiating a turn will affect the lateral force generation ability of the tires.

Robust Control System

The control system used in the present study is based on a typical PI controller. The control algorithm is linear and the controller has no information about the saturation state of the tire lateral forces. In this case, if the forward velocity of the vehicle is higher than a certain value for a given steering command, such that the vehicle can never reach the reference state due to limited lateral forces, the controller will steer the wheels indefinitely, leading to vehicle instability. This shortcoming can be eliminated by using a

nonlinear robust controller. A quantitative stability analysis of the control algorithm should be carried out.

Severe Test Conditions

Vehicle behavior in severe conditions, such as side wind disturbance, double lane-change and split-μ maneuver can be examined to establish the robustness of the independent control technique.

Integrated Control

In the proposed control algorithm, only one wheel was controlled at a time. The *equalized* tire work-loads of the front tires in the present study are results of yaw-rate control, and are not *optimized* directly. If both front wheels are controlled independently with optimized steer angles, tire work-load can be *optimized* along with yaw-rate. Furthermore, the proposed AIFS can be integrated with other conventional control techniques, such as DYC to realize full vehicle control, i.e., yaw-rate and vehicle side-slip control.

Other Applications

The proposed mechanism with a full control capability at front wheels can be used for an optional drive-by-wire technology in future. The 2-DOF planetary gear system opens the possibility of controlling the vehicle path on automated guided highways and lane-keeping without any driver interference and without disturbing the steering wheel. This

mechanism can also be used in "automatic parking", already available in certain production cars, again, without disturbing the driver steering wheel.

Other major application of AIFS control technique could be the stability control in split-μ tracks. As shown in Figure 7.1, independent steering system makes it possible to actively steer only left wheel to generate lateral forces and counter moments, while the right tire on low friction surface is held straight to generate maximum possible longitudinal force for braking purpose, without risking it to get "locked".

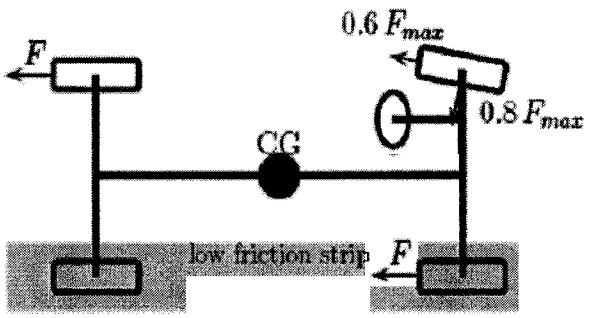

Figure 7.1: AIFS in split-μ condition

These arguments further establish the potential of AIFS control technique to improve the vehicle handling performance and hence, further research in this area would certainly take active steering control to another level.

References

1. Stanton, N.A. and Marsden, P. "From Fly-by-Wire to Drive-by-Wire: Safety Implications of Automation in Vehicles"; Safety Science, Oct 1996, Vol. 24 (1), pp. 35-49.

2. Stanton, N.A., Young, M., and McCaulder, B. "Drive-by-Wire: The Case of Driver Workload and Reclaiming Control with Adaptive Cruise Control"; Safety Science, Nov 1997, Vol. 27 (2), pp. 149-159.

3. Favre, C. "Fly-by-Wire for Commercial Aircraft - The Airbus Experience" in "Advances in Aircraft Flight Control"; Taylor & Francis, London, 1996, pp. 211-229.

4. D. Stoll and S. Bourne, "The National Advanced Driving Simulator: Potential Applications to ITS and AHS Research," Proceedings of 6th ITS (Intelligent Transportation Society) American Annual Meeting, ITS America, Washington, D.C., Apr. 1996.

5. Daganzo, C. "The Cell Transmission Model. Part I: A Simple Dynamic Representation of Highway Traffic". California Partners for Advanced Transit and Highways (PATH). Research Reports: Paper UCB-ITS-PRR-93-7, Jan. 1, 1992.

6. UMTRI Transportation Data Center Data Set Codebook, No. 2005-2, June 2005.

7. Stanton, N. and Marsden, P. "Drive-by-Wire Systems: Some Reflections on the Trend to Automate the Driver Role"; Proceedings of the Institution of Mechanical Engineers Part D: Journal of Automobile Engineering, 1997, Vol. 211 (4), pp. 267-76.

8. Sweet, W. "Glass Cockpit"; IEEE Spectrum, Vol. 32 (9), pp. 30, 1995.

9. Pant, A.G. "Meshed Stability of Formations of Unmanned Aerial Vehicles"; Ph.D. Thesis, University of California, Berkely, 2002.

10. Golconda, S. "Steering Control for a Skid-Steered Autonomous Ground Vehicle at Varying Speed"; Master's Thesis, University of Louisiana, Lafayette, 2005.

11. Marquard, E. "Fortschritte in der Berechnung von Fahrzeug-Zusammenstoben", Automobiltechnis-che Zeitschrift; 1966, Vol: 68 (3), pp. 74–80.

12. Hegazy, S., Rahnejat, H. and Hussain, K. "Multi-Body Dynamics in Full-Vehicle Handling Analysis under Transient Manoeuvre", Vehicle System Dynamics, July 2000, Vol. 34 (1), pp: 1–24.

13. Kiencke, U. and Nielsen, L. "Automotive Control Systems"; Springer-Verlag, New York, USA, 2000.

14. Williams, R.A. "Automotive Active Suspensions Part 1: Basic Principles"; Proceedings of the Institution of Mechanical Engineers Part D: Journal of Automobile Engineering, 1997, Vol. 211 (6), pp 415-426.

15. Cech, I. "Anti-Roll and Active Roll Suspensions"; Vehicle System Dynamics, 2000, Vol. 33, pp. 91–106.

16. Wong, J.Y. "Theory of Ground Vehicles"; 3rd Edition, Wiley-Interscience, New York, NY, USA, 1978.

17. Ackermann, J., Odenthal, D. and Bunte, T. "Advantages of Active Steering for Vehicle Dynamics Control"; 32nd International Symposium on Automotive Technology and Automation, Vienna, Austria, 1999, pp. 263-270.

18. Mokhiamar, O. and Abe, M. "Active Wheel Steering and Yaw Moment Control Combination to Maximize Stability as well as Vehicle Responsiveness during Quick Lane Change for Active Vehicle Handling Safety"; Proceedings of the Institution of Mechanical Engineers Part D: Journal of Automobile Engineering, 2002, Vol. 216 (2), pp. 115-124.

19. Mokhiamar, O. and Abe, M. "Effects of Model Response on Model Following Type of Combined Lateral Force and Yaw Moment Control Performance for Active Vehicle Handling Safety"; JSAE Review, Vol. 23 (4), Oct. 2002, pp. 473-480.

20. Velardocchia, M., Morgando, A. and Sorniotti, A. "Four-Wheel-Steering Control Strategy and its Integration with Vehicle Dynamics Control and Active Roll Control"; SAE paper no. 2004-01-1061.

21. Brown, G.L., and Hung, J.C. "A Mathematical Model for Vehicle Steering Control"; 20th International Conference on Industrial Electronics, Control and Instrumentation (IECON '94), Bologna, Italy, 5-9 Sep 1994, Vol. 3, pp. 2027-2032.

22. Sienel, W. "Estimation of the Tire Cornering Stiffness and its Application to Active Car Steering"; Proceedings of the 36th Conference on Decision & Control, San Diego, California, USA, Dec. 1997, pp. 4744-4749.

23. Horiuchi, S., Okada, K. and Nohtomi, S. "Improvement of Vehicle Handling by Nonlinear Integrated Control of Four Wheel Steering and Four Wheel Torque"; JSAE Review, Vol. 20 (4), Oct. 1999, pp. 459-464.

24. Pacejka, H.B., Bakker, E., and Nyborg, L. "Tyre Modeling for Use in Vehicle Dynamics Studies"; SAE paper no. 870421, 1987.

25. Hebden, R.G., Edwards, C and Spurgeon, S.K. "Automotive Steering Control in a Split- μ Manoeuvre Using an Observer-Based Sliding Mode Controller"; Vehicle System Dynamics, 2004, Vol. 41 (3), pp. 181–202.

26. Guvenc, B.A., Bunte, T., Odenthal, D. and Guvenc, L. "Robust Two Degree-of-Freedom Vehicle Steering Controller Design"; IEEE Transactions on Control Systems Technology, July 2004, Vol. 12 (4), pp. 627- 636.

27. Chang, Y.P., Moustafa, E.G. and Streit, D.A. "Literature Survey of Transient Dynamic Response Tyre Models'; International Journal of Vehicle Design, 2004, Vol. 34 (4), pp. 354-386.

28. Sharp, R. S. and El-Nashar, M. A. "A Generally Applicable Digital Computer Based Mathematical Model for the Generation of Shear Forces by Pneumatic Tyres"; Vehicle System Dynamics, 1986, Vol. 15, 187-209.

29. Bernard, J. E., Segel, L. and Wild, R. E. "Tire Shear Force Generation during Combined Steering and Braking Maneuvers"; SAE paper no. 770852, 1977.

30. Pacejka, H. B. "Analysis of Tire Properties" Chapter 9 in "Mechanics of Pneumatic Tires" (Ed. S. K. Clark), 2nd edition, NBS Monograph 122, Washington, D.C., 1981.

31. Flegl, H., Foldi, T. and Witte, L. "Handling Characteristics of Four-Wheel Drive Vehicles"; Proceedings of the 8th Symposium on The Dynamics of Vehicles on Roads and on Railway Tracks, 1984, pp. 165-178.

32. Segel, L. "The Tire as a Vehicle Component"; Mechanics of Transportation Suspension Systems, The Winter Meeting of the ASME, Houston, Texas, 30 Nov.-5 Dec., 1975.

33. Lugner, P., Lorenz, R. and Schindler, E. "The Connexion of Theoretical Simulation and Experiments in Passenger Car Dynamics"; Proceedings of the 8th IAVSD Symposium on The Dynamics of Vehicles on Roads and on Railway Tracks, 1984, pp. 317-330.

34. Allen, R. W., Magdaleno, R. E., Rosenthal, T. J., Klyde, D. H. and Hogue, J. R. "Tire Modeling Requirements for Vehicle Dynamics Simulation"; SAE paper no. 950312 (SP-1074), 1995.

35. Russo, M., Russo, R. and Volpe, A. "Car Parameters Identification by Handling Manoeuvres"; Vehicle System Dynamics, 2000, Vol. 34, pp. 423–436.

36. Best, M.C., Gordon, T.J. and Dixon, P.J. "An Extended Adaptive Kalman Filter for Real-time State Estimation of Vehicle Handling Dynamics"; Vehicle System Dynamics, 2000, Vol. 34 (1), pp. 57 – 75.

37. Jang, B. and Karnopp, D. "Simulation of Vehicle and Power Steering Dynamics Using Tire Model Parameters Matched to Whole Vehicle Experimental Results"; Vehicle System Dynamics, 2000, Vol. 33 (2), pp. 121–133.

38. Mammar, S. and Koenig, D. "Vehicle Handling Improvement by Active Steering"; Vehicle System Dynamics, 2002, Vol. 38 (3), pp. 211-242.

39. Sharp, R. S., Casanova, D. and Symonds, P. "A Mathematical Model for Driver Steering Control, with Design, Tuning and Performance Results"; Vehicle System Dynamics, 2000, Vol. 33 (5), pp. 289–326.

40. Sharp, R.S. "Testing and Improving a Tyre Shear Force Computation Algorithm"; Vehicle System Dynamics 2004, Vol. 41 (3), pp. 223–247.

41. Beato, M., Ciaravola, V., Russo, M. and Volpe, A. "Lateral Tyre Force by a Milliken Test on a Flat Track Roadway Simulator"; Vehicle System Dynamics, 2000, Vol. 34 (2), pp. 117–129.

42. Samadi, B., Kazemi, R., Nikravesh, K.Y. and Kabganian, M. "Real-Time Estimation of Vehicle State and Tire-Road Friction Forces"; Proceedings of the American Control Conference, Arlington, VA, USA, June 25-27, 2001, Vol. 5, pp. 3318-3323.

43. Yi, K., Hedrick, K. and Lee, S.C. "Estimation of Tire-Road Friction Using Observer Based Identifiers"; Vehicle System Dynamics, 1999, Vol. 31 (4), pp. 233–261.

44. Sayers, M.W. "Vehicle Models for RTS Applications"; Vehicle System Dynamics, 1999, Vol. 32 (4-5), pp.421–438.

45. Sharp, R.S. and Bettella, M. "Tyre Shear Force and Moment Descriptions by Normalisation of Parameters and the "Magic formula"; Vehicle System Dynamics, 2003, Vol. 39 (1), pp. 27–56.

46. Bolzern, P., Cheli, F., Falciola, G. and Resta, F. "Estimation of the Non-Linear Suspension Tyre Cornering Forces from Experimental Road Test Data"; Vehicle System Dynamics, 1999, Vol. 31 (1), pp. 23–34.

47. Liu, C.S. and Peng, H. "Road Friction Coefficient Estimation for Vehicle Path Prediction"; Vehicle System Dynamics, 1996, Vol. 25 Suppl., pp.413-425.

48. Park, K., Heo, S.J. and Baek, I. "Controller Design for Improving Lateral Vehicle Dynamic Stability". JSAE Review, 2001, Vol. 22 (4), pp. 481–486.

49. Bernard, J.E., Segel, L. and Wild, R.E. "Tire Shear Force Generation during Combined Steering and Braking Maneuvers" SAE paper no. 770852, 1977.

50. Bernard, J., and Clover, C. L., "Tire Modeling for Low-Speed and High-Speed Calculations"; SAE paper no. 950311, 1995.

51. Sakai H. "Theoretical and Experimental Studies on the Dynamic Properties of Tyres. Part 3: Calculation of the Six Components of Force and Moment of a Tyre"; International Journal of Vehicle Design, 1981, Vol. 2(3), pp 335-372.

52. Deur, J., Asgari, J. and Hrovat, D. "A 3D Brush-type Dynamic Tire Friction Model"; Vehicle System Dynamics, 2004, Vol. 42 (3), pp. 133–173.

53. Denti, E. and Fanteria, D. "Models of Wheel Contact dynamics: An Analytical Study on the In-Plane Transient Responses of a Brush Model", Vehicle System Dynamics, 2000, Vol. 34 (3), pp. 199–225.

54. Svendenius, J. "Tire Models for Use in Braking Applications"; Licentiate thesis, ISRN LUTFD2/TFRT--3232--SE, Department of Automatic Control, Lund University, Sweden, November 2003.

55. Szostak, H.T., Allen, R.W. and Rosenthal, T.J. "Analytical Modeling of a Driver Response in Crash Avoidance Maneuvering Volume II: An Interactive Tire Model for Driver/Vehicle Simulation"; U.S. Department of Transportation, Report No. DOT HS 807-271, April 1988.

56. Schuring, D.J. "Tire Parameter Determination, Volume I – Summary"; NHTSA DOT HS 802-086, Nov 1976.

57. Schuring, D.J. "Tire Parameter Determination, Volume II – Technical Report: Part I, Test Methodology"; NHTSA DOT HS 802-087, Nov 1976.

58. Ray, L.R. "Nonlinear State and Tire Force Estimation for Advanced Vehicle Control"; IEEE Transactions on Control Systems Technology, March 1999, Vol. 3 (1), pp. 117-124.

59. Ray, L.R. "Non-linear Tire Force Estimation and Road Friction Identification: Simulation and Experiments"; Automatica, 1997, Vol. 33 (10), pp. 1819-1833.

60. Stengel, R. F. "Stochastic Optimal Control: Theory and Application"; John Wiley and Sons, New York, 1986.

61. Kalman, R.E. "A New Approach to Linear Filtering and Prediction Problems"; Transactions of the ASME- Journal of Basic Engineering, 1960, Vol. 82, pp. 35-45.

62. DiMaggio, S.J. and Bieniek, M.P. "Vehicle Dynamics Using a Limit Surface Treatment of the Tyre-Road Interface"; Proceedings of the Institution of Mechanical Engineers Part D: Journal of Automobile Engineering, 1998, Vol. 212 (5), pp. 347-356.

63. Maurice, J.P., Berzeri, M. and Pacejka, H.B. "Pragmatic Tyre Model for Short Wavelength Side Slip Variations"; Vehicle System Dynamics, 1999, Vol. 31 (2) pp. 65–94.

64. Milliken, W.F. and Miliken, D.L. "Race Car Vehicle Dynamics"; SAE International, Warrendale, PA, USA, 1998.

65. Qu, Q. and Liu, Y. "On Lateral Dynamics of Vehicle Based on Nonlinear Characteristics of Tires"; Vehicle System Design, 2000, Vol. 34 (2), pp. 131-141.

66. Lacombe, J. "Tire Model for Simulations of Vehicle Motion on High and Low Friction Road Surfaces"; Proceedings of the 32nd conference on Winter simulation, Orlando, Florida, USA, 2000, pp. 1025–1034.

67. Park, J.H. and Kim, C.Y. "Wheel Slip Control in Traction Control System for Vehicle Stability"; Vehicle System Dynamics, 1999, Vol. 31 (4), pp. 263–278.

68. Huh, K. "Active Steering Control Based on The Estimated Tire Forces"; Proceedings of the American Control Conference, San Diego, California, USA, June 1999, Vol. 1, pp. 729-933.

69. Segel, L. "Theoretical Prediction and Experimental Substantiation of the Response of the Automobile to Steering Control"; Proceedings of the Institution of Mechanical Engineers, Automotive Division, 1956, pp. 26–46.

70. McHenry, R. R., "An Analysis of the Dynamics of Automobiles during Simultaneous Cornering and Ride Motions, in Handling of Vehicles under Emergency Conditions"; Proceedings of the Institution of Mechanical Engineers, 1968-9, No.13, pp. 28-48.

71. Shladover, S. E. et al "Steering Controller Design for Automated Guideway Transit Vehicles"; Journal of Dynamic Systems, Measurements and Control, 1978, Vol. 100, pp. 1-8.

72. Yih, P., Ryu, J. and Gerdes, J.C. "Modification of Vehicle Handling Characteristics via Steer-By-Wire" In Proceedings of the American Control Conference, 2003, Vol. 13 (6), pp. 965- 976.

73. Ryu, J., Rossetter, E. and Gerdes, J.C. "Vehicle Sideslip and Roll Parameter Estimation using GPS"; In Proceedings of the 6th International Symposium on Advanced Vehicle Control (AVEC'02), Hiroshima, Japan, 2002.

74. Bevly, D.M., Gerdes, J.C. and Wilson, C. "The use of GPS Based Velocity Measurements for Measurement of Sideslip and Wheel Slip"; Vehicle System Dynamics, 2002, Vol. 38 (2), pp. 127-147.

75. Shaout, A., Jarrah, M.A., Al-Araji, H. and Al-Tell, K. "A Nonlinear Optimal Four Wheels Steering Controller"; Proceedings of the 43rd IEEE Midwest Symposium on Circuits and Systems, 08 Aug.-08 Nov., Lansing, MI, USA, 2000, Vol. 3, pp. 1426-1429.

76. Elbeheiry, E.M., Zeyada, Y.F. and Elaraby, M.E. "Handling Capabilities of Vehicles in Emergencies Using Coordinated AFS and ARMC Systems"; Vehicle System Dynamics, 2001, Vol. 35 (3), pp. 195-215.

77. You S-S. and Jeong S-K. "Vehicle Dynamics and Control Synthesis for Four-Wheel Steering Passenger Cars"; Proceedings of the Institution of Mechanical Engineers Part D: Journal of Automobile Engineering, Dec. 1998, Vol. 212 (6), pp. 449-461.

78. Ackermann, J. and Odenthal, D. "Damping of Vehicle Roll Dynamics by Gain Scheduled Active Steering"; Proceedings of European Control Conference, Karlsruhe, Germany, 1999.

79. Tahami F., Farhangi, S. and Kazemi, R. "A Fuzzy Logic Direct Yaw-Moment Control System for All-Wheel-Drive Electric Vehicles"; Vehicle System Dynamics 2004, Vol. 41 (3), pp. 203–221.

80. Nagai, M., Shino, M. and Gao, F. "Study on Integrated Control of Active Front Steer Angle and Direct Yaw Moment"; JSAE Review, July 2002, Vol. 23 (3), pp. 309-315.

81. Furukawa, Y. and Abe, M. "Advanced Chassis Control Systems of Vehicle Handling and Active Safety"; Vehicle System Dynamics, 1997, Vol. 28 (2-3), pp. 59-86.

82. Timothy, J.G. and Best, M.C. "Lyapunov Control of Vehicle Handling Dynamics", JSAE Review, March 1999, Vol. 20, pp. 453-458.

83. Rossetter, E.J. and Gerdes, J.C. "A Study of Lateral Vehicle Control Under a 'Virtual' Force Framework"; Proceedings of 6th the International Symposium on Advanced Vehicle Control (AVEC'02), 2002, Hiroshima, Japan.

84. Huh, K., Kim, J. and Yi, K. "Monitoring System Design for Estimating the Lateral Tyre Force"; Proceedings of the Institution of Mechanical Engineers Part D: Journal of Automobile Engineering, April 2003, Vol. 217 (4), pp. 247-256.

85. Venhovens, P.J.Th. and Naab, K. "Vehicle Dynamics Estimation Using Kalman Filters"; Vehicle System Dynamics, 1999, 32 (2-3), pp.171–184.

86. Takezono, S., Minamoto, H. and Tao, K. "Two-Dimensional Motion of Four-Wheel Vehicles"; Vehicle System Dynamics, 1999, 32 (6), pp. 441–458.

87. Kasselmann, J. and Keranen, T. "Adaptive steering"; Bendix Technical Journal, 1969, Vol. 2, pp. 26-35.

88. Abe, M., Kano, Y., Suzuki, K., Shibahata, Y., and Furukawa, Y. "Side-Slip Control to Stabilize Vehicle Lateral Motion by Direct Yaw Moment"; JSAE Review, Oct. 2001, Vol. 22 (4), pp. 413-419.

89. O'Kane, C.M., and Timoney, S.S. "Investigation of Four-Wheel Steering Algorithms for a Formula SAE Car"; SAE 2004 World Congress & Exhibition, March 2004, Detroit, MI, USA, paper No. 2004-01-1066 (SP-1869).

90. Gordon, T., Howell, M. and Brandao, F. "Integrated Control Methodologies for Road Vehicles", Vehicle System Dynamics, 2003, Vol. 40 (1-3), pp. 157–190.

91. You, S.S and Kim, H.S. "Lateral Dynamics and Robust Control Synthesis for Automated Car Steering"; Proceedings of the Institution of Mechanical Engineers Part D: Journal of Automobile Engineering, Jan. 2001, Vol. 215 (1), pp. 31-43.

92. Lv, H.M., N. Chen, N. and Li, P. "Multi-Objective H Optimal Control for Four-Wheel Steering Vehicle Based on Yaw Rate Tracking"; Proceedings of the Institution of Mechanical Engineers Part D: Journal of Automobile Engineering, October 2004, Vol. 218 (10), pp. 1117-1123.

93. Mammar, S. "Two-Degree-of-Freedom H∞ Optimization and Scheduling for Robust Vehicle Lateral Control"; Vehicle System Dynamics, 2000, Vol. 34 (6), pp. 401–422.

94. Mammar, S., Iaona, T.R., Glaser, S. and Duc, G. "Lateral Driving Assistance Using Robust Control and Embedded Driver-Vehicle-Road Model"; Vehicle System Dynamics Supplement, 2004, Vol. 41, p.311-320.

95. Velenis, E., Tsiotras, P., Canudas-de-Wit, C. and Sorine, M. "Dynamic Tyre Friction Models for Combined Longitudinal and Lateral Vehicle Motion"; Vehicle System Dynamics, 2005, Vol. 43(1), pp. 3-29.

96. Tsiotras, P., Velenis, E. and Sorine, M. "A LuGre Tire Friction Model with Exact Aggregate Dynamics"; Vehicle System Dynamics, 2004, Vol. 42 (3), pp. 195-210.

97. Canudas-de-Wit, C. and Tsiotras, P. "Dynamic Tire Friction Models for Vehicle Traction Control"; Proceedings of 38th IEEE Conference of Decision and Control, Phoenix, AZ, USA, 1999.

98. Canudas-de-Wit, C. and Horowitz, R. "Observers for Tire/Road Contact Friction using only Wheel Angular Velocity Information"; Proceedings of 38th IEEE Conference of Decision and Control, Phoenix, AZ, USA, 1999.

99. Yi, J., Alvarez, L., Horowitz, R. and Canudas-de-Wit, C. "Adaptive Emergency Braking Control in Automated Highway System using Dynamic Tire/Road Friction Model" Proceedings of 38th IEEE Conference of Decision and Control, Sydney, Australia, 2000.

100. Claeys, X., Yi, J., Alvarez, L., Horowitz, R. and Canudas-de-Wit, C. "A Dynamic Tire/Road Friction Model for 3D Vehicle Control and Simulation"; Proceedings of 2001 IEEE Intelligent Transportation Systems Conference, Oakland, CA, USA, August 25-29, 2001.

101. Canudas-de-Wit, C., Olsson H., Astrom K. J. and Lischinsky, P. "A New Model for Control of Systems with Friction" IEEE Transactions on Automatic Control, March 1995, Vol, 40 (3), pp. 419–425.

102. Dihua, G., Jin, S. and Yam, L.H. "Establishment of Model for Tire Steady State Cornering Properties using Experimental Modal Parameters", Vehicle System Dynamics, 2000, Vol. 34 (1), pp. 43-56.

103. Shang, J., Guan, D. and Yam, L.H. "Study on Tire Dynamic Cornering Properties Using Experimental Modal Parameters"; Vehicle System Dynamics, 2002, Vol. 37(2), pp. 129-144.

104. Cadiou, J.C., Hadri, A.E.L. and Chikhi, F. "Non-Linear Tyre Forces Estimation Based on Vehicle Dynamics Observation in a Finite Time"; Proceedings of the Institution of Mechanical Engineers Part D: Journal of Automobile Engineering, Dec. 2004, No. D12, pp. 1378-1391.

105. Cadiou, J.C. and Hadri, A.E.L. "Transversal Tyre Road Characteristic Estimation"; Proceedings of the Institution of Mechanical Engineers Part D: Journal of Automobile Engineering, Oct. 2004, Vol. 218 (10), pp. 1099-1110.

106. Fukada, Y. "Slip-Angle Estimation for Vehicle Stability Control"; Vehicle System Dynamics, 1999, Vol. 32 (4-5), pp. 375–388.

107. Kyong-su, Y. "Road Friction Estimation using Wheel Speed Sensors"; 5th World Congress on ITS, Seoul, Korea,1998.

108. Umeno, T. "Estimation of Tire-Road Friction by Tire Rotational Vibration Model"; Toyota Central R&D Labs Inc. R&D Review of Toyota CRDL, 2002, Vol.37 (3), pp. 53-58.

109. Ray, L.R. "Experimental Determination of Tire Forces and Road Friction"; Proceedings of the American Control Conference, June 1998, Vol. 3, pp. 1843–1847.

110. Hahn, J.O., Rajamani, R. and Alexander, L. "GPS-Based Real-Time Identification of Tire-Road Friction Coefficient"; IEEE Transactions on Control Systems Technology, March 2002, Vol. 10 (3), pp. 331-343.

111. Guo, K., Cheng, Y. and Ding, H. "Analytical Method for Modeling Driver in Vehicle Directional Control"; Vehicle System Dynamics, 2004, Vol. 41 Suppl., pp. 401-410.

112. Limpibunterng, T. and Fujioka, T. "Bilateral Driver Model For Steer-By-Wire Controller Design - The Improvement of Lane-Change Stability Using Optimal *SA7*Rate Feedback + Lead Steering Method"; Vehicle System Dynamics, 2004, Vol. 41 Suppl., pp. 381-390.

113. Noomwongs, N., Yoshida, H., Nagai, M., Kobayashi, K. and Yokoi, T. "Study on Handling and Stability using Tire Hardware-in-the-Loop Simulator". JSAE Review, 2003, Vol. 24, pp. 457–464.

114. Cabrera, J.A., Ortiz, A., Simon, A., Garcia, F. and de la Blanca, A. P. "A Versatile Flat Track Tire Testing Machine"; Vehicle System Dynamics, 2003, Vol. 40 (4), pp. 271-284.

115. Klier, W. and Reinelt, W. "Active Front Steering (Part 1): Mathematical Modeling and Parameter Estimation"; SAE World Congress Detroit, Michigan, USA, March 8-11, 2004, SAE paper no. 2004-01-1102.

116. Koehn, P. and Eckrich, M., 'Active Steering – The BMW Approach towards Modern Steering Technology'. SAE World Congress Detroit, Michigan, USA, March 8-11, 2004, SAE paper no. 2004-01-1105.

117. Smith, C. "Tune to Win"; Aero Publishers, Fallbrock, CA, USA, 1978.

118. Valkenburgh, P.V. "Race Car Engineering & Mechanics"; Seal Beach, CA, USA, 1992.

119. Velenis, E., Tsiotras, P. and Canudas-de Wit, C. "Extension of the Lugre Dynamic Tire Friction Model to 2D Motion"; Proceedings of the 10th IEEE Mediterranean Conference on Control and Automation – MED2002, Lisbon, Portugal, 9–12 July, 2002.

120. Gaffney III, E. F. and Salinas, A.R. "Introduction to Formula SAE Suspension and Frame Design"; SAE paper no. 971584, 1997.

121. Bamsey, I. and Lis, A. "Competition Car Controls"; Haynes Publications Inc., Newbury Park, CA, USA, 1990.

122. Kuo, B. C. "Automatic Control Systems" 7th edition, Prentice-Hall International Inc., Englewood Cliffs, N.J., USA, 1995.

123. Shigley, J.E., and Uicker, Jr, J.J. "Theory of Machines and Mechanisms"; 2nd Edition, McGraw-Hill, New York, USA, 1995.

124. Orozco, A.R. "Evaluation of an Active Steering System"; Master's Degree Project Stockholm, The Royal Institute of Technology (KTH), Sweden 2004.